MODIFICATION OF AUSTENITIC CAST IRON (NI-RESIST) WITH HIGH MANGANESE CONTENT BY USING HEAT TREATMENT
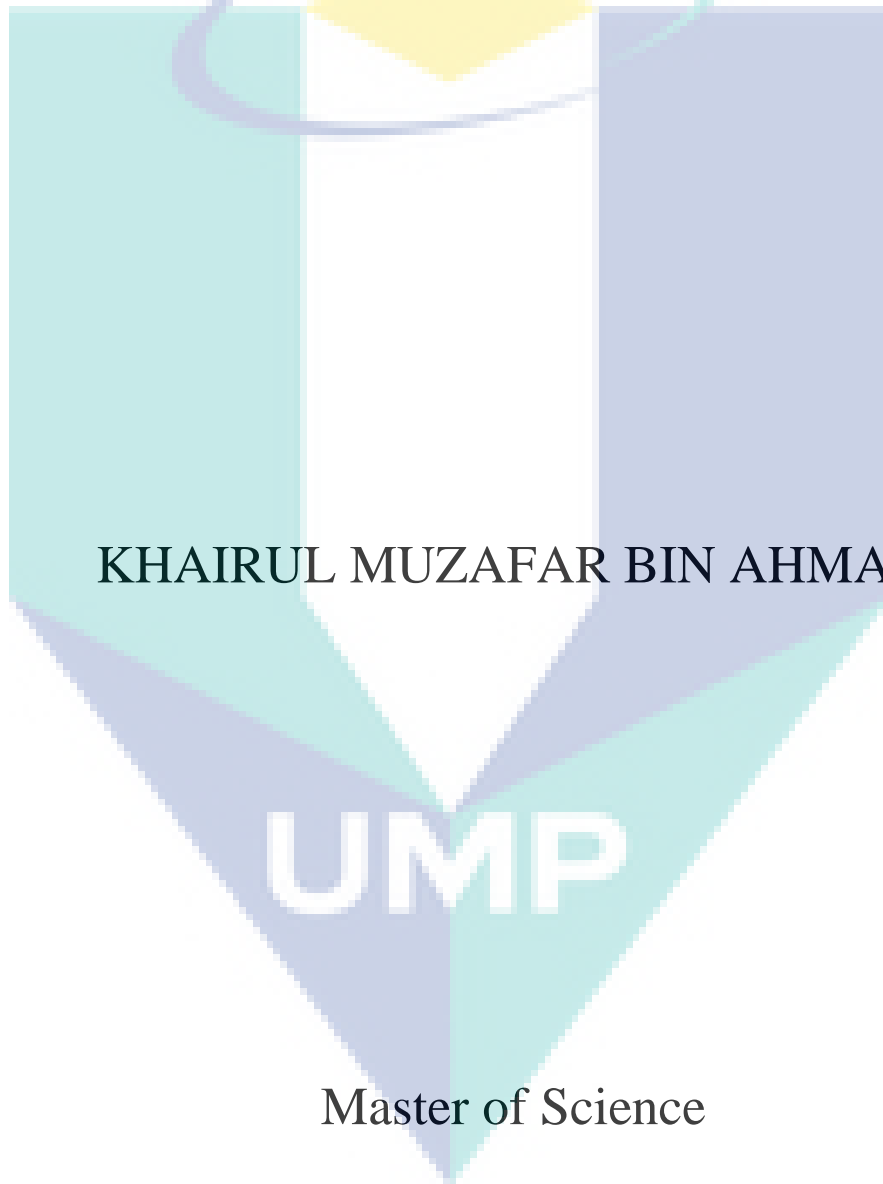
KHAIRUL MUZAFAR BIN AHMAD

Master of Science

UNIVERSITI MALAYSIA PAHANG

UNIVERSITI MALAYSIA PAHANG

DECLARATION OF THESIS AND COPYRIGHT

Author's Full Name : _____

Date of Birth : _____

Title : _____

_____

_____

Academic Session : _____

I declare that this thesis is classified as:

☐ CONFIDENTIAL (Contains confidential information under the Official Secret Act 1997)*

☐ RESTRICTED (Contains restricted information as specified by the organization where research was done)*

☑ OPEN ACCESS I agree that my thesis to be published as online open access (Full Text)

I acknowledge that Universiti Malaysia Pahang reserves the following rights:

1. The Thesis is the Property of Universiti Malaysia Pahang
2. The Library of Universiti Malaysia Pahang has the right to make copies of the thesis for the purpose of research only.
3. The Library has the right to make copies of the thesis for academic exchange.

Certified by:

_____   _____
(Student's Signature)   (Supervisor's Signature)

_____   _____
New IC/Passport Number   Name of Supervisor
Date: Date:

NOTE : * If the thesis is CONFIDENTIAL or RESTRICTED, please attach a thesis declaration letter.

THESIS DECLARATION LETTER (OPTIONAL)

Librarian,
Perpustakaan Universiti Malaysia Pahang,
Universiti Malaysia Pahang,
Lebuhraya Tun Razak,
26300, Gambang, Kuantan.

Dear Sir,

CLASSIFICATION OF THESIS AS RESTRICTED

Please be informed that the following thesis is classified as RESTRICTED for a period of three (3) years from the date of this letter. The reasons for this classification are as listed below.

Author's Name
Thesis Title

Reasons   (i)

                    (ii)

                    (iii)

Thank you.

Yours faithfully,

_____
     (Supervisor's Signature)

Date:

Stamp:

Note: This letter should be written by the supervisor, addressed to the Librarian, *Perpustakaan Universiti Malaysia Pahang* with its copy attached to the thesis.

SUPERVISOR'S DECLARATION

I/We* hereby declare that I/We* have checked this thesis/project* and in my/our* opinion, this thesis/project* is adequate in terms of scope and quality for the award of the degree of *Doctor of Philosophy/ Master of Engineering/ Master of Science in ……………………………..

_____
(Supervisor's Signature)
Full Name   :
Position   :
Date   :

_____
(Co-supervisor's Signature)
Full Name   :
Position   :
Date   :

STUDENT'S DECLARATION

I hereby declare that the work in this thesis is based on my original work except for quotations and citations which have been duly acknowledged. I also declare that it has not been previously or concurrently submitted for any other degree at Universiti Malaysia Pahang or any other institutions.

_____

(Student's Signature)

Full Name   : KHAIRUL MUZAFAR BIN AHMAD

ID Number   : MMM 14014

Date   : 28 June 2017

MODIFICATION OF AUSTENITIC CAST IRON (NI-RESIST) WITH HIGH
MANGANESE CONTENT BY USING HEAT TREATMENT

KHAIRUL MUZAFAR BIN AHMAD

Thesis submitted in fulfillment of the requirements
for the award of the degree of
Master of Science

Faculty of Mechanical Engineering

UNIVERSITI MALAYSIA PAHANG

OCTOBER 2017

ACKNOWLEDGEMENTS

ABSTRAK

Besi Tuangan Austenitic (Ni-resist) digunakan secara meluas dalam industri kimia dan loji kuasa, automotif dan industri minyak dan gas. Bahan ini menawarkan ketidakstabilan sifat yang luar biasa pada suhu yang cukup tinggi dan ketahanan terhadap pengaratan dan hakisan seperti yang dituntut oleh industri. Struktur mikro Austenitic dalam Ni-melawan wujud kerana pengaruh nikel sebagai pemangkin austenitic matrik yang utama. Walau bagaimanapun, menggunakan nikel sebagai aloi tambahan utama untuk pengeluaran Ni-menolak Alloy adalah mahal kerana mempunyai harga yang tidak stabil. Oleh itu, menggunakan mangan sebagai pengganti nikel atau campuran keduanya untuk memangkin matriks austenit adalah pilihan yang boleh diambil kira dalam mengurangkan jumlah kos pemprosesan. Oleh itu, kajian ini bertujuan untuk meneroka kemungkinan untuk mengurangkan penggunaan nikel dengan penggantian mangan untuk menjana struktur austenit Ni-resist. Selain itu, penyiasatan mengenai kesan sifat-sifat ke arah perubahan Ni-resistif (Mn-Ni-resist) sebelum dan selepas rawatan haba adalah menarik untuk dikaji. Bahan besi austenit mangan yang lebih tinggi dengan kandungan nikel yang dikurangkan (Mn-Ni-resist) dihasilkan dengan kandungan mangan 9 wt%, 10 wt%, 11wt% dan 12wt% menggunakan blok Y berdasarkan piawaian ASTM A436 dengan menggunakan acuan pasir hijau . Sampel kemudian dipanaskan pada suhu 700ºC, 800 ºC, 900 ºC, dan 1000 ºC selama 3 jam sebelum perlahan-lahan didinginkan ke suhu bilik dalam suhu relau. Hubungan kompleks antara pembangunan mikrostruktural pemejalan dan membina pemisahan mikro disebabkan peningkatan Mn wt% dalam Mn-Ni-resist diperoleh dengan menggunakan analisis lengkung haba pendinginan dan dibantu dengan pemerhatian mikroskopik dan ujian mekanik. Eksperimen menggambarkan pencirian mikrosegregasi dalam Mn-Ni-resist telah dibuat menggunakan kiraan mikroanalisis di sepanjang mikrostruktur. Hasilnya menunjukkan bahawa penambahan mangan dan rawatan haba mempengaruhi struktur mikro dan sifat mekanik. Lenkung penyejukkan menurun dan morfologi austenit lengan dendrite dilihat memendek sebagai peningkatan Mn wt%. Kemudian, kekuatannya berkurangan dan lebih rendah berbanding dengan besi tuang konvensional. Pemerhatian mikrostruktur menunjukkan bahawa Mn-Ni-resist terdiri daripada serpihan grafit yang tertanam dalam matriks austenitik dan karbida terkumpul di dalam bingkai grafit yang berbentuk roset dimana dikenali juga sebagai rantau membekukan terlambat(LTF). Suhu *annealed* yang lebih tinggi pada Mn-Ni-resist telah berjaya mengurangkan pembentukan karbida dan sedikit meningkatkan kekuatan tegangan. Suhu *annealed* yang lebih tinggi menunjukkan karbida diubah menjadi saiz yang lebih kecil dan menyebar melalui struktur matriks austenit. Saiz karbida menurun dengan peningkatan suhu *annealed* seperti yang diperhatikan dalam struktur mikro. Sebaliknya kekerasan berkurangan apabila suhu annealed bertambah.

ABSTRACT

Austenitic cast iron broadly used in chemical and power plant, automotive and oil and gas industry. This material offers outstanding properties instability at a moderately high temperature and resistance to corrosion and wear which demanded by the industry. Austenitic microstructure in Ni-resist exists due to the influence of nickel as prime austenitic matrix promoter. However, using nickel as prime alloy addition for the production of Ni-resist Alloy is expensive due to its unstable prices. So, employing manganese as nickel replacement or mixing with for austenitic matrix promoter is an option that may reduce total processing cost. Therefore, the present study aims to explore the possibility to reduce nickel consumption by manganese substitution to generate the austenitic structure of Ni-resist. Furthermore, an investigation on the effect of the properties towards modified Ni-resist (Mn-Ni-resist) before and after heat treatment is appealing. Higher manganese austenitic cast iron with reduced nickel content (Mn-Ni-resist) was produced with manganese content nine wt%, ten wt%, 11 wt% and 12 wt% through Y-block according to ASTM A436 by using a green sand mold. Samples were then annealed at 700ºC, 800 ºC, 900 ºC, and 1000ºC for 3 hours before slowly cooled to room temperature in furnace temperature. The complex relationship between the development of the solidification microstructures and build up of micro-segregation due to increasing Mn wt% in Mn-Ni-resist was obtained by using cooling curve thermal analysis and complemented by microscopic observation and mechanical properties. Experimental describe the characterization of microsegregation in Mn-Ni-resist was made using point counting microanalysis along the microstructure. The result showed that manganese addition and heat treatment affect the microstructure and mechanical properties. Solidification cooling curve decreased, and the morphology of austenite dendrite arm shortened as the Mn wt% increased. Then, the strength reduced and more inferior compared to conventional cast iron. Microstructure observations revealed that Mn-Ni-resist consists of flake graphite embedded in the austenitic matrix and the accumulative of carbide at the frame of the rosette flake graphite and also known as late to freeze region (LTF). Higher annealing temperature on the Mn-Ni-resist has successfully reduced carbide formation and slightly increases tensile strength. The higher annealing temperature shows carbide altered into a smaller size and disperses through the austenitic matrix structure. The size of carbide decreased with increasing annealing temperature as observed in the microstructure. On the other hand, hardness diminished as the annealing temperature increases.

TABLE OF CONTENT

LIST OF TABLES

LIST OF FIGURES

xi

LIST OF SYMBOLS

γ	Austenitic
α	Ferrite Iron
T_{liq}	Liquidus temperature
T_{und}	Undercooling temperature
T_{eut}	Eutectic temperature
T_{end}	End of solidification temperature
dT / dt	1st derivation
T_L	Austenite liquidus temperature
T_E	Equilibrium point of graphite eutectic temperature
T_C	Equilibrium point of carbide eutectic temperature
V	Volume
P	Density
C_p	Heat capacity
Q_L	Heat of solidification
T	Time
H	Convection heat transfer coefficient
A	Area
T	Temperature
D	Diffusion rate of carbon in austenite
R	Nodule size of graphite
S	Distance
X	Molar fraction
K_s	Segregation Coefficient

LIST OF ABBREVIATIONS

T-T-T	Time –temperature-transformation
ASTM	American standard for testing material
ADI	Austempered ductile iron
Ni-resist	Austenitic cast iron
TA	Thermal analysis
DNR	Ductile ni-resist
FCC	Face centered cubic
BCC	Body centered cubic
TAL	Temperature of the liquidus arrest
TES	Temperature of eutectic nucleation
TEU	Temperature of eutectic undercooling
TER	Temperature of eutectic recalescence
TEE	Temperature of the end of eutectic solidification
DTA	Differential thermal analysis
LTF	Last to freeze
DAS	Dendrite arm spacing
SDAS	Secondary dendrite arm spacing
TC	Total carbon
CEV	Carbon equivalent
CAE	Calculation of liquidus value
NiFe	Nickel Ferro
FeMn	Ferromanganese
MgFeSi	Magnesium ferrosilicon
FeSi	Ferrosilicon
SEM	Scanning electron microscopy
EDX	Energy dispersive X-ray spectroscopy
OM	Optical microscope
XRD	X-ray diffraction
kW	Kilowatt
HCL	Hydrochloric
KOH	Kalium hydroxide
NaOH	Natrium hydroxide
HMV	Hardness micro Vickers
HV	Hardness Vickers

CHAPTER 1

INTRODUCTION

1.1   Introduction

Austenitic cast irons are also known as Ni-resist are essential materials, and their use is justified by mechanical properties which can be achieved, associated with their outstanding abilities on withstanding the effects of corrosion (Rashidi & Hasbullah, 2013), heat and wear. It is the most widely utilized materials in corrosive environments, due to its excellent resistance to corrosion (Alabbasian, Boutorabi, & Kheirandish, 2016; Alzafin, Mourad, Zour, & Abuzeid, 2009; Yang, Cao, Lian, & Yu, 2011; Zeng, Xie, Hu, & Yung, 2001). These materials have been used for more than 50 years, dating back to the early of 1930 (McKay & Robert, 1936).

Austenitic cast irons microstructure contained a high austenitic matrix composition. The appearance of this matrix is contributed by the influence of nickel contained in the composition that acts as austenite matrix promoter. Nickel is the main element to achieve austenitic matrix, and its content varies from 13 to 37 wt%. Nickel forms a continuous series of solid solutions with iron and has almost unlimited solubility in austenite. It maintains the austenitic matrix both during elevated and room temperature. It happened because austenitic matrix evades matrix volume changes from room to elevated temperature operation. Thus the influence of ferrite and austenite towards volume changes suffered like conventional cast iron was minimized.

Ni-resist able to stay consistent in the austenitic matrix at all temperatures and have avoided this type of transformation (Rashidi & M. Hasbullah, 2013). It can be achieved by the suitable addition of alloying elements. The time–temperature–transformation (T–T–T) curve is pushed to the right. So, the solidification curve at room temperature stands a chance to miss the 'nose' of the T–T–T curve(Forrest, 1983;

1

A. N. Volkov, Lyadskii, & Stanehev, 1968). Nickel broadens the temperature range in which austenite exists. Thus the austenitic matrix can stable at room and lower temperatures (Aptekar' & Abramenko, 1977). The austenite matrix in these alloys is a metallic phase with an FCC lattice, consisting of a solid solution based on iron.

Although numerous data have been published on the advantages of this excellent material, the uses of nickel resist still have a major drawback especially associated with production cost. The high price is contributed by the cost of nickel as an alloying element (Oshima, 2007). There is increasing concern about the uncertainty of Ni-resist prices. So, there is demand for improvement in the design, properties, alloying elements and microstructure of Ni-resist to overcome these challenges. It is mere to ensure that Ni-resist will be more sustainable and adaptable for robust, economical and extreme operations in the future (Covert, 1998; Warda, 1998).

Some efforts have been made to reduce nickel content in Ni-resist iron. Several investigations reported the use of manganese and copper as nickel replacement due to its relatively cheaper. They have been the object of a long time ago until recent studies like (A. Janus & K. Granat, 2014; Cox, 1988; Rashidi, Hasbullah, & Shayfull, 2013; Shebatinov & Abramenko, 1986). Furthermore, manganese is also believed to be better austenite promoter than copper (Cox, 1988).

Manganese seems a good prospect to be used as alternative austenitic promoter despite suspected to interrupt the nodularisation phase during solidification (Roula & Kosnikov, 2008). It is also can act as a sulphur controller (Gundlach, Meyer, & Winardi, 2015). However, manganese is also well known as carbide promoter (Murthy, Sampathkumaran, & Seetharamu, 2009; Rashidi & Hasbullah, 2014; Yaer, Shimizu, Matsumoto, Kitsudo, & Momono, 2008). The concentrations of this element in the austenite usually differ from the average concentration of the cast iron. This occurrence is due to the limited solubility of the manganese in the liquid or solid solution.

Manganese is partially soluble in iron and furthermore encourages the formation of carbide. The existence of carbide is an undesirable element in producing iron. Manganese segregates severely in inter graphite area and in the last to freeze (LTF) region (Ahmadabadi, Niyama, Tanino, Abe, & Ohide, 1994; Alabbasian et al., 2016; Rashidi & Hasbullah, 2014; Rashidi & M. Hasbullah, 2013). Another researcher

discovered this region is enriched with positive segregation elements such as Mn and Cr (Owhadi, Hedjazi, Davami, Fazli, & Shabestari, 1997).

Several restrictions limit the production of austenitic cast iron with high manganese content. Larger manganese content promoted the precipitation of eutectic carbide throughout austenite matrix and expected to reduce martensite start line (Ms) temperature as reported in the previous report (Dasgupta, Mondal, Chakrabarti, & Ganguli, 2012). The presence of carbide in the matrix microstructure is predicted strongly detrimental to alloyed mechanical properties and processing parameter. So there is a possibility that manganese affected the alloyed iron cooling rate and its microstructure.

There are two different approaches that can be used to minimize carbide in alloyed iron. The first approach would be to avoid carbide precipitation during solidification. This circumstance can be achieved by maximizing the efficiency of inoculation. Proper inoculation technique managed to reduce carbide precipitation during solidification and improves its mechanical properties. The second approach would be to eliminate the carbide precipitated during solidification by using a dissolution heat treatment.

It is believed that heat treatment utilizing annealing process can minimize the formation of excessive carbide in microstructure due to manganese influence. This information based on the previous study (Stanchev, Rublev, Sednev, & Filatov, 1976). Annealing is a heat treatment process for the purpose of obtaining certain desirable conditions or properties by utilizing elevated temperature method.

This study is an attempt to combine high manganese content (9wt% to 12wt %) with reduced nickel content (10wt%) in the production of Ni-resist. Then annealing was applied to lessen the drawback of the manganese on the microstructure. The aim is to investigate the effect of manganese on flake graphite of Mn-Ni-resist and annealing temperature on the microstructure of Mn-Ni-resist. The annealing temperature varies from 700°C up to 1000°C. A large Ni-resist block casting that was inoculated with the optimum amount of inoculant (0.5 wt% FeSi) (Rashidi et al., 2013) and alloying with high manganese content was selected for that purpose. With the hope, this investigation

3

will shed some light on the understanding of the relation between flake graphite, heat treatment, and carbide appearance.

1.2   Problem Statement

Nowadays, Ni-resist was produced by using a large amount of Ni as their austenitic promoter. The common microstructure from pearlite and ferrite was transformed to austenite structure due to the effect of Ni. However, the price of Ni is affected by the higher price of the global commodity. As the result, the Ni price is high that influences the price of Ni-resist production cost. So there is an opportunity to reduce the overall processing cost by searching an alternative for Ni as Ni-resist austenitic promoter.

Cu and Mn are also capable of acting as austenitic promoter. However, Cu was damaging the structure of graphite upon solidification. Meanwhile, Cu also has limited solubility in the iron matrix after solidification. So there is the tendency of Cu to solidify in Last to Freeze region instead in grain size. Consequently, the usage of Cu is neglected to produce Ni-resist.

Another option that capable to act as an austenitic promoter is Mn. However, current knowledge on manganese effect on Ni-resist processing availability is limited. Usage of manganese as austenite stabilizer was ignored because of side effect on the iron's properties. This circumstances influence related industrial player to accept only Ni as matrix promoter that led to higher processing cost.

In theory, there are two types of structure of Ni-resist which can be developed; spheroidal or flake graphite structure alloyed iron. However, the research to date has tended to focus on spheroidal graphite alloyed iron only rather than flake graphite structure. Most studies in flake graphite have only been carried out in a small number of areas, insufficient and already out dated.

As for carbide formation issues, heat treatment seems to be a promising alternative method for overcoming and increasing the alloying austenitic cast iron's microstructure, mechanical, corrosion properties. Heat treatment means controlled utilization of temperature and time to alter the overall properties of the newly developed iron.

The present study investigates the effects of manganese addition and effects of heat treatment on the Mn-Ni-resist with flake graphite. The impact of manganese alloying on the microstructure and mechanical aspects of iron was observed and analysed. The effects of heat treatment on the microstructure and mechanical of the iron also determined. The effects of the necessary operating conditions were studied.

1.3   Objectives of the Study

The main purpose of the research is to find out the effects of higher manganese addition and heat treatment on austenitic cast iron with flake graphite. The specific objectives are:

1. To modified austenitic cast iron at a different loading of manganese content.

2. To characterize the austenitic cast iron with high manganese content in term of microstructure and its relation with mechanical properties.

3. To observe and analyze the effect of heat treatment on microstructure changes and mechanical properties of the high alloyed austenitic cast.

1.4   Significant of Study

This research introduces the novel usage of manganese as one of alloying element in austenitic iron which leads to noticeable favourable changes in the material mechanical properties. Manganese element was added more than 9 wt% to 12 wt% in austenitic cast iron with reduced nickel content to 10 wt%. Previously, manganese content was kept low because of its behaviour in promoting carbide although it is one of the austenite promoters.

Then the use of the heat treatment is to refine the properties of iron. The enhancements of the properties through the implementation of heat treatment are expected to bring several benefits as the constituted material imparts higher strength and toughness. This versatility leads to an expansion in the engineering applications of as cast iron, thus produces material with reduced cost and comparable in term of performances wise. Furthermore, there is a requirement needed to formulate brand new materials and enhancement continuously for those already in the account.

1.5 Scope of the Study

This study covered the scopes as stated below:

1.5.1 Phase 01

Pig iron, pure nickel (Ni), ferromanganese (FeMn), ferrosilicon (FeSi), Magnesium-ferrosilicon (MgFeSi) was checked using spectrometer test machine to collect chemical concentration data. At the same time, a pattern with "Y" block shape was fabricated according to ASTM A436.

1.5.2 Phase 02

Austenitic cast iron developed using a mixture of pig iron, pure nickel, Ferromanganese, and Ferrosilicon and scrap materials. Melting process was held in an induction furnace at 1500 ± 50°C. Nickel content was adjusted to 10 wt% and manganese content as manipulating factor increase from 9 wt% to 12 wt% according to the calculation. Then melt was poured into mold cavity fabricated using the green sand material. Ferro silicon introduced to the melt through the in-mould reaction chamber. Austenitic cast iron with high manganese content was developed and tested to obtain the material mechanical and physical properties.

1.5.3 Phase 03

Austenitic cast iron samples from 9 wt% chose and heated to temperature 700°C, 800°C, 900°C and 1000°C for at least 2 hours and slow cooling in a furnace until ambient temperature for heat treatment.

1.5.4 Phase 04

Austenitic cast iron produced then analyses of its carbide formation, graphite type, tensile strength and hardness using a spectrometer, image analyzer, scanning electron microscopy (SEM), Brinell hardness testing machine and universal tensile testing machine.

1.6   Limitation of Study

Although the investigation was able to be performed as initially intended, however, a number of caveats need to be noted regarding the present study.

1. The current study has only examined the effect of manganese to the Ni-resist. There is the possibility of using copper to the investigation. It is more to deep the understanding the effect of manganese on flake graphite, carbide formation, mechanical properties and thermal analysis as indicated in the objective of the research in Chapter 01, Section 1.3.

2. There is another's method of heat treatment that is applicable for producing Ni-resist iron. However, through this investigation, it is limited to the single heat treatment as according to the scope. It is believed more in-depth understanding may be achieved if another type of heat treatment held for comparison.

3. The current research was not specifically designed to evaluate factors related to optimization of manganese content in Mn-Ni-resist. It is more on the understanding of the effect of manganese to the Ni-resist since it was alloyed with a high quantity of manganese.

CHAPTER 2

LITERATURE REVIEW

2.1   Introduction

This chapter gives a brief introduction to the overview and also references used to complete this study. It is to ensure that all information written and quoted is based on a reliable source which includes books, conference papers, published journals and also internet sourcing.
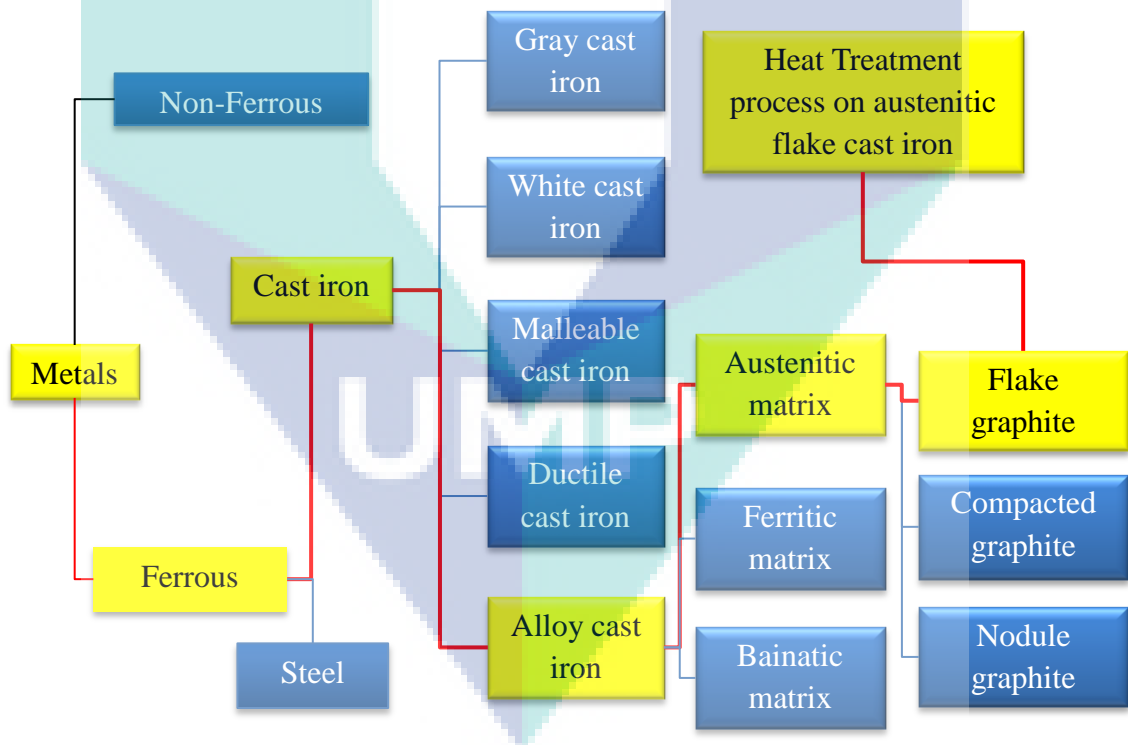
Figure 2.1   Research tree

Overall this research started with investigating about metal which is widely used nowadays as illustrates in Figure 2.1. From this point, there are two types of metal known as ferrous and non-ferrous. As illustrated, besides steel cast iron is a family of ferrous metal which widely used in industry due to its low price. It is about 70% of total world casting tonnage produced every year was cast iron to meet industry demand (D. M. Stefanescu, 2005). This metal can be converted to 5 types of cast iron. Gray cast iron is the first product in this family before others and still being used until today. However, on alloyed cast iron produce with a combination of high alloyed metal and thus have very special properties compared to other. This metal usually is expensive due to the production cost especially austenitic matrix which was produced through alloying with high nickel content. So, this investigation is focusing on this type of material.

2.2   Cast Iron

Cast irons are in the class of ferrous alloy with carbon contents in between 2.0 wt% to 4.5 wt% with the addition of variety other alloying elements like Si, Mn, P, S and trace elements such as Ti, Sb and Sn (Doru M. Stefanescu, 1993). However, in practice, most cast irons are containing between 3.0 and 4.5 wt% C. It is an important and special metallic materials Fe–C alloy, which is most widely used on Earth because of its excellent casting ability, other favourable properties in variety of combination, and relatively cheaper material to produce (Calister & Rethwisch, 2010). Warda (1998) indicated that the term "cast iron" refers not to a single material, but to a generic term for a series of alloys of an iron family who's primarily constituent is iron (majority). Cast irons are iron-carbon base alloys that solidify with a eutectic because the carbon is more than the amount which can be retained in solid solution in austenite at the eutectic temperature as shown in lower part of Figure 2.2 (A644, 2003).
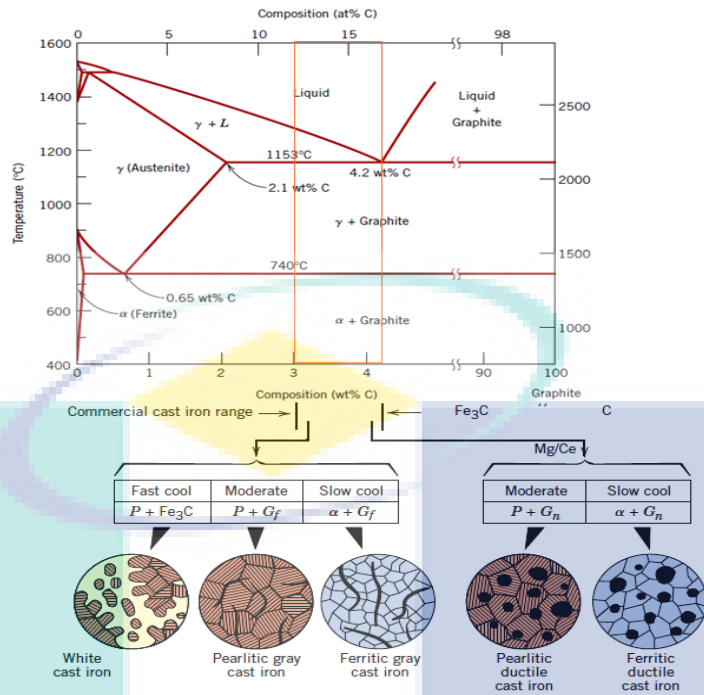
Figure 2.2   The iron–carbon phase diagram with composition ranges for commercial cast irons.

Source: Calister and Rethwisch (2010)

Depending on chemical specifications cast iron can be non-alloyed or alloyed. Wide variations in properties can be achieved by varying the balance between carbon and silicon, by alloying with various metallic or non-metallic elements, and by varying melting, casting, and heat-treating practices (Doru M. Stefanescu, 1993). The carbon in cast iron will be precipitates either as graphitic carbon or as iron carbide based on the silicon concentration (Walton, 1993). Cast irons containing iron carbide (cementite) are named "white" whereas those in which carbon is present as graphite are called "gray" irons.

Cementite precipitated in cast iron during solidification commonly known as iron carbide. These elements relatively are very hard and have excellent abrasion resistance. It forms a brittle white cast iron, and its applications are limited where only wear resistance is of importance involving wear surfaces components. In contrast, graphite is a crystalline form of pure carbon that is soft and very easily fractured. Another essential alloying element is silicon. According to Verhoeven (2007), Silicon content will reduce the chance of carbide to form since silicon is one of graphitizes agent like nickel. Silicon assists in graphite formation (graphitization) above than 1.0

10

wt% in concentrations. Silicon presence lowers the temperature of the austenite to cementite (Fe_3C) graph formation while increase austenite to graphite graph formation (Johansson, 1977). It can be noted that the addition of silicon makes it harder to form Fe_3C. Aside from chemical composition, slower cooling rate during solidification also favours graphite formation instead of carbide. In contrary fast cooling contribute to the precipitation of Fe_3C or white structure.

Calister and Rethwisch (2010) notes that cast iron is classified by a rather simple somewhat archaic system. There are four factors which lead to the different types of cast irons namely, the carbon content, the alloy, the impurity content, the cooling rate and the heat treatment after casting process. However, before 1860, D. M. Stefanescu (2005) reported that there were only two different types of cast irons known based on appearances which are the cast iron that has a gray fracture appearance and the cast iron that has a white fracture appearance. Thus, the names gray iron and white iron evolved. Then, those irons that have a mixed gray and white appearance then called as mottled iron. Only after 50 years, other cast irons start discovered and have names associated with a mechanical property, such as malleable iron and ductile iron. After that compacted graphite iron and austempered ductile iron has been introduced. Several types of cast iron were shown in Figure 2.3.

(a)   (b)

| (c) | (d) |
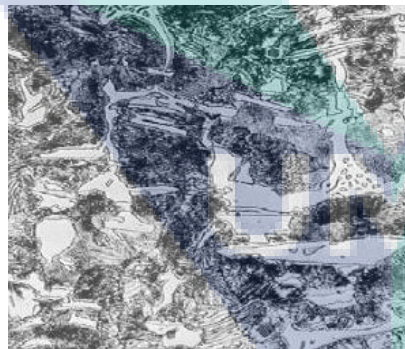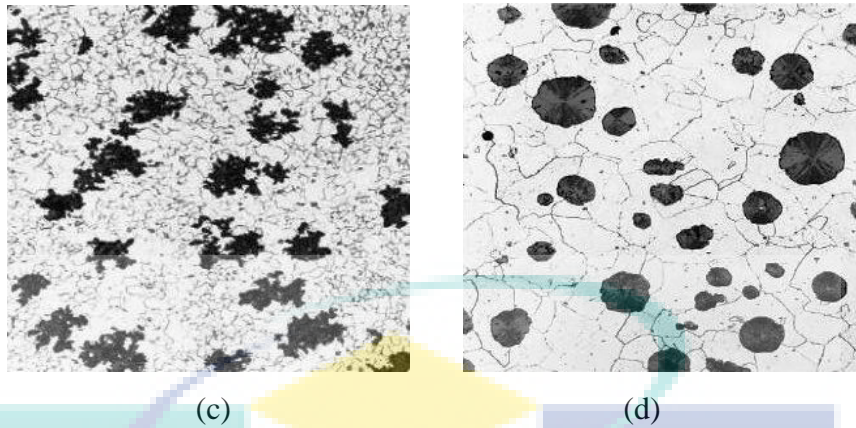
Figure 2.3   Microstructure of (a) White iron, (b) Gray Iron, (c) Malleable iron and (d) Ductile iron at 200 times magnification

Source Radzikowska (2004)

Closed control on the microstructure and metal matrix are the major components which determined the mechanical and physical properties of cast iron. Tensile strength, hardness, and impact properties are the most discussed as these are the primary determinant that differentiates the mechanical properties. Summary of cast iron and steel mechanical properties is shown in Table 2.1.

Table 2.1   Mechanical properties of 4 types of cast iron

Material	Tensile strength [MPa]	Elongation [% (in 2 inches)]	Hardness [Brinell]
Grey cast iron	138-345	0.6	180
Ductile iron	414-552	3-18	170
White cast iron	276	0	450
Malleable iron	345-414	10	130

Source: Siti Khadijah (2010)

Although the conventional cast irons are brittle and have lower strength than steels, they are cheaper and have better castability. In fact, cast irons also have other useful properties which are by the implementation of proper alloying, good foundry control, and through appropriate heat treatment. Furthermore, the properties of cast iron may be varied over a wide range such as comparative strength and hardness, excellent abrasion and corrosion resistance and not to mention its low cost. However, their most significant benefits would be their castability that makes it possible to produce numerous shapes near to net shape to the finished product, thus eliminating major finishing processes. Significant developments in foundry control have led to the production of enormous tonnage of cast iron with consistent properties makes cast iron

12

more competitive in the engineering field. Thus it has been used in widespread engineering applications.

2.3   Austenitic Cast Iron

Recent developments in the production of cast iron have led to renewed interest in austenitic matrix types of cast iron which is also known as High-Nickel Austenitic Cast Iron or Ni-resist. Ni-resist designed with both ductile and flake graphite grades and being covered by national and international specification standard. Despite that, some investigation has been done on austenitic compacted cast iron. Its special abilities in becoming resistant to corrosion, heat and non-magnetic, low temperature and special expansion properties make it very convenient in industries applications. Ni-resist with spheroidal graphite form known as austenitic spheroidal iron or by the trade name Ductile Ni-Resist (DNR). While Ni-resist with flake type graphite form known as austenitic gray cast iron. Ni-resist iron is a family of versatile cast irons exhibiting a broad range of mechanical properties stemming from the microstructure control.   It contains some carbides and sufficient alloy content to produce an austenitic structure (A439, 2001).

Ni-Resist austenitic alloy irons offer an outstanding combination of properties that meet a variety of industrial demands in withstanding the effects of corrosion, heat, and wear (Covert, 1998). Austenitic cast iron can be an economical alternative to stainless steel as it is easier to cast and therefore suitable for precision casting of complicated shaped parts with an arrow wall thickness. Furthermore, it has been produced for many years to meet a broad range of applications requiring special chemical, mechanical and physical properties combined with the economy and ease of production of Cast Iron (Warda, 1998). It is becoming increasingly difficult to ignore the advantages of austenitic cast iron which are developed with the expectation to meet a broad range of applications requiring special chemical, mechanical and physical properties combined with the economy and ease of production of Cast Iron (Warda, 1998).

Ni-resist iron is an iron with the austenitic matrix in room temperature as describe in Figure 2.4. While common iron usually is in the form of pearlite or ferrite matrix in ambient temperature condition as shown in Figure 2.2. Austenitic structure

happens due to the alloying process for the purpose of special properties or demands of service conditions. However, these properties cannot be achieved by the conventional iron or austempered process because only limited percentages of alloying elements will solute inside the iron structure. So alloying during melting is required which Ni-resist material fit easily.

(a)   (b)
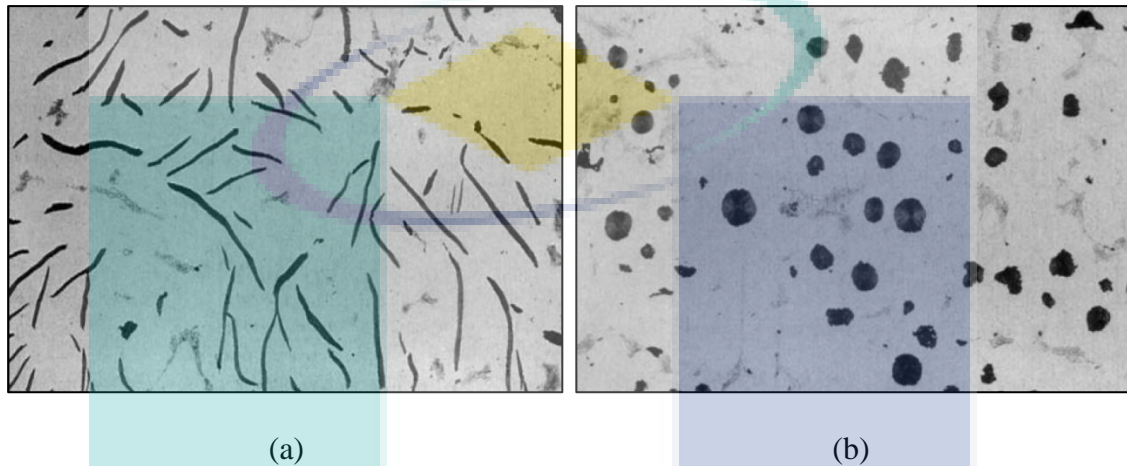
Figure 2.4   Typical microstructure of Ni-resist (a) Gray Ni-resist (b) Ductile Ni-resist

Source: Covert (1998)

Ni-resist has been used in many applications due to its stability as an austenitic metallic matrix in a broad temperature range. It is possible to employ at high temperatures as high as 950 °C (1740 °F) and low temperature as reported by Aptekar' and Abramenko (1977). The homogeneity of the austenitic matrix is responsible for the high resistance to corrosion and erosion, scale resistance, and excellent machinability and ductility. Austenitic irons also have the advantages in mechanical properties such as greater toughness and thermal shock resistance than the other heat-resistant alloy irons, although their strength is rather low (Jenkins & Forrest, 1993).

2.4   Properties of Austenitic cast iron

As According to ASTM A436 (2001), there are eight types of Ni-resist as shown in Table 2.2, with differs in term of their characteristic. Each type of Ni-resist iron has their specific field of application and condition. The feature of the iron based on the chemical composition which was controlled by its alloying elements.

Table 2.2   Chemical composition of Austenitic ductile iron

Ni-resist	Element					
	Carbon	Silicon	Manganese	Copper	Nickel	Chromium
Type 1	3.00	1.00-2.80	0.50-1.50	5.50-7.50	13.50-17.50	1.50-2.50
Type 1b	3.00	1.00-2.80	0.50-1.50	5.50-7.50	13.50-17.50	2.50-3.50
Type 2	3.00	1.00-2.80	0.50-1.50	0.5 max	18.00-22.00	1.50-2.50
Type 2b	3.00	1.00-2.80	0.50-1.50	0.5 max	18.00-22.00	3.00-6.00
Type 3	2.60	1.00-2.00	0.50-1.50	0.5 max	28.00-32.00	2.50-3.50
Type 4	2.60	5.00-6.00	0.50-1.50	0.5 max	29.00-32.00	4.50-5.50
Type 5	2.40	1.00-2.00	0.50-1.50	0.5 max	34.00-36.00	0.10 max
Type 6	3.00	1.50-2.50	0.50-1.50	3.50-5.50	18.00-22.00	1.00-2.00

Source: ASTM A436 (2001)

Ni-resist type 1 – Good resistance to corrosion in alkalis, dilute acids, sea water, and other salt solutions which have moderate temperature and wear resistance. Used for pumps, valves and products selection where wear resistance is required. It is also used for piston ring inserts because of its matching expansion characteristics such as aluminum piston alloys.

Ni-resist type 1b – Similar applications as Ni-Resist 1, but has superior corrosion-erosion resistance. Higher chromium content produces an alloy that is harder and stronger.

Ni-resist type 2 – Higher nickel content makes this alloy more corrosion resistant in alkaline environments. It was applied for handling soap, food products, rayon, and plastics. It can be used where freedom from copper contamination is required.

Ni-resist type 2b – Greater hardness improves corrosion-erosion resistance. This alloy performs well in metal-to-metal wear situations.

Ni-resist type 3 – Resistant to corrosion in wet steam and corrosive slurry. Can be used where it is necessary to match the coefficient of expansion of gray cast iron or steel at temperatures around 260°C (500°F). Applications include pumps, valves, and machinery castings.

Ni-resist type 4 – Has excellent stain resistance. It is superior proportionate to other Ni-Resist alloys concerning corrosion-erosion resistance.

Ni-resist type 5 – Has the lowest coefficient of thermal expansion of Ni-Resist alloys. Provides dimensional stability for machine tool parts, forming dies, instruments, and expansion joints.

Ni-resist type 6 – Is an uncommon alloy. When produced, it is used for pumps and valves handling corrosive solutions.

2.5   Solidification of Austenitic Cast Iron

A clear understanding of solidification principle enables the casting practitioner to predict the practical design of high-quality casting of Ni-resist and reduce undesirable defect. Influence of alloying element on solidification stage is the heart of the understanding of processing Ni-resist (Rashidi, 2014). To date, nickel has widely accepted as a prime alloying addition element in the production of Ni-resist by the industries. The International standard also accepts it and being referenced by many concerned parties. A considerable amount of literature has been published on nickel as an austenitic promoter in Ni-resist. Ni is ranging from 13.5 to 36% in the international standard for industry practice such as ASTM, ISO, and DIN for acquiring a stable austenitic characteristic (Covert, 1998). This range of nickel in standard manages to achieve austenitic matrix structure. Furthermore, this matrix enhances corrosion, wear, and oxidation and heat resistance characteristic. However, most studies in solidification of Ni-resist were produced in a small number of publications and some of them out-dated.

2.5.1   Matrix Formation

It is becoming increasingly difficult to ignore the importance of controlling matrix structure because it will determine the properties and potential applications of the cast iron especially austenite matrix as remarked by (Forrest, 1983). The key control over this matrix utilization depends on its cooling rate and chemical composition. The majority of cast iron is produced with matrix structures consisting ferrite and pearlite or a combination of this matrix. However, to produce cast iron with stable austenite structure (Ni-resist), it depends on alloying element for the purpose to generate the austenitic matrix. Generally, Nickel is being used as the austenitic promoter.

The austenitic structure is achieved by introducing suitable alloy which resists high fraction of the elements inhibiting transition. This phenomenon exists during non-equilibrium cooling of casting. This element minimizes diffusion rate of carbon in austenite. Then it is influenced eutectoid and bainitic transition area in the T-T-T diagram to the right adequately. Later it will reduce the martensite, (Ms) temperature to the lowest working temperature of the casting (Aptekar' & Abramenko, 1977).
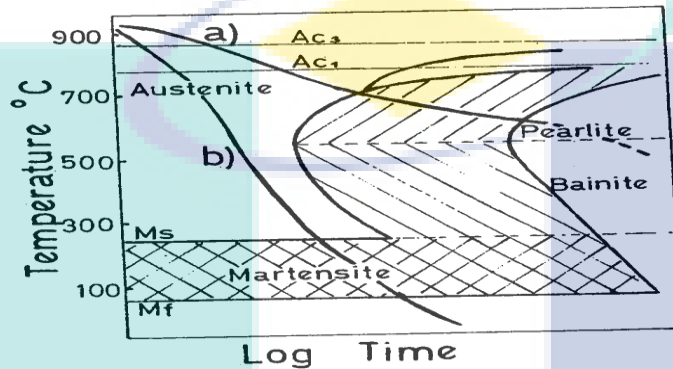
Figure 2.5   Typical time-temperature-transformation curve (T-T-T) for cast iron.
Source: Morrison (1998)

Several publications described the role of nickel on Ni-resist. The review by Forrest (1983) is somehow less extensive but covers more on the importance of matrix control in determining the properties. This publication also defined the influence of alloying elements on the transformation characteristics of austenite. According to his research, the as-cast austenitic microstructure of Ni-Resist occurs due to the effect of nickel contain in the composition that acts as austenitic matrix promoter. The graph in

Figure 2.5 illustrates the mechanism in which nickel suppresses austenite (γ) to ferrite (α) change in conventional iron. Generally, as the solidification in normal condition (slow cooling) either ferrite or pearlite matrix or a combination of this two matrix are expected to exist as described in Figure 2.2. The control of this constituent depended on cooling rate and chemical composition. This fact was supported in

Figure 2.5 which represent a slow and rapid cooling rate situation. Line (a) cuts through the pearlite "nose." While Line (b) misses the "nose" and consequently happen to transform to martensite structure. Martensite was produced when the matrix is rapidly cooled to room temperature and entering Ms region.

17

There were claims that with a suitable concentration addition of alloying elements, the time–temperature–transformation (T–T–T) curve is moved to the right, making it possibly to miss the 'nose' of the T–T–T curve (Forrest, 1983). This statement supports the earlier investigation by Yatsenko and Martsiniv (1968), which discovered that the development of the transformation in casting sections is corresponding to specific elements of the primary structure. It is evidently due to intra-crystalline segregation of nickel and the enriched excess austenite and eutectic austenite which normally are formed at elevated temperature. Figure 2.6 (a-c) shows an overlap of the stable and metastable eutectoid transformations which is a characteristic of these cast irons, that prevents complete ferritization of the matrix by the reaction $\gamma - \alpha + G$. Nickel increases this overlapping, by narrowing $\gamma - \alpha + G$ region. At a high nickel concentration, ferrite formation is suppressed as shown in (Figure 2.6(c)). The eutectoid transformation at $\gamma - \alpha + C$ precede the formation of structurally free carbide (Figure 2.6c, lines 1-2) in the form of austenite grain boundaries network (in contrast to the ferrite network in the lower-nickel concentration of cast iron).
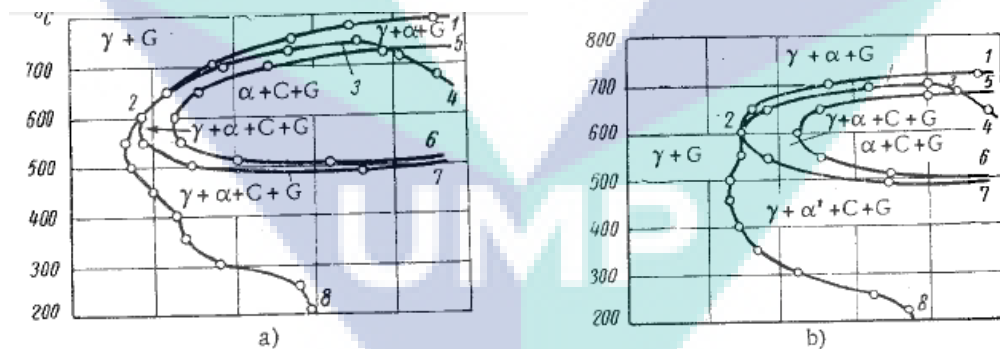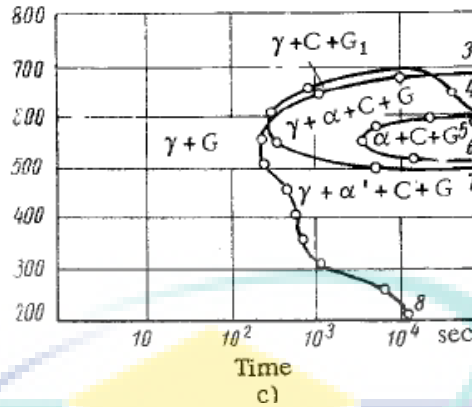
Figure 2.6 Isothermal transformation diagram of austenite in cast iron. a) Without nickel; b) with 3.15% Ni; c) with 6.25% Ni

Source: Yatsenko and Martsiniv (1968)

A suitable amount of Ni is required in order to acquire fully austenitic matrix in the microstructure. The microstructure of Ni-resist will be in the single white matrix together with dark graphite nodules or flake embedded in its matrix. According to ASTM A436 (2001) and ASTM A439 (2001), the minimum amount of nickel demanded to produce a sound Ni-resist is 18wt% for spheroidal type and 13.5 wt% Ni for the gray type. However, this 13.5 wt% Ni is assisted by 5.50 to 7.50 copper wt%. Copper also acts as an austenitic promoter and discussed in Section 2.5 (Kalinina, Mayurnikov, Porublev, & Mayurnikov, 1975). Furthermore, Fatahalla, AbuElEzz, and Semeida (2009) reported that with low nickel content (range 1–9 wt % Ni) sound production of Ni-resist was impossible as indicated in Figure 2.7 (a-b). The appearance of pearlite and martensite was also used as an indicator of insufficient of nickel allocation. That means the Ms temperature line still higher than normal temperature. Another finding was Ni-resist having wholly austenitic matrix can be achieved at 13.5% of nickel addition as shown in Figure 2.7 (c-d).
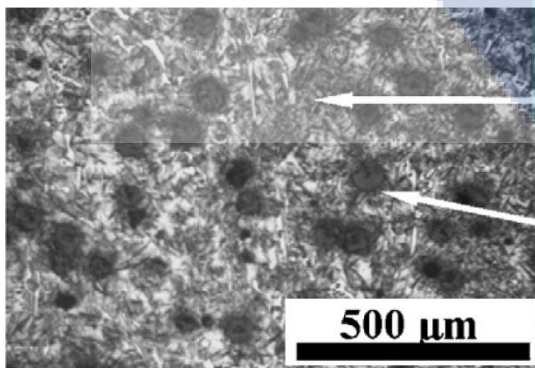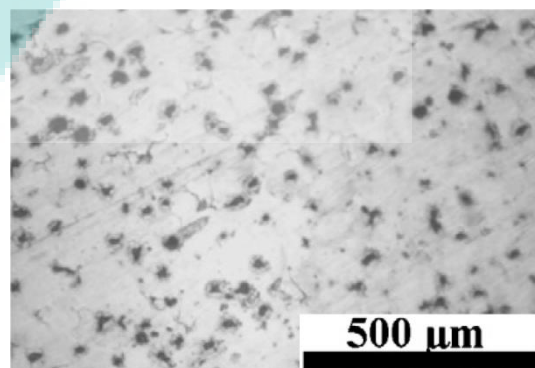
a) 4.99 wt%   b) 9.09
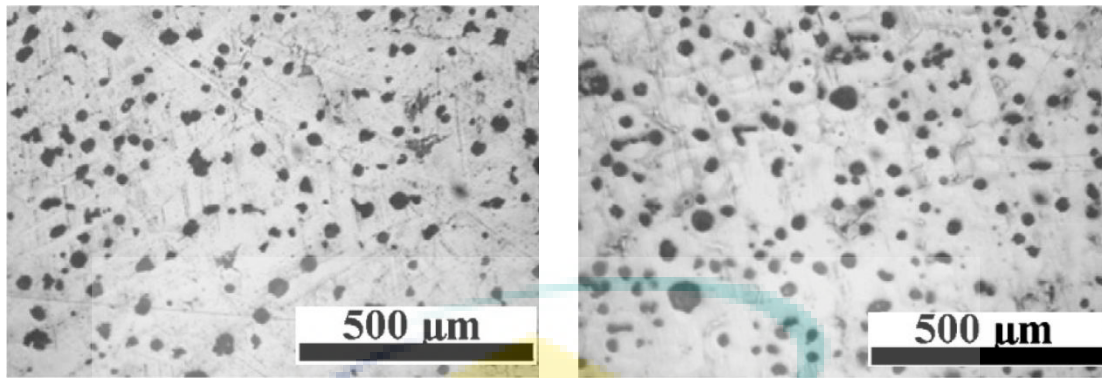
<div align="center">c) 13.5 wt%   d) 16.10 wt%</div>

Figure 2.7   Effect of nickel on the microstructure of Ni-resist (a) with 4.99wt % (b) with 9.09 wt %Ni (c) with 13.5 wt%Ni (d) with 16.10wt%Ni

Source: Fatahalla et al. (2009)

On the other hand, Janus and Kurzawa (2013) proposed that the austenite matrix stability can be controlled by nickel equivalent (Eq_{uni}) as shown in Equation 2.1. However, it is a calculation method based on the concentration of their total elements. This equation not only considers element which stabilizes austenite matrix but also the role of carbon and silicon which was believed to influence the intensity of entire austenite stabilizing process (A. Janus & M. Stachowicz, 2014).

$$Eq_{uni} = 0.32C + 0.13Si + Ni + 2.48Mn + 0.53Cu[\%] \qquad 2.1$$

According to them, previous literature has not indicate the solid value of Eq_{uni} needed for producing sound austenitic cast iron. Consequently, there are still in an ambiguous way to conclude the exact formulation. However, they proved that the minimum value of Eq_{uni} for Ni-resist is 16 (Janus & Kurzawa, 2013). Any casting with Eq_{uni} below than 16 will results of partial austenite–martensite transition occurs. The decrease of equivalent nickel value will result in increasing in the austenite decomposition rate. Fortunately, whole Eq_{uni} value of ASTM A436 type Ni-resist is above 16.

The M_s line temperature change also happened to depend on the chemical composition in the metal and heat treatment (Aptekar' & Abramenko, 1977). The initial temperature of the martensitic transformation (M_s) depends above all on the chemical composition of the alloying elements. An increase of Mn, Cr, Ni, St, or Mo in austenite by 0.1°C lowers Ms respectively by 3.3, 2.2, 1.7, 1.1 and 1.1 °. Cu and C also believed

<div align="center">20</div>

to decrease the Ms temperature line. From this literature, Mn gives higher impact on reducing Ms line (Barton, 1958). The implication from the addition of nickel in cast iron expected to affect the line of martensite transformation commences. Hence it is possible to attain stable phase austenitic matrix at room temperature or below than that. The alloying making the Ms pushed downward. From the Fe-graphite phase diagram in Figure 2.2 the austenite region will be modified and expanded at significant proportion. The expansion may grow from high to room temperature depending on the concentration of austenitic promoter contained. The conventional phase diagram in Figure 2.2 consequently is transformed to phase diagram in Figure 2.7.
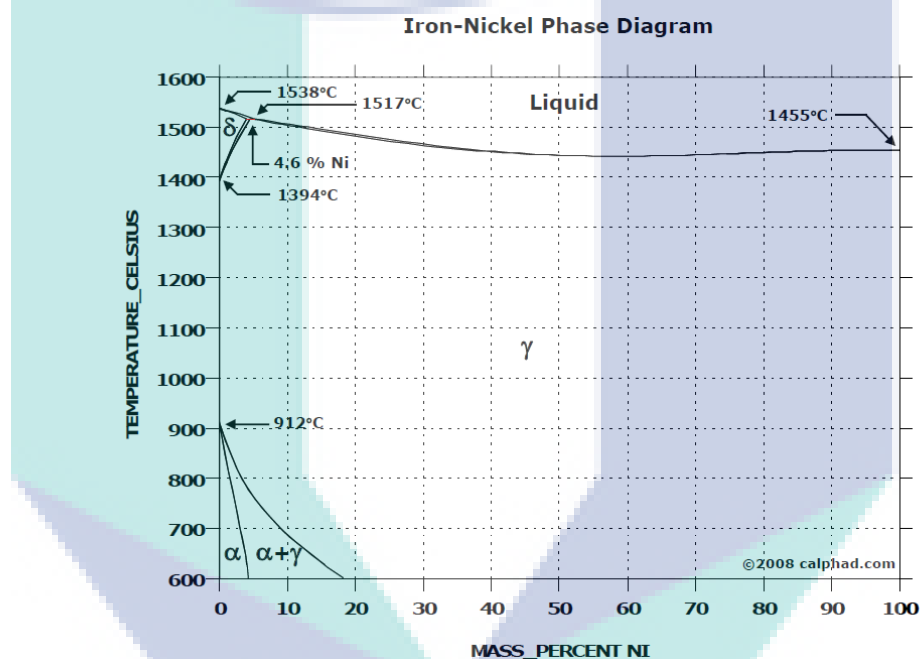
Figure 2.8   Iron- nickel equilibrium phase diagram

Source: CHALPAD Calculation of phase diagram (1st ed) Cambridge: Pergamon Materials Series, Elsevier Science Ltd.

Figure 2.8 shows iron-nickel equilibrium phase diagram by Saunder (1998). It was reported that the normal phase diagram could be modified using the large addition of the alloying element of nickel. This phase diagram remarks that Nickel broadens the temperature range in which austenite exists and stabilizes it at room and lower temperatures. Austenite region encloses most of the phase diagram. Austenite region covers most of the iron structures at room temperature starting from 20% Ni content. Ms temperature line is expected to be below the ambient temperature.

2.5.2 Segregation

Segregation will be the center of discussion and be one of the significant issues in cast iron production, especially Ni-resist. Previous literature indicates how this segregation phenomenon affects the properties of cast iron. It shows a need to be explicit about exactly what is meant by the word segregation. Segregation can be divided into two categories macro-segregation and micro-segregation. According to Hasse Fredriksson and Ulla A ˚ kerlind (2006), segregation can be elaborated as the concentration of the alloying element will be unevenly distributed in the metal when an alloy solidifies by dendritic solidification. While Jiyang (2009b) state that micro segregation is also called short range segregation; which is a phenomenon of non-uniform chemical composition in grain scale. It is with the same meaning but in a different term.

There are several factors influenced the occurrences of micro-segregation. Firstly is the alloying process factor. Various alloying elements have very different partition constants and different tendencies of segregation which depending on its degree of segregation (Jiyang, 2009a). Cr, Mn, V, Mo and much more have a tendency of positive segregation. While constituents such as Si, Al, Cu and much more known as the inverse (negative) segregation element. This segregation led to structural diversity which meant a region rich with the certain element and then prone to precipitate into carbide or eutectic. This non-uniform distribution of alloying elements will affect the solid transformation during cooling or heat treatment.

During solidification, the concentration of the alloying element is levelled out between the solid phase and the melt and lastly pushes to last to freeze region (LTF) (Hasse Fredriksson & Ulla A ˚ kerlind, 2006) as shown in Figure 2.9 below. All the impurity pushes to the area between dendrite (high impurity level region), because of the solid dendrites cannot hold virtually another element, these atoms must be repulsed from the growing dendrite arms into the liquid region between the two dendrites. The composition of positive segregation element in the interdendritic liquid is greater approximate to the base of the dendrites at the bottom of the picture, and eventually, it became high enough to solidify solid and combine with carbon which will encourage micro segregation further severe. The micro segregation is then ended up lying between dendrite arms.
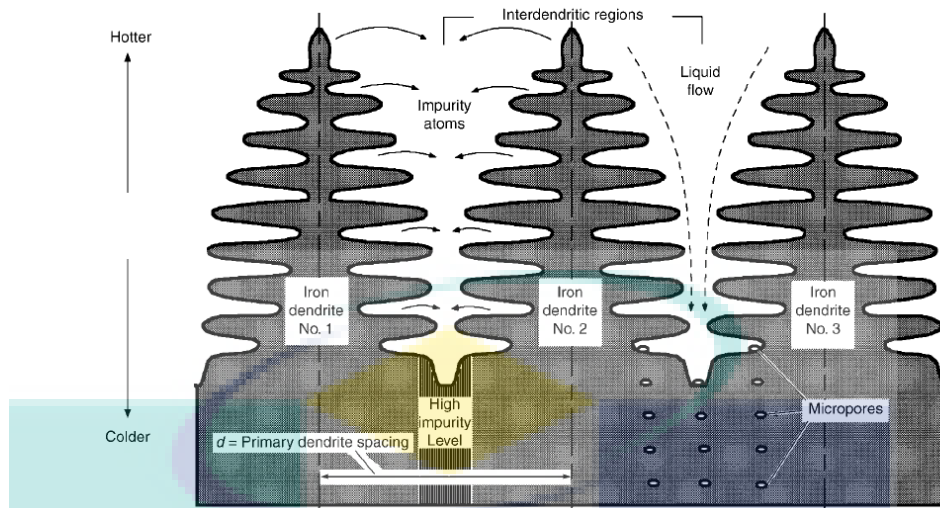
Figure 2.9   Three iron dendrites growing vertically into the liquid during solidification

Source: Verhoeven (2007)

Secondly is the process factor or the possibility of cooling rate influence the segregation of element. If the cooling rate increases as in proper procedure, the segregation tendency becomes less greatly and better (Hasse Fredriksson & Ulla A ̊ kerlind, 2006). In slow cooling casting usually, have strong grain boundary segregation at eutectic cell boundary especially in heavy section casting. It is due to positive element have enough time to be repulsed to the LTF and combine with carbon there.

The third factor that influenced the segregation is the interaction of alloying elements. It should be emphasized that the interactive effect between the presences alloying elements influence the segregation ratio of other elements (Jiyang, 2009a). The high Si content, for example, reduces the uneven balance of other constituents at the cell boundaries. However, when another constituent with higher segregation tendency introduced like high Mn content, the results of silicon in pushing outside from the center of LTF region. It is undoubtedly competition of constituent. Then LTF region will be remarkably filled with Mn in the form of carbide (Owhadi et al., 1997).

Micro-segregation in a solidified material can be determined by using a microprobe. Microsegregation is classified according to its form; segregation can be divided into cellular, dendrite and intergranular segregation (Rashidi, 2014). However, carbide segregation existence from positive carbide promoter likely is undesirable. This element usually ignored or keeps at low concentration in cast iron. In the case where the

presence of carbide enormous, there is two approaches can be applied to reduce the carbide first is maximizing the efficiency of inoculant and second by using heat treatment. These two approaches will be discussed later in the separate chapter.

2.6   Inoculation

Inoculation nowadays is a common applied metallurgical treatment carried out by foundries to improve the mechanical properties of commercial alloys. It is essential in producing a sound cast iron. The comparison between uninoculated and inoculated iron in lamellar graphite is severe and easily revealed as shown in Figure 2.10. The essence of the cast iron inoculation consists in changing the physicochemical state of molten metal. According to ELKEM (2012), inoculation is a mean of controlling the structure and properties of cast irons by minimizing undercooling and increasing the number of nucleation sites. Later the availability of nucleation site will encourage the growth of graphite flakes in gray irons or graphite nodules in ductile irons rather than precipitated as iron carbide during solidification. The purpose of inoculation means to prevent the undercooling to temperature below the metastable eutectic where carbide structures are formed as shown in Figure 2.11.

There are many advantages of inoculation such as to avoid eutectic carbide, ensure distribution of graphite and refine eutectic cell size. Typically, inoculation also reduces the tendency of shrinkage formation (Popovski, 2004). At the same time, it is also found that a homogeneous manganese and sulphur composition is necessary for the precipitation of graphite as stressed by I. Riposan, M. Chisamera, S. Stan, and D. White (2009). This relationship suggested that MnS inclusion could act as a nucleation site for graphite flakes and probably manage to produce a sufficient nucleation site for type A flake graphite as investigated.

Lux (1968) suggested that a method by introducing a small amount of inoculant to the cast iron of low graphite nucleation shortly before pouring has a capability to increase the number of active nuclei. The main key ingredient behind successful inoculant which makes the purpose of inoculation working is the combination of some element with a rare earth such as Al, Ba, Sr and other trace elements (M. Chisamera, Riposan, & Liliac, 1995). Most of the inoculants are based on ferrosilicon containing about 70-75% Silicon, or on ferrosilicon - graphite mixtures. In flake irons, the normal

levels of inoculant ladle addition raise the silicon content by about 0.2% - 1.0%. However, there is an alternative technique of nucleation such as late inoculation which capable to reduce the inoculant lowers than half as stated by Olsen, Skaland, and Hartung (2005).

(a) un-inoculated   (b) inoculated
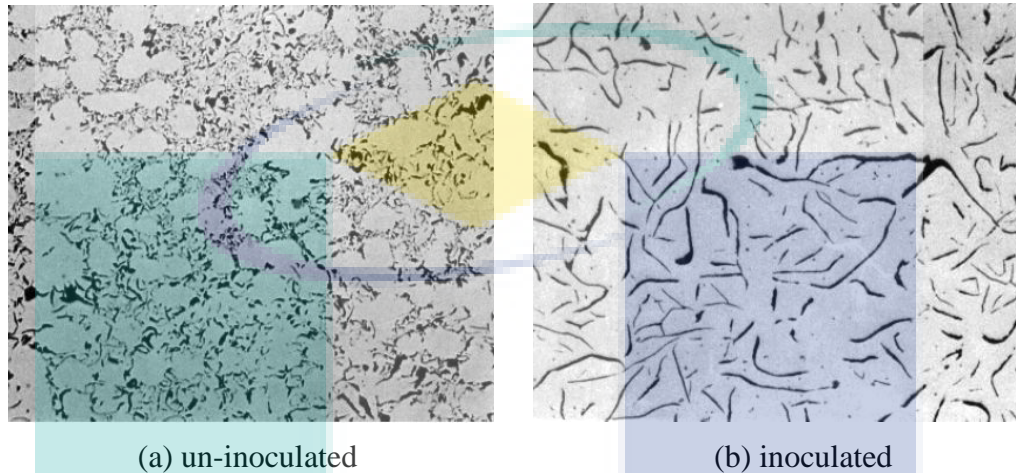
Figure 2.10   Examples of structures in uninoculated and inoculated

Source: ELKEM (2004)

Popovski (2004) stated that iron solidification mechanism is prone to form chilled iron structures when inoculation is inadequate. It is associated with shrinkage due to the unavailability of carbon for graphite expansion throughout the solidification range. Chilled structures contained higher hardness and severely damage machine tool and raise processing cost. However, over-inoculation is lead to waste and may cause shrinkage. Over inoculation can cause excessive early graphite growth that may lead to a lack of available graphite for expansion at the end of freezing. Their situation favoured to the possibility of the micro-shrinkage formation. Also, excessive early graphite growth may cause mold wall expansion which resulting in macro-shrinkage.

(a)   (b)
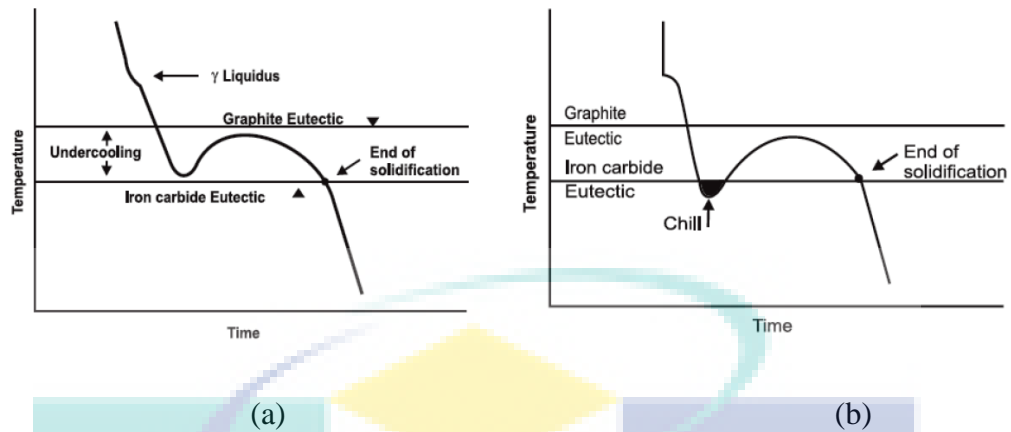
Figure 2.11   Cooling curve (a) without chill formation (b) with chill formation
Source: S.C.Borse (2014)

One of the most significant current discussions in reducing carbide segregation formation in Ni-resist is the application of inoculation process. There is a possibility to eliminate carbide formation. Inoculation manages to increase the properties and eventually help in reduce carbide formation by rearranging the microstructure. It happens during solidification stage which is reducing the gap between dendrite arm and at the same time increase the graphite count in the microstructure. This approach proposes by D. M. Stefanescu (2005) whom stated that there is a possibility of minimizing segregation by controlling branching of primary austenite dendrite for graphite aggregates. The right amount and better application of inoculant practice makes it possible to achieve this objective. However, inoculation technique does not mean to remove the carbide completely from the iron.

A considerable amount of literature has been published with extensive investigation according to the inoculation practice, which allows us to increase properties of cast iron and understand the role of inoculant in solidification of Ni-resist. There is probably some interaction of inoculant and another variable that might lead and link to segregation. Pearce (2008) believed inoculation is responsible in reducing carbide segregation as described in previous studies. Rashidi and Hasbullah (2014) concur this statement through investigation which evidently shows how 1 wt% of inoculation successfully increases mechanical properties and also reduce carbide in the microstructure.

The tensile strength of inoculated cast iron is related to the changes of graphite precipitates characteristic. Inoculation increase the distance between the graphite flakes (and the length of these flakes) between the grains of the graphite eutectic. An effective inoculation treatment of cast iron will change the graphite distribution from interdendritic of type D into a uniform of type A. The character of graphite precipitates depends on interrelations between the interfacial distance of eutectic grains and interdendritic distance of primary austenite. Therefore it could be assumed that the inoculation treatment will also have a substantial effect on the number and shape of the dendrites of primary austenite.
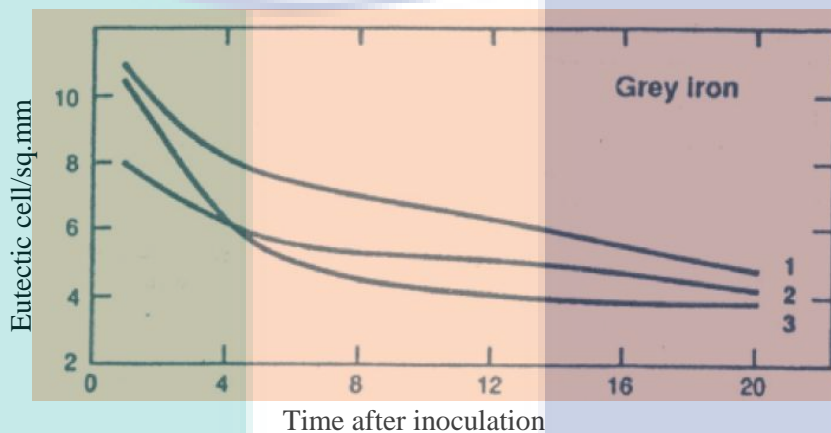
Figure 2.12   Fading of inoculation effect on eutectic cell counts in gray iron. 1. FeSi with Ba and Ca 2. FeSi with Sr and low AI 3. FeSi regular foundry-grade.
Source: Pearce (2008)

Unfortunately, Pearce (2008) remarks the effects of inoculation treatments are transient, and they become reduced with time when the inoculated metal is held in the ladle before castings are poured. This phenomenon is called as 'fading.' According to Popovski, Misterek, and Kaiser (2005), this fading of inoculation will eventually result in carbide formation and poor graphite structures if the iron is held for a prolonged time before pouring. Fading in flake irons leads to a greater tendency to form chill, and increases in eutectic cell size thus decreasing tensile strength. The effects of fading of three common inoculant materials in gray iron can be seen in Figure 2.12. Verhoeven (1975) explains that the reason for this fading loss is coarsening and growth of micro-inclusion which is known as Ostwald Ripening Effect. It is seen that the rates of fading are highest immediately after inoculation.

The majority of researcher and foundry practitioner might agree that to reduce the effects of fading, which molten metal should be poured as soon as possible after inoculation treatment. However often in production situations, this practice cannot always be achieved. Skaland (1999) purpose that the problems of inoculant fade in cast iron can be reduced by using late treatments via pouring stream or in the mold techniques. This technique was agreed by Mihai Chisamera, Riposan, Stan, Stefan, and Costache (2009) through extensive investigation that discovered the in-mould inoculation has a more significant effect compared to ladle inoculation, especially at lower inoculant usage (less than 0.20 wt.%). An earlier investigation by Olsen et al. (2005) also found the required inoculant addition rate may be as high as 1 wt%, while the alternative late in-stream inoculation may need only 0.1 wt% additions which still providing a sufficient or even better inoculation effectiveness. It is primarily due to the late addition method giving lesser time available for particle towards coarsening and fading effects.

2.7   Austenitic Promoter

The principal of alloying element in producing all types of Ni-Resist is Ni, and it has been widely accepted by the industries. However, Ni is comparably expensive material and face economic limitation due to high price for alloying purpose compared to the conventional austenitic stainless steels. Therefore, there has been increasing awareness in the importance of rare source saving by reducing materials demand on Ni. Controlling chemical composition of the alloy is one of the ways in achieving required matrix. It is apparent that by using alloying element, the phase diagram can be altered. There are several types of alloying element that have been used in iron such as silicon, nickel, manganese, copper, molybdenum, and so on. However, there are potential of certain elements that can be used as austenitic promoter besides nickel. From the previous studies, Ni, Cu, and Mn found to be good austenitic matrix promoter of cast iron.

Figure 2.13 shows austenitic promoter elements shows the element that can be used as austenitic matrix promoter.
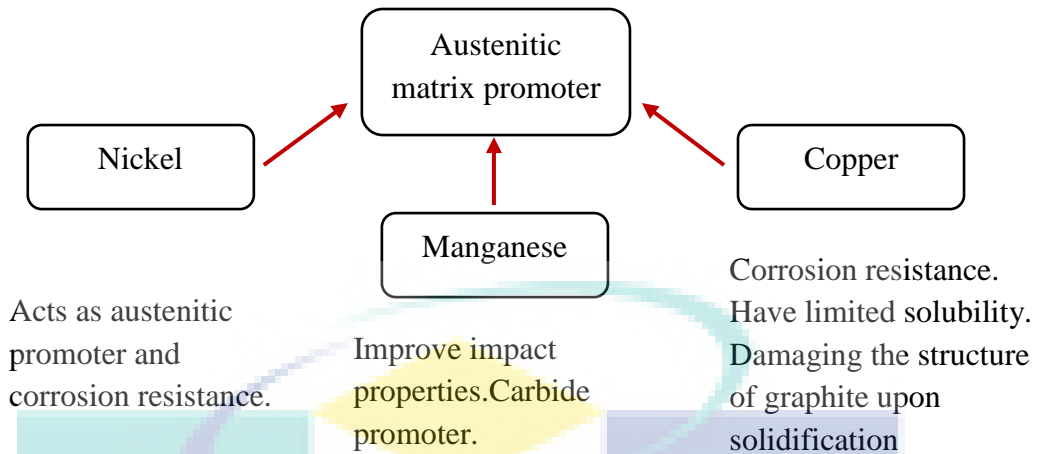
Figure 2.13   Austenitic promoter element

Forrest (1983) and Cox (1988) discussed the influence of various alloying element in austenitic cast iron characteristic. By addition, alloying elements such as copper and manganese, the same effect as the nickel which is the T-T-T curve moving to the right was produced. However, the use of copper has a deleterious effect on nodule graphite of Ductile Ni-resist (DNR), and manganese also has a disadvantage because of its behaviour towards promoting carbide formation.

2.7.1   Manganese

Sulphur is a residual element and should be as low as is commercially feasible. Several previous investigation notes have shown that sulphides in the microstructure degrade abrasion resistance. According to Gundlach et al. (2015) sulphur is a surface active element that can exhibit many adverse effects, including the promotion of degenerate graphite forms, intercellular carbides, increased chilling tendency and high hardness pearlite. When manganese is not present at sufficient concentrations, sulphur reacts with iron to produce a low-melting phase (FeS) that may produce hot shortness. Consequently, industry has always added Mn to control S. It has the ability to neutralize sulphur which is also known as a deoxidizing effect (Ozaki, Okada, & Miyake, 1968). Manganese more than the amount needed to scavenge sulphur mildly suppresses pearlitic for the nation. Davis (1996) remark that manganese will combine with sulphur to form manganese-sulphides (MnS) and thus avoid the undesirable consequences of high S such as lowers the unfavourable effect of iron sulphides. It is of particular importance for free cutting because it reduces the risk of red shortness or decreases the

depth of chill until the residual concentration has been neutralizing. However, Mn reduces the critical cooling rate substantially and thus increases hardenability. Yield point and strength are increased by the addition of Mn.

Manganese also widely known as a relatively strong austenite stabilizer and is usually kept below about 0.7% in martensitic white irons. When the manganese content exceeds about 1.3%, the strength and toughness of martensitic irons begin to drop. Abrasion resistance also drops, mainly because of austenitic retention as reported by Davis (1996). ASTM A128 (2001) indicate that in cast steel, 11 wt% Mn is enough to produce the austenitic matrix in microstructure which is known as Hadfield austenitic manganese steel castings. However, there is no specific standard for austenitic cast iron despite there already several attempts have been made to utilize manganese in cast iron such as Rashidi (2014), Janus and Kurzawa (2013), Cox (1988) and Poyet, Couchinave, and Dancoisne (1984).
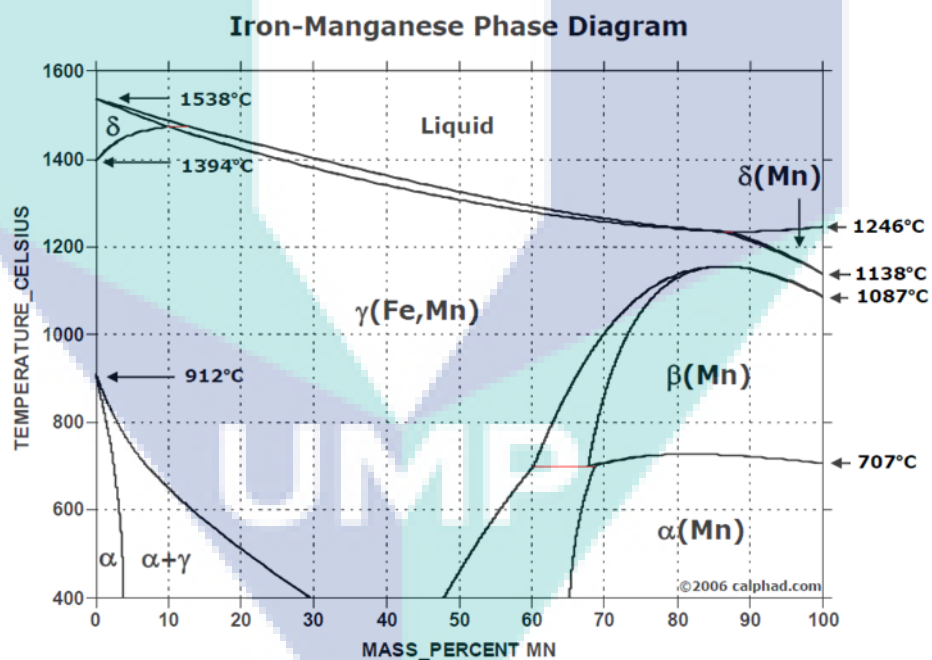
Figure 2.14   Iron- Manganese equilibrium phase diagram

Source: CHALPAD Calculation of phase diagram (1st ed) Cambridge: Pergamon Materials Series, Elsevier Science Ltd.

Figure 2.14 illustrate the Iron-manganese phase diagram with enlarged austenite region compares to conventional iron-carbide phase diagram. Although its austenite behaviour does not expand at significant proportion as when alloyed with high nickel

30

content, high manganese content still provides austenitic characteristic to the cast iron. To get the stability of austenite at lower temperature required high manganese content which is led to increasing in carbide formation. Based on the characteristic of nickel and manganese phase diagram it is possible to alter the phase diagram into the desired one which contained high manganese and nickel without sacrifice the stability of the austenite and reduces carbide formation as suggested by Zhang et al. (2009).

Instead of good austenite stabilizer manganese also well known as a potent promoter of hardenability in cast iron but it also segregates severely and encourages the formation of carbides in the matrix (A. N. Volkov, 1974). Consequently, the use of manganese is limited in cast irons, even though it is one of the least expensive alloying elements. Thus, it is suggested that when the Mn content is high, attempts should be made to minimize the Mn segregation.

Poyet et al. (1984) stated that cast iron which containing more than 7 wt% Mn contents will encourage austenitic matrix because Mn enlarges the y-range considerably. Such iron will experience severe strain hardening of the surface when exposed to impact stresses, while the core remains tough. They are therefore highly wearing resistant in case of impact stresses (Lyadskii, 1963). This investigation supported by latest publication by Rashidi (2014) who reported that using 10 wt% Ni with 9 – 12 wt% Mn manages to produce austenitic cast iron. It is also recorded that from 6 – 8 wt % Mn still produce martensite only completely dissolve when it reaches 9 wt% Mn. However, it comes with severe segregation of carbide in the intercellular region.

Austenitic cast iron made from manganese tends to be less resistant to the effects of oxidation and corrosion as reiterated by Aptekar' and Abramenko (1977). They also tend to be brittle, which is not desirable for structural materials, but the fluidity and ease of casting make it an excellent candidate for non-structural applications.

This discovery supports the earlier research statement made by McKay and Robert (1936) that 20 wt% – 30% wt nickel able to produce an austenitic structure in the cast iron microstructure. He also proposed that manganese may also be employed to help in the production of the austenitic structure with less corrosion resistance.

2.7.2 Copper

The discovery of copper as an austenitic promoter has lifted up the hope of replacing nickel as a main alloying element in Ni-resist (Aptekar' & Abramenko, 1977). Increasing Cu in Ni-resist improved the corrosion resistance in mildly acidic acid and avoided in Ni-resist production (Rashidi & Hasbullah, 2013). However, more is not necessarily better when Cu additions are considered the gray type of Ni-resist. Copper is also known as a pearlitic promoter while manganese ferritic promoter (Sertucha, Larrañaga, Lacaze, & Insausti, 2010). However copper can have a pearlite promoter role only when combined with a low addition of manganese instead of austenite structure as stated by Boudot, Gerval, Oquab, Lacaze, and Santos (1997).

According to Hayrynen (2002), levels more than 0.80 wt% can create diffusion barriers around the graphite nodules and inhibit carbon diffusion during austenitizing. Nickel additions are essential when the level of Cu has been maximized. Ni additions of up to 2 % are typically made. Beyond that, the price becomes an important consideration. In ASTM standard for Ni-resist, a maximum of Cu content is up to 7.50 wt% (type 1b). Seidu, Owoeye, and Owoyemi (2015) affirm that copper up to 2.0% exhibited excellent corrosion resistance in alkali and marine environment. While more than 2.5wt. % of copper is show good corrosion behaviour all in salt water and basic environments but poorly in an acidic environment.

The effect of copper relatively mild compared to that of nickel and because of the limited solubility of copper in austenite, copper addition probably should be limited to about 2.5% or less. This limitation means that copper cannot completely replace nickel in Ni-Hard-type iron (Davis, 1996). Park, Heo, Na, and Kang (2012) attempt to reduce Ni content by using Cu and Mn as replacement find out that bainite and cementite were formed in high Cu content. The formation of Cu-Mn/MnS and those phases decreased the effect of Cu and Mn on austenite formation.

2.8   Thermal analysis

Solidification of casting processes is best described using cooling curves features based on the thermal analysis (Paulik, Paulik, & Erdey, 1966). Thermal analysis covers a range of techniques used to determine the physical or chemical properties of a substance as it is heated, cooled or held at constant temperature. Thermal

analysis (TA) (also called cooling curve analysis, CCA) can provide a complete insight into the dynamic changes occurring upon melting and during melt treatment of casting alloys. Cooling curves record the changes in temperature with time as a consequence of a change of energy within the system. A deviation from normal cooling indicates the occurrence of a source of heat such as the heat of crystallization released by a precipitating phase. D. M. Stefanescu (2015) stated that its interpretation is based on the belief that all the events occurring during solidification leave their mark on the shape of the cooling curve.

It was decided that the best method adopt for thermal analysis be by submerging the tip of the thermocouple into solidified material. Liquid metal is removed from the furnace or ladle and poured into a sample cavity with a thermocouple embedded in it (Emadi, Whiting, Nafisi, & Ghomashchi, 2005). The temperature changes during solidification were recorded and monitored by the data logger and transmit to attach computer. It is crucial because cast iron solidifies with two parts known as primary and eutectic phase solidification. The solidification features initial phase network formed the matrix, eutectic cell, and eutectic morphology. From this information chemical composition based on the phase diagram can be calculated, or the crystalline structure of the cast sample can be estimated. The interaction of these structures also will determine the properties of cast iron (Rashidi, 2014).

In this method, the temperature changes in the sample are recorded from fully liquid to fully solidified phase producing a curve plot of temperature as a function of time. A cooling curve reflects the release of latent heat of solidification. This liberates latent heat in multi-component alloys changes the slope of the cooling curve which is then used to detect the characteristics of transformations and phase reactions during solidification (Farahany, Ourdjini, & Idris, 2012). However, due to the faster reaction during solidification, the small amounts of heat evolved in some phase transformations may not be obvious on the cooling curve. Thus, to reveal the appropriate temperature and time of certain reactions such as start and end of the transformation, the first derivative cooling curve (dT/dt) is employed. These identities are known as solidification point and were synthesized using Differential Thermal Analysis (DTA) (Bhadeshia, 2002). Sparkman (2010) once have stated that the temperature cooling

curve has much information hidden in it. However, if the dT/dt (delta Temperature/delta time) curve is plotted, that information becomes visible.

Differential Thermal Analysis (DTA) was utilized to determine precise temperature point, especially for cast iron solidification. It manages to predict not only the chemistry of the melt but also the nucleation potential (degree of inoculation), the shrinkage tendency, the dendrite arm spacing and the grain size, the graphite shape, the solidification microstructure, and even the room temperature microstructure (D. M. Stefanescu, 2015). Furthermore, cooling curve method is useful for commercial applications for some reasons: it is simple, inexpensive and provides consistent results. This technique is an excellent choice for drawing fundamental relationships between cooling curve characteristics, alloy composition, and melt treatment.
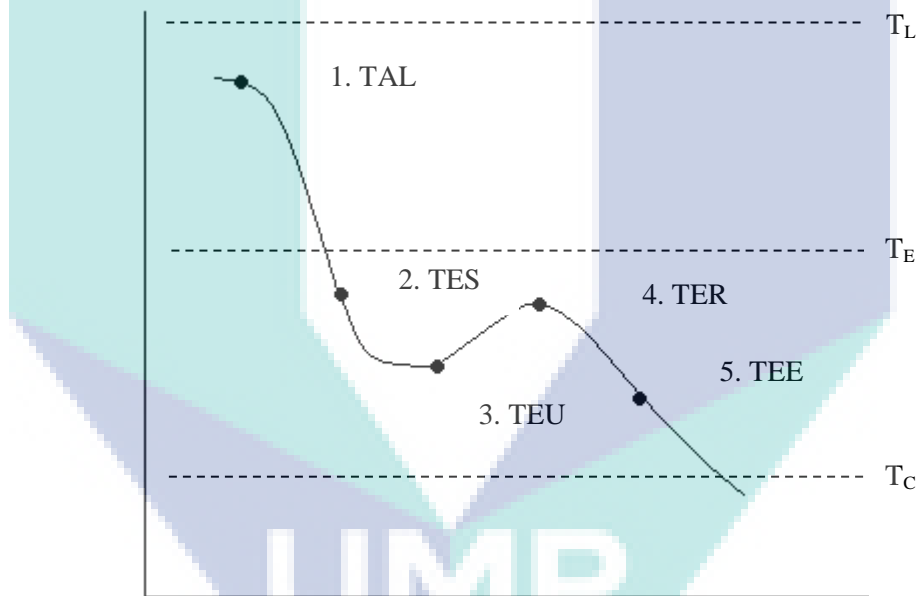
Figure 2.15   Schematic of cooling curve temperature point
Source: Elliott (1988)

Elliott (1988) proposed five important temperature points for the typical cooling curve of hypo eutectic gray cast iron as shown in Figure 2.15. The cooling curves were characterized by; T_L is the austenite liquidus temperature, T_E is the equilibrium point of graphite eutectic temperature, and T_C is the equilibrium point of carbide eutectic temperature. Point 1 as illustrated is known as the temperature of the liquidus arrest (TAL), point 2 is the temperature of eutectic nucleation (TES), and point 3 is the temperature of eutectic undercooling (TEU). While point 4 is the temperature of

eutectic recalescence (TER) and point 5 is the end of eutectic solidification (TEE). Despite that, there is a different opinion on the important temperature point which proposed only 4 temperature point TAL, TES, TEU and TER (Boeri, 1989). Mampaey (2002) express this temperature point in a more simple way as shown in Figure 2.16.
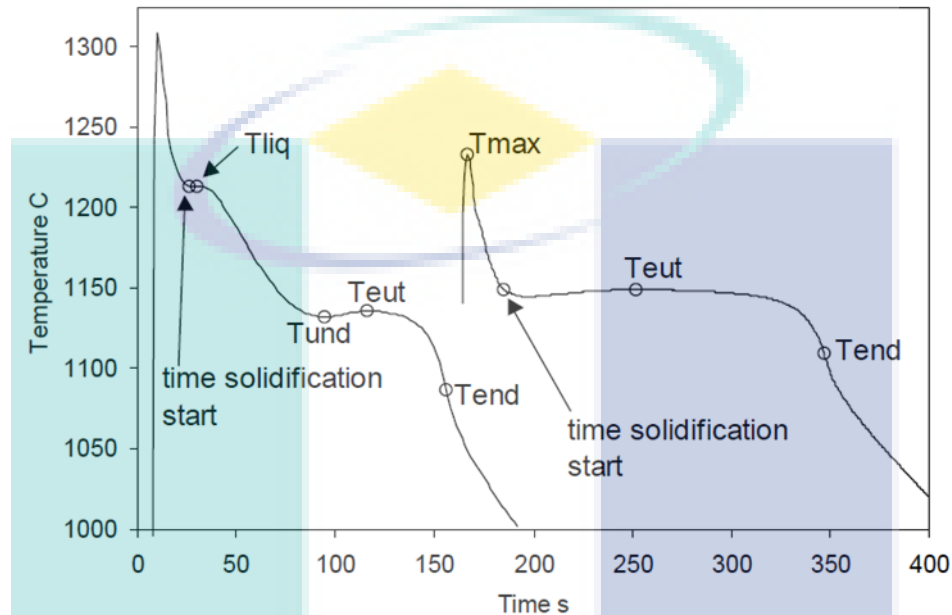
Figure 2.16   Definition of characteristic points on a solidification mode. Hypoeutectic (left) and a eutectic (right) cooling curve.

Source: M. Chisamera, Stan, Riposan, Costache, and Barstow (2008)

In recent years there are many investigations recorded using the DTA such as M. Chisamera et al. (2008) whose investigated the solidification pattern of In-Mold and Ladle Inoculated gray cast irons by various inoculant reading evaluated using solidification cooling curve and DTA. A thermocouple located inside the mold as according to DTA set up. Various cooling curve information was successfully obtained as shown in Figure 2.17. The result showed the difference between uninoculated and inoculated irons is strongly affected by the addition alloy rate, much more for ladle inoculation. In all cases, the in-mold/cup inoculation is clearly more efficient than the in ladle inoculation as represented in DTA.
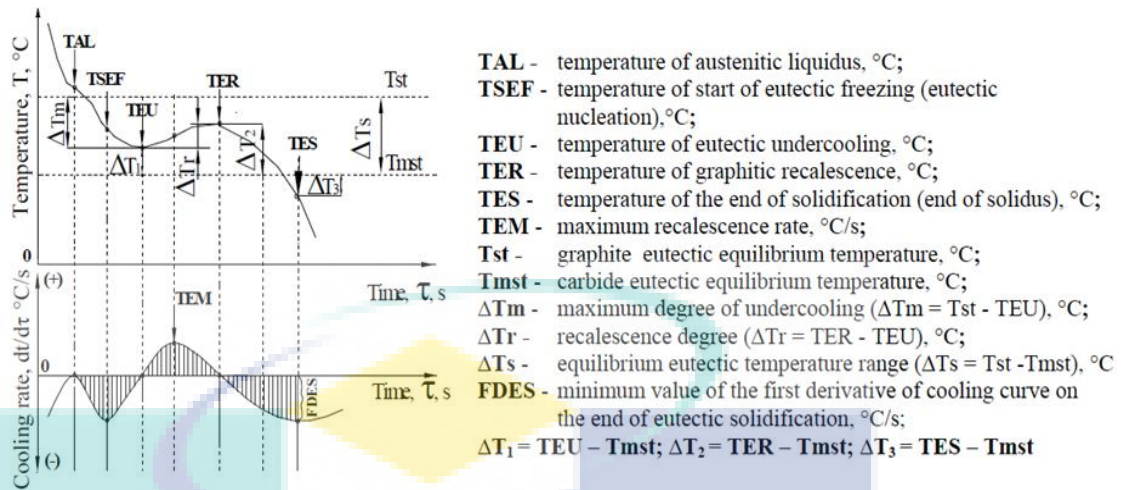
Figure 2.17   Typical cooling curve and its first derivative

Source: M. Chisamera et al. (2008)

Gagne and Labreque (2007) investigate the effect of different thickness on solidification of austenitic type D5-S where the cooling curve shows the most rapid cooling rate occurred during thinner casting and in the opposite direction during thick casting size. However, the cooling needs to be analysed thoroughly to reveal point temperature arrest. This finding was supported by Alabbasian et al. (2016) which acknowledged the effect of casting thickness affected the carbide formation and suggested using proper inoculation procedure to get the best casting result. Unfortunately, this report does not support using TA.

While Rashidi and Hasbullah (2014) reveal that by the addition of mass carbide promoter element such as manganese will encourage carbide formation. This occurrence was successfully recorded in the cooling curve by embedded thermocouple inside the mold and was analyze using DTA method. Higher Mn wt% alloyed iron has a decreased solidification cooling curve temperature. Dt/dt curve shows the point temperature arrest better than the typical cooling curve.

Knowledge of phase diagrams and phase transformations is critical in understanding the structure of metals and alloys, and controlling their solidification and subsequent modification to achieve desired properties and attributes Emadi et al. (2005). Thermal analysis and cooling curves analysis (DTA) are excellent tools to control the quality of the base and to observe the behaviour during solidification. It gives better insight during solidification (Cabanne, 2006).

2.9   Heat Treatment of Austenitic Cast Iron

When a metal is in a liquid state, it is homogeneous. That is, the metal properties (especially composition) are the same everywhere. However, during freezing, there is a redistribution of alloying elements and impurities called segregation (the concentration of solute is not constant throughout the casting). Segregation has a significant influence on casting quality. Understanding the process is useful for the casting engineer or metallurgist for decision making (Geoffrey, 2014).

According to Glicksman (2011), segregation occurs by the various elements that exists in the melt such as Mn and Cr. There is two types of segregation are microsegregation and macrosegregation. Microsegregation is the variation in composition on a minuscule scale which occurs over distances comparable to the size of the dendrite arm spacing. This occurrence as a result of the first solid formed being of a lower concentration than the final equilibrium concentration, resulting in partitioning of the excess solute into the liquid so that solid formed later has a higher concentration. The gathering of these elements led to the formation of eutectic carbide.

It is desirable to prevent segregation during casting, to give a solid billet that has uniform properties throughout. Microsegregation effects can be removed after casting by using homogenization. It can carry out by implementing annealing process at high temperatures where the diffusivity is higher. However, segregation profiles formed initially during solidification cannot be removed completely by subsequent heat treatment.

Giacopini, Boeri, and Sikora (2013) make an attempt to investigation the dissolution by annealing of carbides present in thin walled and found out that the dissolution rate was fast at both 900°C and 950°C. Dorazil (1991) stated that increasing the austenitizing temperature in the range 850°C-1000°C for 1 h leads to a slight reduction in the degree of chemical micro inhomogeneity. Jolley and Gilbert (1967) and Harding (1986) have shown that even after a long annealing cycle, the Mn content at the cell boundary could be more than twice that formed close to the nodules. However, it has been suggested that long-term austenitizing may be useful to revolutionise the as cast carbides.

In cast iron, tight control of austenitizing temperature is imperative if consistent properties are to be obtained. The austenitizing temperature has a significant effect on the hardenability and transformation behaviour at higher temperatures, the matrix carbon content increases and the austenite grain size is enlarged. This change increases hardenability and reduces the rate of reaction and thus permits larger castings to be treated or less efficient quenching baths to be used.

The austenitizing temperature should be selected to ensure sufficient carbon transfer from the graphite to the austenite matrix. The carbon solution process is both time and temperature dependent, thus high austenitizing temperatures shorten the time necessary to attain uniform carbon content in the matrix structure. However, scaling and casting distortion may result if austenitizing is carried out at higher temperatures.

Lower austenitizing temperatures may be specified for castings which are to be machined after annealing. Lowering the austenitizing temperature lowers the volume of untransformed austenite. On the other hand, a decrease in austenitizing temperature frequently results in incomplete austenitization and associated problems with the microstructure and mechanical properties.

In this study, the austenitizing temperatures investigated were 700°C, 800°C, 900 °C, and 1000 °C. It is believed that such an investigation will help to establish the optimum austenitizing temperature. Previous studies suggest that this temperature would be within the proposed range. Fallon (1993) suggest the suitable range of annealing temperature is 875°C to 900°C. However, the early investigation by Lyadskii, Mairansaev, and Teshaev (1967) try annealing the cast iron with high manganese content from 500°C to 1000°C. The result obtained from this investigation shows increasing and decreasing pattern of the graph which 800°C is the peak of the chart. At 1000°C there is a major reduction of carbide observed.

2.10   Summary

Traditionally, steel has been chosen as corrosion resistance material for application such as gas turbine components, power plant steam compressor housing and automotive gasoline power engine turbine manifold. It happens because of steel characteristic that stable at a medium high temperature up to 500°C. However, a major problem with this kind of application is numerous. Steel is comparatively expensive

material and also harder to manufacture due fluidity problem compare to iron. Another option capable and have a similar character with steel (in term of resist characteristic) is austenitic cast iron (Ni-Resist).

To date, there has been an increasing interest in austenitic cast iron due to its excellent quality in easier to cast and cheaper processing cost. Furthermore, it is advantages cannot be neglect anymore regarding the properties and also ability in operation at high temperature and the very corrosive environment. There are a considerable amount of literature has been published on austenitic cast iron. However, one of the most significant current discussions on the problematic issue still unsolved, regarding the setback due to volatile price of alloying elements such as nickel in the market. There has been little agreement on what another alternative available to reduce Ni consumption to produce competitive austenitic cast iron component (Morrison, 1998).

Based on the literature review above, there are several approaches discovered on how to reduce the drawback-effect of costly element Ni:

a. Minimize the use of nickel as a main alloying element.

b. Replacing completely Ni with another austenitic element promoter such as Mn and Cu.

c. The combination of Ni with others austenitic promoter materials (Ni and Cu).

d. Use low austenitic promoter element or partial austenitic cast iron and generate full austenitic matrix using heat treatment.

Although extensive research has been conducted on an alternative alloying element such as copper and manganese which is a potential candidate can be utilized as an austenitic promoter there is still no profound study exist on the investigation of this method on the flake graphite austenitic cast iron. By using this method probably manage to reduce the price of Ni-resist since copper and manganese is cheaper than a nickel in the market. Manganese is believed as right austenite promoter better than copper. However, the use of manganese leads to mass production of carbide as the manganese content increase as suggested by Fallon (1993). Low content manganese

favourable in hardenability of cast iron especially heat treatment and classified as free graphite. Despite, when it is in high quantity (more than 6%) it starts to produce carbide (Morrison, 1998). Manganese also demanded when it comes to producing white cast iron which able the manganese to react with another element inside the iron (Fredrickson, 2006 and Elliot, 1988). Manganese seems to be a good material as the investigated material since it has been used to produce austenitic manganese cast iron a long time ago (Lyadskii et al., 1967). It is favourable to use it together with nickel as to produce comparable Ni-resist with some countermeasure approaches.

Inoculation is reported successfully increase the properties of cast iron families included Ni-resist. Pearce (2008) stated that by using inoculation process makes the nucleating site of graphite increase and simultaneously reduce carbide formation. Earlier extensive work supported this statement by Patterson and Ammann (1959) who demonstrate the relationship of undercooling and eutectic cell count. Furthermore, the main role of inoculant is to produce nuclei in the liquid iron melt which enhance the graphite nucleation with a low degree of undercooling as stated by (ELKEM, 2012). Latest investigation evidently shows the effect of inoculation on reducing the tendency of carbide formation provide better chances for graphite to precipitate (Rashidi et al., 2013). Solidification cooling curve changed by reducing the degree of undercooling (TER-TEU temperature differences) of liquid iron during eutectic solidification results in less risk of carbide formation (Asenjo et al., 2007). However, control over the amount of inoculant used need to be optimum because excessive of inoculant (more than 1.0 wt%) mean nothing to the properties and lastly become waste. Rashidi (2014) reiterates that inoculation process manages to reduce carbide formation and able to increase properties of Ni-resist. It is because of inoculation reduces the chances of dendrite from growing hence make this size of dendrite smaller with higher inoculant wt%. The decrease in solidification temperature leads to a faster cooling rate that encourages fine dendrite. Rapid cooling produces smaller dendrite, while slow cooling results in large and course dendrite (behman et al., 2010) the phenomenon will also reduce the spacing between the dendrites and minimizes the occurrence of shrinkage as schematically shown. Hence, it is convenient to have this process in Ni-resist with high manganese content.

Segregation profiles formed initially during solidification cannot be removed completely by subsequent heat treatment. Dorazil (1991) stated that increasing the austenitizing temperature in the range 850-1000°C for 1 h leads to a slight reduction in the degree of chemical micro inhomogeneity. Jolley and Gilbert and Harding have shown that even after a lengthy annealing cycle, the Mn content at the cell boundary could be more than twice that formed close to the nodules. However, it has been suggested that long-term austenitizing may be useful to resolutionise the as cast carbides.

Therefore, the aim of this study was to produce, evaluate and validate the effect of Mn on the microstructure and mechanical properties of high manganese austenitic cast iron (Mn-Ni-resist). Particular attentions will wholly direct to the mechanical properties of the alloyed iron about the solidification and microstructural inhomogeneities in casting, dictated by the fact that Manganese elements percentage in Ni-resist are significant. Despite its exploratory nature, this study also will offer some insight of heat treatment manipulation on the enhancement of alloyed iron mechanical properties.

CHAPTER 3

METHODOLOGY

3.1 Introduction

The main objective of this study is to find out the effects of manganese addition on Ni-resist and heat treatment on the high manganese alloyed austenitic cast iron with reduced nickel concentrations as stated in Chapter 1. In this particular chapter, the research methodology used in the study is described in several purposes according to the scope of the study.

All the methodology employed was according to the conclusion from the literature in Chapter 2 to ensure the quality and credibility of this research secured.

3.2 Flow Chart

The experimental work was divided into four phases as described in the scope of the research in Section 1.6. In the first phase, the study focuses more on the preparation of the material and fabrication of pattern for casting. The second phase of the research is the metal casting process. The addition of pure nickel and ferromanganese to the melting is the main factor to produce this alloy. The parameter of manganese is 9 wt%, 10 wt%, 11wt% and 12wt% as a manipulating factor, while nickel remains 10 wt% Ni throughout the phase. Inoculation processes were carried out by adding 0.1-0.2% FeSi respectively. Cast iron produces observed its microstructure under an optical microscope. The appearance of flake graphite inside a bright white matrix is the sign of preliminary phase completed. The third phase is heat treatment process on the product of the casting. Ni-resist with higher manganese content or Mn-Ni-resist was introduced to heat treatment. The fourth phase is analysis on post process. The analysis will be conducted to determine mechanical properties, corrosion rate and microstructure of Ni-

resist. This research flow was summarized in Figure 3.1. It is can be referred to appendix A for detail information.
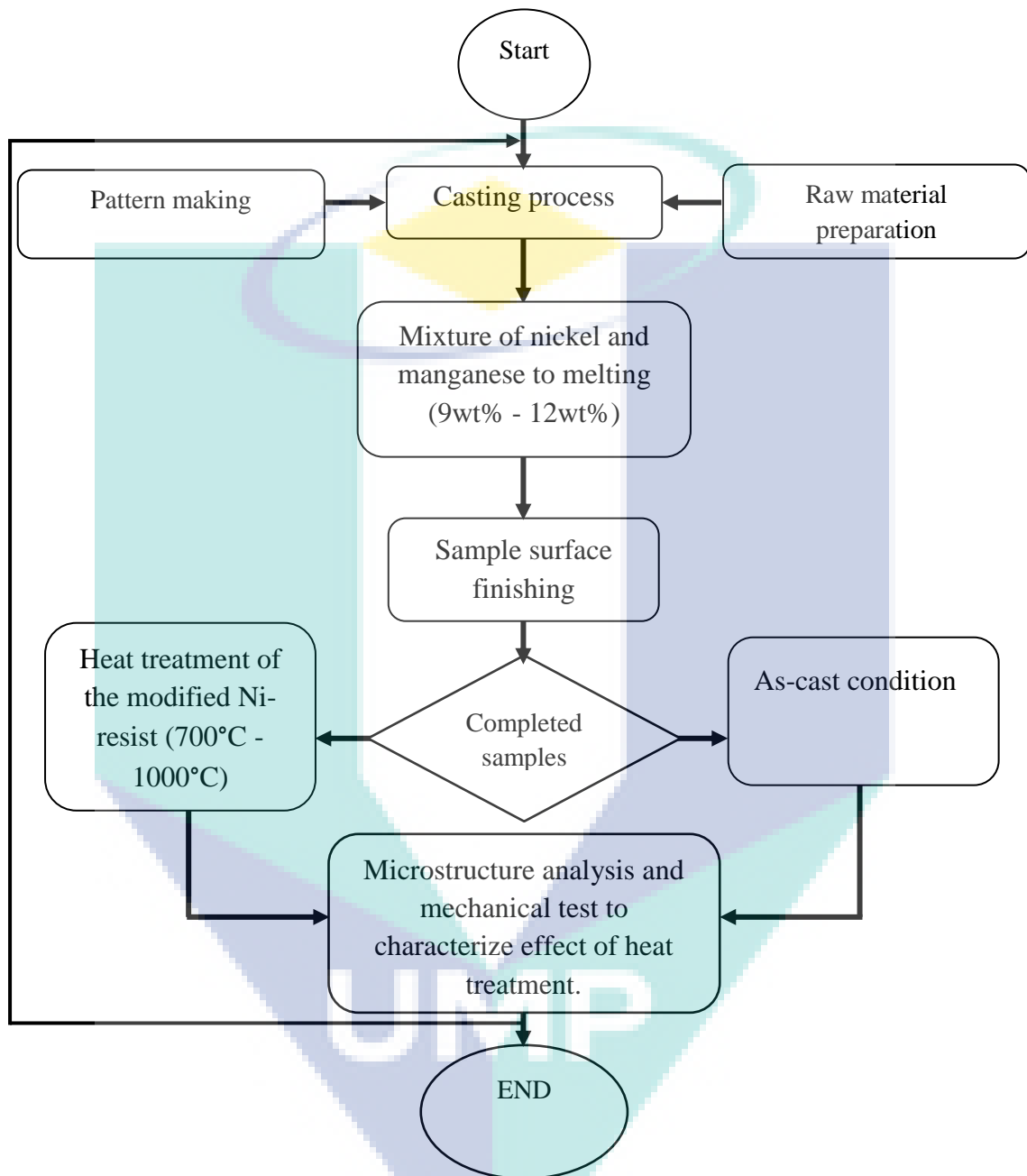
Figure 3.1   Experiment flow chart

3.3   Pattern and mould fabrication

Austenitic cast iron with controlled manganese content was produced which was followed by heat treatment process. At the beginning of the research, a pattern was

studied and fabricated according to ASTM 436 and dimensioned as in Figure 3.2. Y-block casting specification. The dimensions are in mm.

Source (ASTM A439). Pattern assembly was incorporated into the gating system and reaction chamber for In-Mould treatment as shown in Figure 3.3.
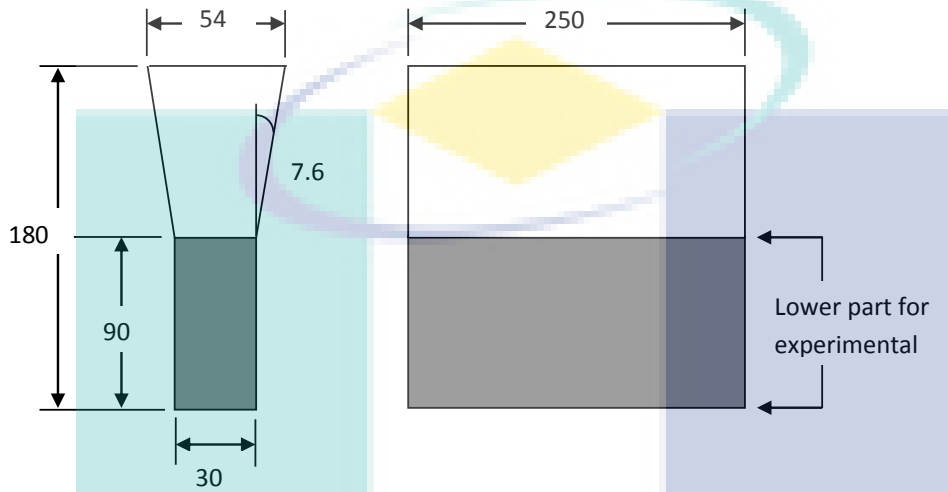
Figure 3.2   Y-block casting specification. The dimensions are in mm
Source: ASTM A439 (2001)

The mold was prepared by using green sand. The green sand was rammed, and the hardness then tested using equipment named Hardness Tester 'B' Scale for rigidity purpose. The readings of the mold were in the range of 80-90 unit of spring loaded steel ball. The material used to build the mold as listed in Table 3.1. Pattern's draft is paramount to avoid cracking during mold fabrication.

(a)   (b)
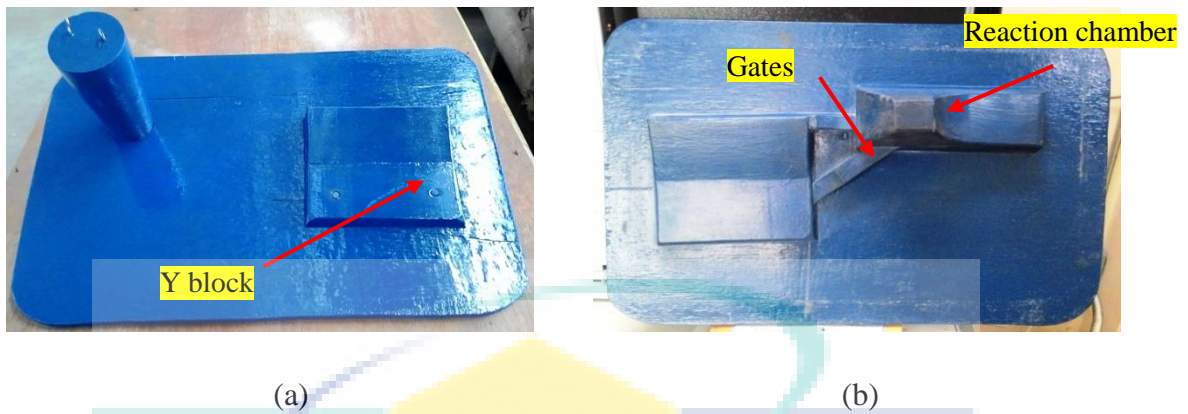
Figure 3.3   Pattern was fabricated according to ASTM standard (a) upper side of the pattern (b) below side of the pattern

When all the material homogeneously mixed, the mixture (melt) was poured into the flask as a mold structure as shown in Figure 3.4.

Figure 3.4   Casting Mould

Table 3.1   Casting mold preparation

Material content	Composition wt%	Purpose
Silica sand	95	Major molding portion
Clay - bentonite	2	Binder
moisture	3	Clay activation and plasticity

Pattern assembly was fabricated complete with gating system. Mould material used in this experiment was green sand since it has an ability to withstand high temperature and reusable. During mold making, the green sand was rammed, and hardness test was held using equipment named Hardness Tester 'B' Scale for rigidity purpose. The molten metal temperature is around 1500°C ±10 if the mold cannot withstand this high temperature then it probably affects the casting process. The reading needed in the range 80-90 unit of spring loaded steel ball.

3.4 Melting

3.4.1 Base iron preparation

There are several materials used in producing austenitic iron such as pig iron, nickel, Ferromanganese, and steel. The iron used in this study was pig iron with its majority constituent was ferum. Chemical concentration of each constituent was verified by using the spectrometer. The result listed as shown in Table 3.2 below. The test focused on the percentage of ferum, carbon, silicon, phosphorus, manganese, nickel and sulphur.

Adjustment of chemical concentrations is necessary for producing Ni-resist. Chemical such as carbon, manganese, nickel and chromium that required producing Ni-Resist affects the experimental temperature and alloying parameter. To achieve this target, the process of melting required several preliminary stages; base iron preparation/adjustment, alloying, treatment. Steel scraps were used to control the carbon in the melt.

Table 3.2   Chemical composition of Pig Iron

Composition	Composition wt%			Average
	1	2	3	
Carbon	> 4.50	> 4.50	> 4.50	> 4.50
Silicon	3.28	2.24	1.85	2.460
Manganese	0.414	0.341	0.309	0.354
phosphorus	0.134	0.194	0.180	0.170
Nickel	0.236	0.265	0.287	0.263
Chromium	0.0333	0.0282	0.0266	0.029
Iron	77.40	71.60	73.90	74.30
Sulfur	> 0.150	> 0.150	> 0.150	> 0.150

3.5 Melting and casting

3.5.1 Base iron preparation

Firstly, the pig iron was tested for chemical concentration by using the spectrometer (LECO Glow Discharge Spectrometer, GDS 850A). The result listed is shown in Table 3.2. After knowing the base metal constituent, an adjustment of carbon content takes place. All adjustment was made according to average pig iron mass;

averaging 25 kg -30 kg range. However, the smaller size of pig iron is preferred to accelerate the melting process.

To monitor the carbon content in the preferred range, the mass of steel was calculated using equation 3.1 below.

$$awt\% = \left[\frac{\left[\left(\frac{b}{100xm}\right) + \left(\frac{c}{100xn}\right)\right]}{m+n}\right] x100 \qquad 3.1$$

Where,

a   =   preferred carbon content in melt product.

b   =   carbon content in pig iron.

c   =   carbon content in steel.

m   =   mass of pig iron in kg.

n   =   mass of steel in kg.

3.5.2 Alloying

All the alloying material was placed in the induction furnace. The mixture were added according to the specimen specification such as nickel 10 % of all casting heat and manganese in 9 wt%, 10 wt%, 11 wt%, 12 wt%. The amount of nickel calculated using equation 3.2 and the amount of ferromanganese was calculated using equation 3.3. The chemical composition used for alloying element is shown in Table 3.3.

$$Twt\% Ni = \frac{t}{100\left(m+n\right)} \qquad 3.2$$

Where T is targeted mass of Nickel and t percentage of nickel in the melt.

$$X wt\% Mn = \left[\frac{\left(\frac{x}{100 (n+n)} \right)}{\frac{86}{100}} \right]$$

3.3

Where,

X   =   mass of Ferro-Manganese required.

x   =   percentage of manganese in the melt.

Table 3.3   Element constituent in raw material

Material	Elements (wt. %)										
	C	Si	Mn	P	S	Mg	Ni	Ca	Cr	R.E	Fe
Pig iron	4.5	2.46	0.354	0.170	0.150	0.310	0.263	-	-	-	balance
Steel	0.19	0.15	0.54	0.90	0.02	-	-	-	-	-	balance
Nickel	-	-	-	-	-	-	99.0	-	-	-	balance
FeMn	-	-	86.00	-	-	-	-	-	-	-	-
Inoculant	-	70.00	-	-	-	-	-	2.0	-	-	balance

However for more detail calculation of the mass of mixture can refer to Appendix B.

3.6   Inoculation

FeSi as inoculation materials was smashed using Fast Mill Machine as shown in figure Figure 3.5. It is to make sure all the inoculant uniformly in small size and easy to melt in the base metal.

<div align="center">(a)   (b)</div>

Figure 3.5   Material preparation for treatment a) Fast Mills Machine b) Material container during milling process

Ferro-silicon base was used as an inoculant. This material then was employed together with magnesium-Ferro-silicon in the reaction chamber; nodule in the microstructure was count because it affects the mechanical properties. The amount of FeSi will be calculated using Equation 3.4. Figure 3.6 shows the machined FeSi and MgFeSi in the form of mashed. Figure 3.7 illustrates the location of nodulant and inoculant located in the mold.

$$FeSi = \left(\frac{L}{100 x \ totalmeltweight} \right) \qquad 3.4$$

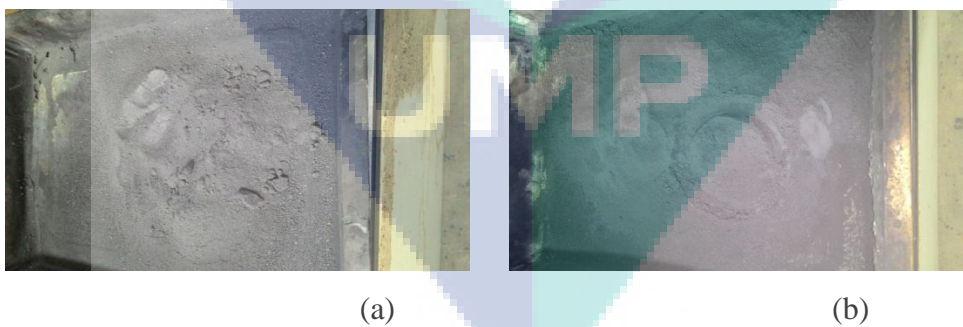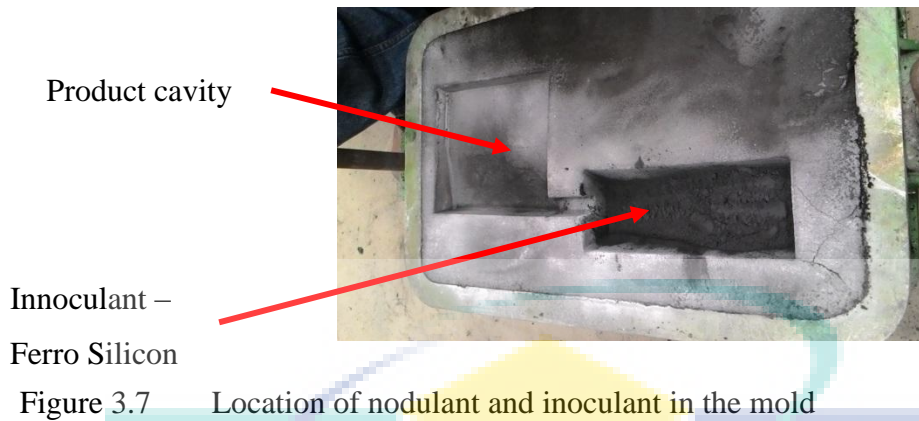Where, L   =   percentage of inoculant in the melt

<div align="center">(a)   (b)</div>

Figure 3.6   Treatment material a) Ferro silicon b) Magnesium Ferro Silicon

Product cavity

Innoculant –

Ferro Silicon

Figure 3.7　　　Location of nodulant and inoculant in the mold

3.7　Thermal analysis

Thermal analysis was used to observe the solidification behaviour and to analysis the interaction between parameter used in the investigation. Any occurrences generally can be detected by irregularity in the normal graph which normally affects the mechanical and microstructure. So to obtain the cooling rate behaviour, two thermocouples type R were placed inside "Y" block cavity inside the mold. Furthermore, the thermocouples were protected by thin walled alumina glass tube to avoid damage to the thermocouple as shown in Figure 3.8.

sprue

Cope

"Y" block cavity shape

Inoculant
Reaction
chamber

Drag

Alumina glass tube temperature tip attached
to thermocouple type R and data logger

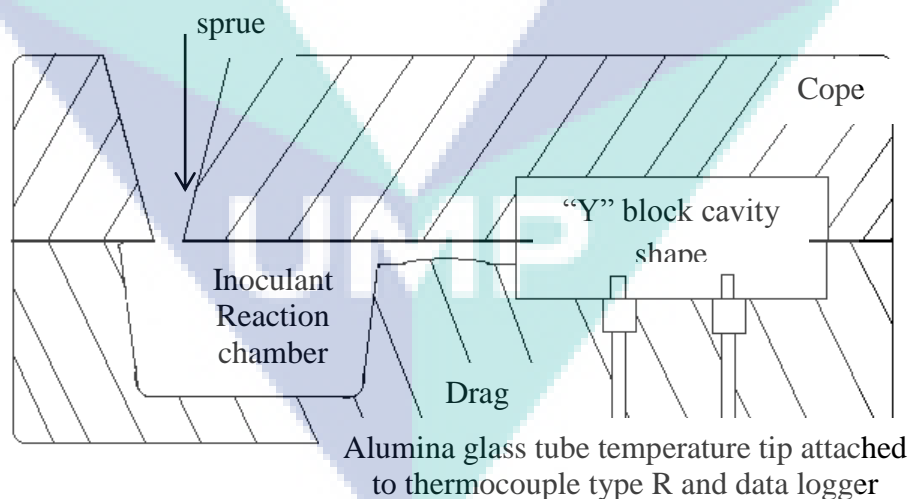Figure 3.8　　　Schematic diagram of temperature monitoring during cooling

The output of thermocouples was measured with a multichannel analog / digital data logger then was uploading to the computer for further analysis. The differential data was analysed to enable the solidification behaviour to be interpreted. Later, the exact position of temperature point of thermal arrest can be determined. The accuracy

of the temperature measurement was -50°C – 1480°C ± 1.5°C. Cooling curves profile at difference stages was obtained in real –time during solidification.

3.8   Heat treatment process

The heat treatment schedule which was outlined in Figure 3.9 was carried out as post process stages. All dog bone samples then were placed in a box-type resistance furnace heated according to its austenitizing temperature at 927°C ±10 and were hold. The holding time was 3 hours and began when it reached the desired temperature. Austenitizing time less than 2 hours was not selected because the complete transformation of the as-cast structure into austenite required at least 2 hours (Putatunda, 2003). The annealing process was held at 700 °C, 800 °C, 900 °C and 1000 °C for 3.0 h. Then the samples cooled down to room temperature by furnace cooling technique respectively. For the purpose of analysis, as shown in Table 4.4, every heat treatment process was named according to its annealing temperature and heat treatment condition.

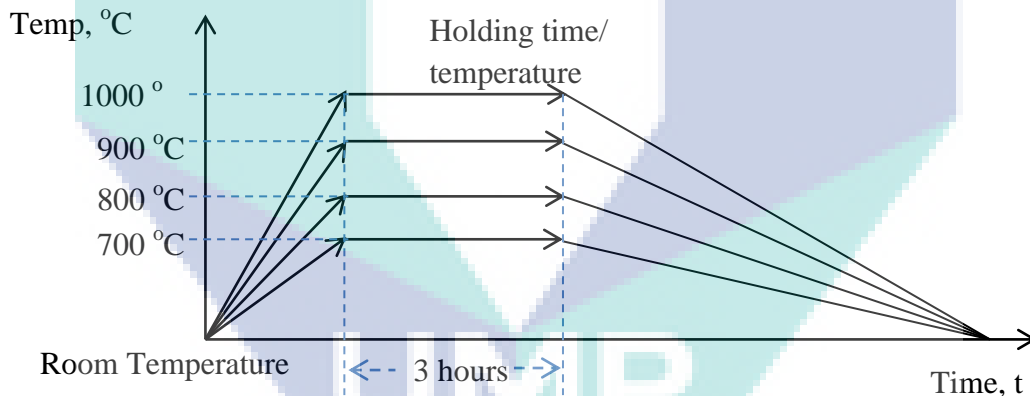Figure 3.9   Heat treatment operation flow

Due to slight oxidation of the surface of cast iron, there is the possibility of scale formation on sample's surface. Moreover, the specimen also tends to not gripped properly in the tensile machine. This problem affects the tensile reading. So, to overcome this specimen were polished to remove the scales from the surface to avoid these difficulties.

3.9   Spectrometer analysis

A spectrometer is an instrument used to measure properties of light over a specific portion of the electromagnetic spectrum, typically used in spectroscopic analysis to identify materials. The variable measured is most often the light's intensity but could also, for instance, be the polarization state. The independent variable is usually the wavelength of the light or a unit directly proportional to the photon energy, such as wavenumber or electron volts, which has a reciprocal relationship to wavelength. A spectrometer is used in spectroscopy for producing spectral lines and measuring their wavelengths and intensities.

The raw material was verified using spectrometer analysis as the data obtained in Table 3.2 and Table 3.3.

3.10   Microstructure analysis

The samples are taken from the edge of the casting product. It was then cut in the form of the square shape of 1.5 cm and be grounded by 240, 320, 600 and 1200 grit abrasive paper respectively. After that, the samples was polished and finally etched. The etchant used in the etching process is nital 4%. It is the most commons etchant used for cast iron. Then the samples were observed under the optical microscope between 5X to 50X magnifications (model OLYMPUS BX60F5). The sample also observed using SEM micrograph capability (model PHILIPS XL40).

Several samples were deeply etched to reveal the iron structure for measurement of primary and secondary dendrite arm spacing. The sample was immersed for 30 to 90 min in 50 wt. % aq. Hydrochloric acid. Every 15 to 20 min., the sample was washed with distilled water, quickly etched in hydrofluoric acid and washed with tap water. Then, the samples were immersed in 5 wt. % aq. NaOH for 10 to 20 min., washed with distilled water in an ultrasonic washer, followed by ethanol, and dried with blowing hot air. The dendritic elements were analysed by SEM EDX.

3.11   Mechanical testing

3.11.1 Hardness test

Hardness test was conducted in two conditions macro hardness test and microhardness test. After heat treatment process a piece of metal was cut from the specimen for hardness test. Hardness test was conducted by using Vickers hardness machine with 125 Kgf loads and for the duration of 15s, while micro hardness was performed by Shimadzu Micro Hardness Tester. The Shimadzu Hardness Testers were attached to optical microscope for measurement purpose.

3.11.2 Tensile test

The tensile test was carried out according to the ASTM E8/E8M (2001) standard. Specimens of dog bone shape shown in Figure 3.10 were prepared for the tensile test, which was machined to 9 mm gauge diameter and 45 mm gauge length after heat treatment process using CNC lathe machine. The test was conducted at room temperature.

Universal testing machine Instron 1195 was connected to a computer to illustrate the stress–strain curves and recording the tensile strength, 0.2 proof stress, and elongation. The test was performed at room temperature (298K). The tensile load of 50 KN was applied to the specimen up to the breaking point.
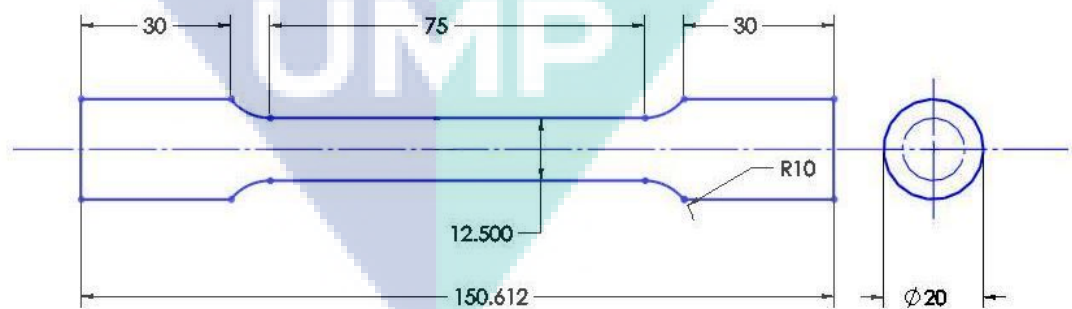
Figure 3.10   Tensile test specimen (measurement in mm)

3.11.3 X-Ray Diffraction (XRD)

Sample preparation for XRD investigation is the same sample for microstructure analysis. The sample was prepared according to ASTM A436 (2001). The sample was obtained from dog bone sample. Philip-PW 1710 XRD was used to identify the phase of the microstructure and was set at 40 kV and 40 mA with copper K-alpha as anode material. Scanning with a step size of 0.02^o per minute was employed commencing from 10° to 90°. Peaks in each of the spectra were identified using Expert High Score software.
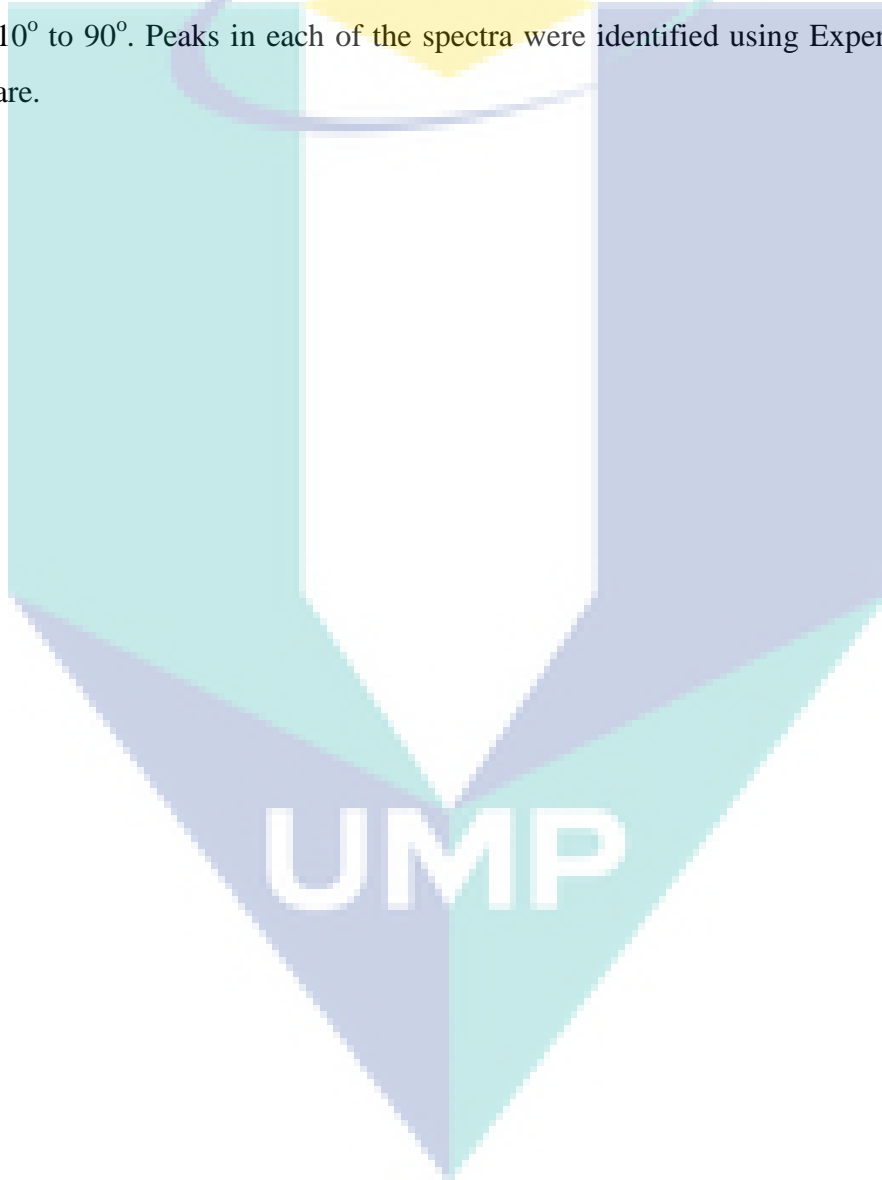
CHAPTER 4

RESULTS AND DISCUSSION

This chapter discusses the results obtained from the experiments conducted in Chapter 3. It comprises of several sections as follows: Section 4.1 describes the results of the as-cast condition experiment to investigate the behaviour of additional alloy without the heat treatment of the desired cast iron. Section 4.2 was describing the influence of annealing parameter on austenitic cast iron with high manganese content.

4.1   As-cast Experiment of Mn Ni-resist

4.1.1   Mechanical properties

The result of tensile test and hardness test conducted on the high manganese austenitic cast iron with reduced nickel content (9wt% Mn to 12wt% Mn) are presented in Table 4.1. wt%. Through this study, the minimum Ni was set at 10wt. %. Every batch of sample namely according to their manganese content added 9 wt% Mn as AI-9, 10 wt% Mn as AI-10, 11 wt% Mn as AI-11, 12 wt% Mn as AI-12. Tensile strength in Table 4.1 concludes that this material is a relatively low strength with lowest reading 56.07 MPa for AI-12 and highest readings 60.1 MPa for AI-9 as recorded. As the comparison to austenitic standard gray cast iron in ASTM A436, the lowest tensile strength in the austenitic gray cast is type 5 with 138 MPa and the highest is type 1b with 207 MPa. The different value of tensile strength is probably due to several factors such as alloy composition and defect. However, the difference in alloy composition effect on the mechanical properties was severe.

Table 4.1   Tensile properties of as-cast high manganese austenitic cast iron

Sample name	Material (Mn%)	Tensile strength (MPa)	Elongation	Macro - Hardness (HV)
AI-9	9	60.10	1.04	102.53
AI-10	10	59.20	1.04	103.00
AI-11	11	57.01	1.04	104.00
AI-12	12	56.07	1.04	106.00

The graph in Table 4.1 shows a clearl decreasing graph pattern for tensile reading and shows increasing pattern of the hardness of investigated iron as the manganese content increases. This investigated macro hardness sample readings recorded are higher than the hardness for austenitic gray cast iron type 5 with 99 HB. With the hardness increased, the tensile strength will also severely affect. It is evident that tensile decrease and hardness increase appreciably with rising in manganese content from 9 wt%Mn to 12 wt%Mn.

It is in agreement with the trend reported earlier work by Rashidi (2014) which evidently show the decreasing trend of mechanical properties and increasing pattern of hardness reading when the manganese increase from 1 wt% to 12 wt%. However, the material used in the report was based on spheroidal and not flake graphite shape. The increased in the mechanical properties was due to the of nodule graphite, which acts like crack arrester in the iron matrix when force is applied. In contradicting, flake graphite acts like crack initiator in the iron matrix. Therefore, the iron with flake graphite drastically reduced the tensile strength of the iron.
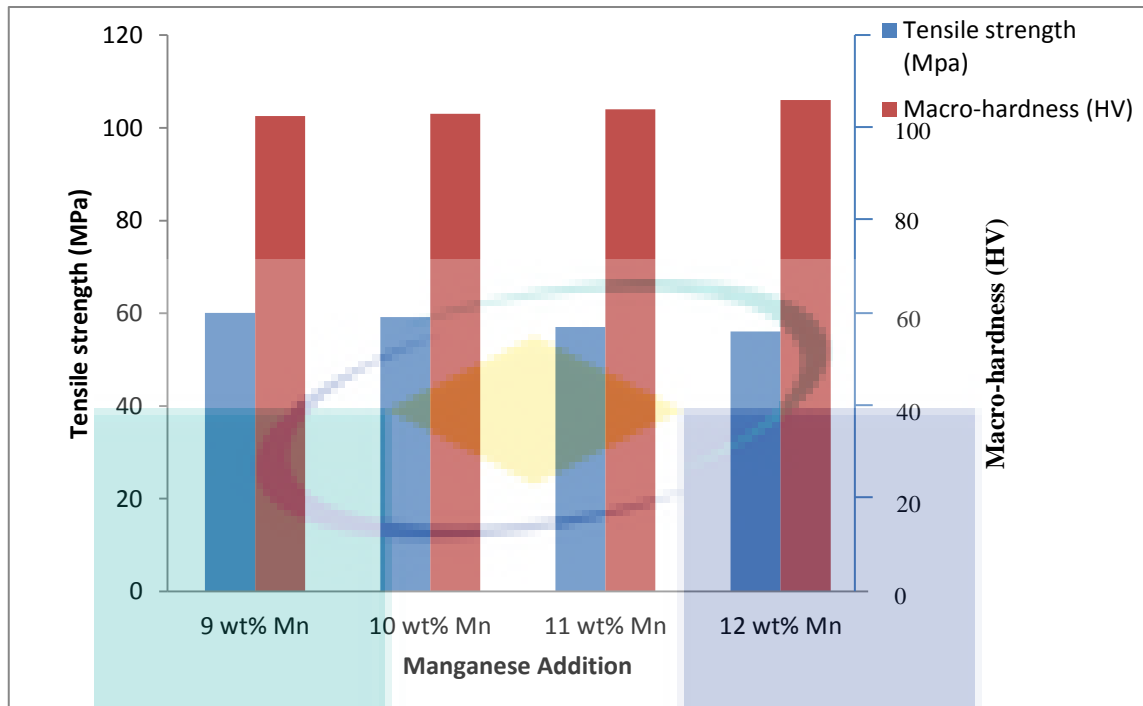
Figure 4.1   Tensile strength and macro-hardness graph

This occurrence believed due to carbide formation during solidification of the material and its effect its properties. Carbide-forming element such as manganese is well known for its austenite promoter ability. However, promote carbide severely at boundary cell, was used in a higher concentration in this investigation. Carbide formation was detected within the microstructure.

4.1.2   Microstructure properties

Every batch of samples shows same microstructure morphology with flake graphite, carbide segregation, and austenite region. Figure 4.2 shows microstructure images based on SEM micrograph with respective magnification. An austenitic microstructure for sample AI-9 solidified with predominantly single bright matrix, and the graphite precipitated predominately in the form of flake graphite. The flake graphite shape is known as type VII or specifically characterized as type B (rosette pattern) of flake graphite as according to ASTM A247 (2001). Dark flake graphite distributed and embedded throughout in the austenite matrix.

While, higher nickel content concentration has produced austenitic matrix. Together with Fe element and dominates the structure of as-cast sample as reported in

the literature (Fatahalla et al., 2009). Austenitic irons must contain sufficient amount of nickel and manganese to promote austenitic characteristic. Even though the combination of higher manganese wt% and less nickel wt% (samples AI-9, AI-10, AI-11, and AI-12) was done, the austenite matrix still stabilized. There are no formations of martensite or pearlite located as the sign of sufficient of austenitic matrix promoter as points out by Janus and Kurzawa (2013).

It also appears that those combinations encourage carbide formation as reported previously (Cox, 1988; Forrest, 1983; Rashidi et al., 2013). It happened because of segregation effect during solidification segregation of element affected Ni-Mn-iron to segregate from each other. The element that attached with an iron will develop as a grain. However, an element that prone to segregation (manganese) tends to segregate away from grain centre. This element accumulates at the edge of the grain and solidifies last. Relatively compare to element solidified in grain structure. This element tends to combine with each other and solidified as carbide as referring to Figure 4.2 and Figure 4.3.
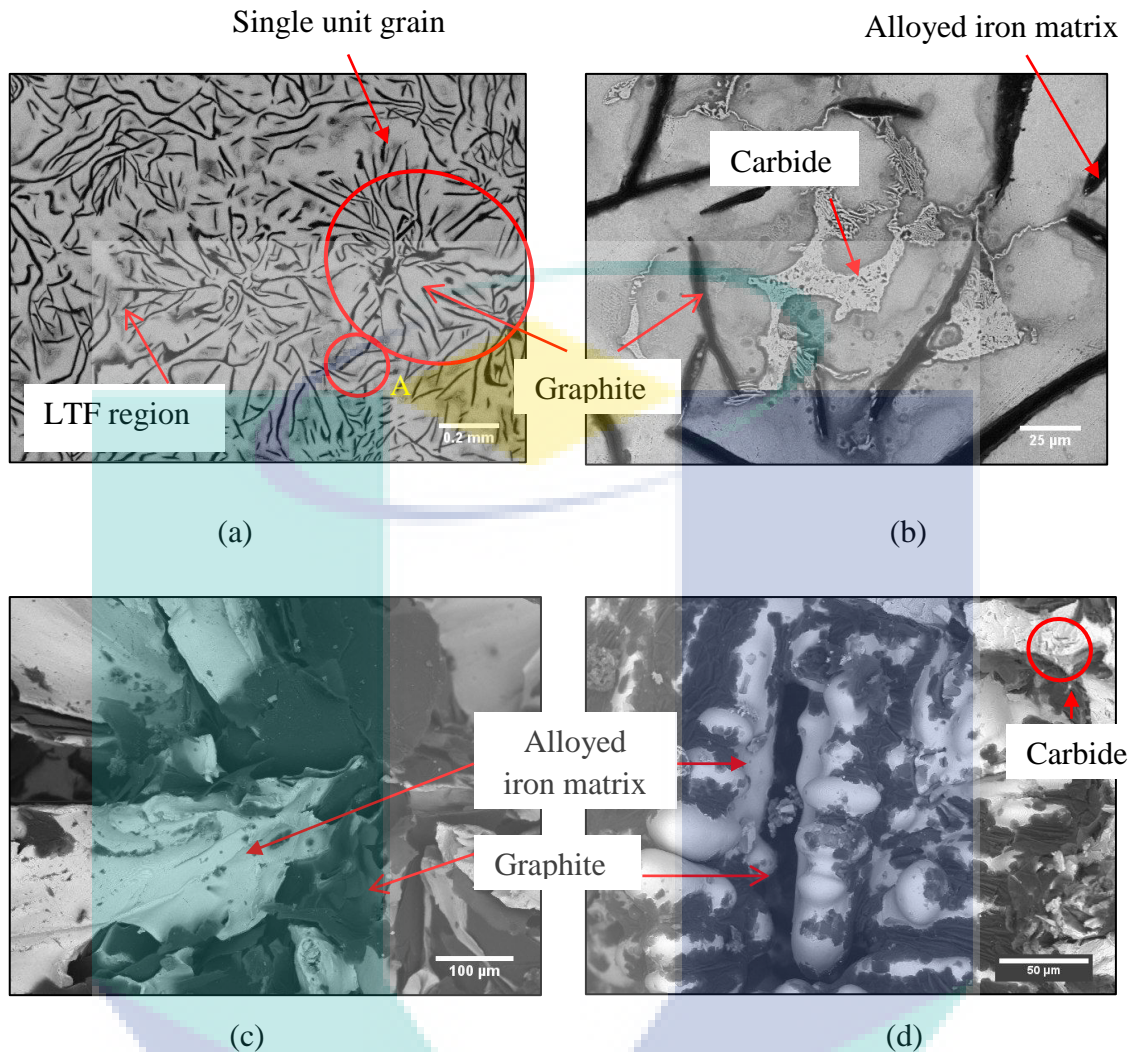
Figure 4.2   Pre-post process microstructure of AI-9 sample (a) microstructure with 100X magnification (b) carbide with 250X magnification (c) fracture morphology with 300X magnification (d) austenite morphology (deep etch) with 600X magnification.

There are several places spotted with a presence of graphite which was darker than others in Figure 4.2(a). According to Aptekar' and Abramenko (1977), this darker region happened to be the dendritic branches accumulated with Ni and Si. Earlier research supported this finding by Szpunar (1968) which claims that this phenomenon is due to the enrichment of elements segregation of axial dendrites because of a preferred solution of another alloying element in this region during etching with an acid solution. On the other hand, Stagno and Pinasco (1970) stated that this area is darker because of impoverishment in chromium as a result of its direct segregation (Aptekar' & Abramenko, 1977). However, the segregation element depends on the alloying used during the melting process.

Carbide formation in Figure 4.2(a) is difficult to be distinguished. However, when the microstructure analyses thoroughly, there are contrast colours in austenite region. The darker region (LTF region) was where the carbide formation laying located and as to make easy view the carbide area was enlarged in Figure 4.2(b). Figure 4.2(b) was previously located at circled area An in Figure 4.2(a). In this Mn-Ni-cast iron carbide, the formation was detected at area inter flake graphite region where located at grain boundary or frame of graphite group. The location of carbide previously expected presence in grain boundary as claimed by Jiyang (2009b). This fact also was supported by Figure 4.2(a) event though the carbide scarcely to be pointed out because of the dark area. As for carbide formation, this occurrence indicates segregated carbide suppress the existences of free graphite as concludes by latest investigation (Rashidi & Hasbullah, 2014).

The formations of the carbide at this region believed to push the graphite aside. It is believed to make the length of graphite increased. During the solidification of iron melt, manganese was pushed away from the solid phase (graphite) which is the first nucleate and solidifies. Manganese becomes the last element solidifies after the nucleation of graphite and austenite. Manganese has been grouping away from the graphite and lastly precipitated as Mn carbide which as shown in Figure 4.3 (b). They were segregated at the alloyed iron grain boundary and identified as the last to freeze (LTF) region.

Needle-shaped crystals with branching were formed implication from cast iron melts solidify also known as dendrite (Hoskin, 1962) can be observed in Figure 4.2 (d). Carbide formation is seen at inter-dendritic morphology and is detected at the frame of the rosette flake graphite in many places as pointed by arrows in circle Figure 4.2 (a). It asserts the fact that carbide only exists and situated at inter-dendritic, sees Figure 4.2(d) in the red circle.
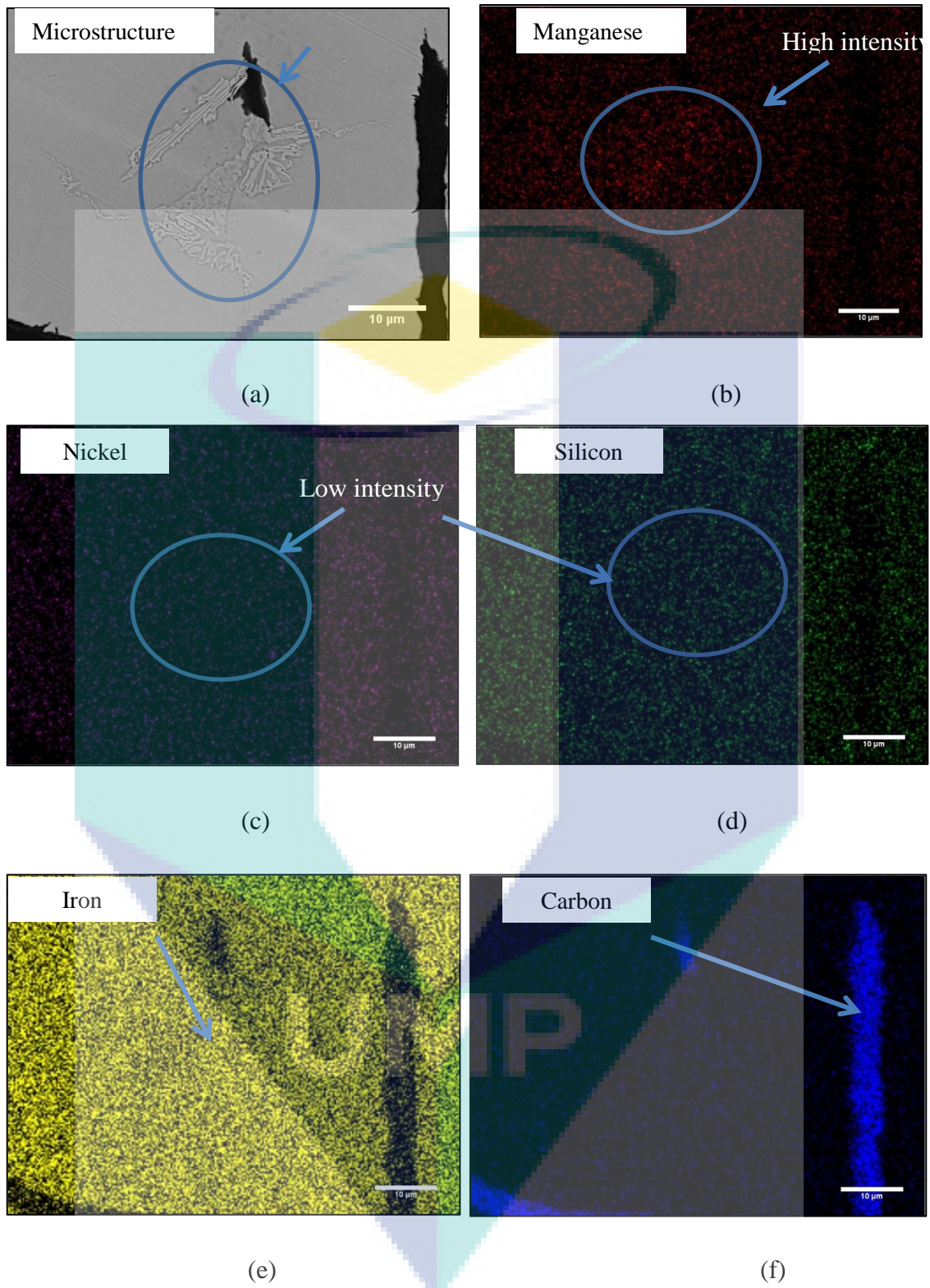
Figure 4.3   Elements mapping showing micro-segregation behavior of the Mn-Ni-resist

The investigation related to element distributions towards carbide formation then was conducted using SEM-EDS as shown in Figure 4.3. This analysis indicates the segregation mechanism activated by a large sum of Mn wt% addition probably influenced the existence of carbide instead of graphite. As the Figure 4.3 (b) shows the distribution of manganese at the centre region of the microstructure is clear which points out the high intensity of manganese. This high intensity of manganese locates exactly at where the accumulative of carbide observed as shown in Figure 4.3 (a). An implication of this is the possibility that the accumulative of manganese tend to react and combine with Carbon to form carbide ($Mn_{23}C_6$) through strong chemical bond since carbon also lightly detected presence at that location as shown in Figure 4.3 (f). On the other hand, Nickel and silicon seem distributed in the trend where low at the centre region. While carbon located accumulated at graphite area and iron highly distribute in the area other than carbon area.

These finding also suggest that higher addition of Mn wt% increase chance of Mn to pull itself to the last region to solidify due to its positive segregation behaviour in the alloyed iron (Henderieckx, 2008). Mn pulls graphite around and encourages both elements to solidify away from the dendritic structure. Later, Mn that acts as carbide forming elements combines with carbon through chemical bonding causing carbon has less chance to precipitate.

4.1.3 Microhardness Test

Micro hardness test confirmed that Ni-resist with the addition of manganese as investigated samples produced carbide at the location of accumulative of manganese. Figure 4.5 shows the 5 indenters position for the microhardness test along with differences of microhardness value in the same place where the manganese segregated. The existence of carbide confirmed spotted in that area and happened same for all of the sampling explained the greater differences in the microhardness value discovered. The hardness reading was obtained through a straight line across the region between flake graphite.

Carbide that is believed to be found at last to freeze (LTF) region, has the highest microhardness value, averaging at 400HB and above as illustrate in Figure 4.5. Micro-hardness of carbidic region between graphite.

Figure 4.4 were located at point C. It is apparently shown that point B and D have less reading than point C with reading 197.97 HV and 235.36 HV nearly half-point C hardness reading while point A and E have the lowest reading among all reading point with reading 81.77 HV and 68.94 HV. It is shows increasing trend data from point A achieved until it arrived at point C then the decreasing trend of data occurred until point E as shown in Figure 4.5. Micro-hardness of carbidic region is between graphite. Hardness value at this region reiterates that this region is where the Mn carbide segregates.

point	hardness
A	81.77
B	197.97
C	403.94
D	235.36
E	68.94

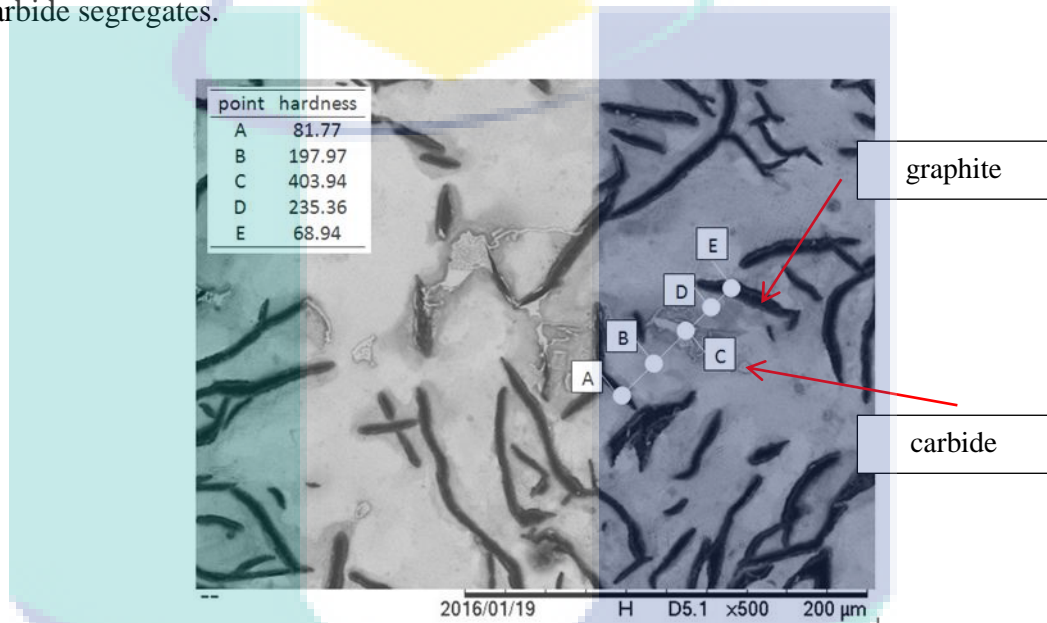2016/01/19   H   D5.1   x500   200 µm

Figure 4.4   Microhardness values in the microstructure.

The behaviour or trend of the microhardness value is due to positive segregation factors such as manganese accumulated more at the outer rim of flake graphite as describe by Jagmohan Datt (2013). Excess manganese tends to form strong bonding with carbon to precipitate as carbide. It was proved by the highest quantitative value of microhardness value in this region. It developed into a complete altered phase compared to the austenitic structure around the dendritic area.

The low microhardness at the area between carbide area and graphite (point B and D) is contributed by the accumulation of negative segregation factors such as nickel and silicon which developed the austenitic structure when alloyed with Fe. Area B and D is whitish area indicates the formation of the austenitic matrix. This element is not known as carbide promoter. However, manganese already well known as carbide promoter and believed segregated at point C then precipitate as Mn carbide (Cox,

1988). The microhardness value for this region was reduced by approximately 50% compared to the carbide region. This is due to the existence of austenite matrix which not as hard as carbide.
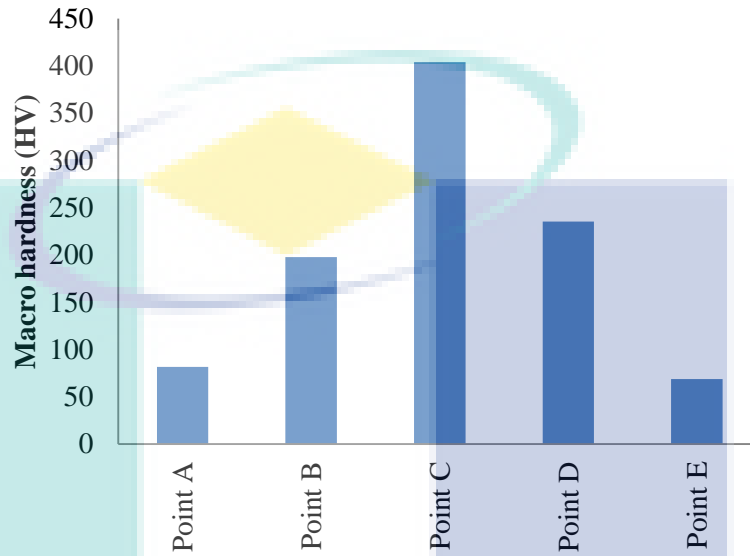

Figure 4.5   Micro-hardness of carbidic region between graphite.

4.1.4   SEM Analysis

The concentration of the elements is unevenly distributed in the microstructure. This phenomenon was known as microsegregation. The investigation related to different elements segregation towards elements distribution was conducted using SEM and EDS for AI-9 sample. The result emphasizes the micro hardness reading. Samples of different Mn percentages like AI-10, AI-11 and AI-12 also show a similar pattern of an uneven element distribution. Based on the previous investigation indicates that the segregation of manganese carbide located at the edge of a single unit of the eutectic cell. The measurement was taken after identification of some region at the edge of the eutectic cell consists of dendritic structure, expected carbide and flake graphite was selected as a center of point location. While LTF point location was identified from one flake graphite to another. Figure 4.6 was obtained at the boundary grain of flake graphite which shows the location of the probe for EDX analysis as referred to Figure 4.2 (a). Electron probe was positioned at different location namely: A – graphite, B – austenite, C – carbide, D – carbide boundary, E – austenite, and F – flake graphite.

While Figure 4.7 and Table 4.2 show the element distribution after examination as according to probe location.
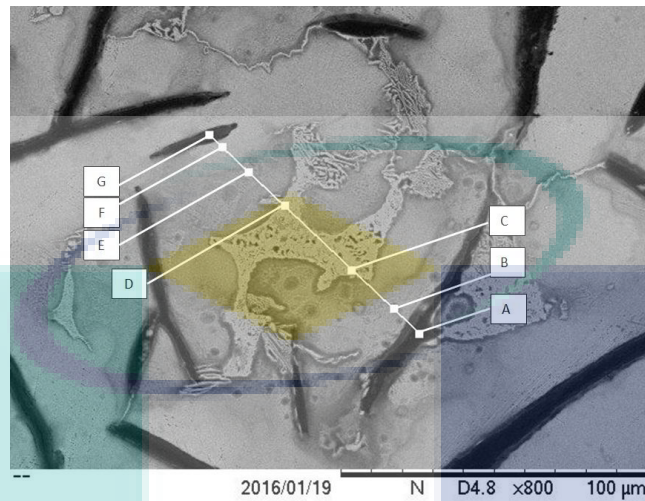

Figure 4.6   The microstructure of high manganese austenitic cast iron with carbide presence.

Figure 4.8 makes clear the trend of the element distribution at Inter graphite area. Nickel reading shows two increasing pattern, and peak reading at point B and E. Silicon also shows same graph pattern as nickel. This pattern indicates that nickel and silicon is positively accumulated at a region between carbide and graphite. However, at accumulated carbide region, nickel and silicon show negative segregation reading with 3.629 wt % Ni and 0.034 wt % Si contrast to manganese where demonstrate peak is reading as 18.007 wt % Mn. As expectedly, manganese reading at the area between accumulative carbide and graphite considerately low as showed at point B and F. When manganese is too much enriched at the area between graphite, thus expectedly leading to the formation of carbide ($Mn_{23}C_6$) as also is proposed by Rashidi and M. Hasbullah (2013) and claims earlier by Fallon (1993) and Morrison (1998).

Table 4.2   Element constituent in the microstructure

Elements	Electron probe location						
	A	B	C	D	E	F	G
Nickel (Ni)	5.094	6.466	3.269	6.594	7.287	3.470	0.231
Manganese (Mn)	2.728	6.616	18.007	12.585	6.138	6.016	0.428
Silicon (Si)	0.762	1.834	0.034	0.752	1.224	0.863	0.772

This quantitative result makes clear the claims before when the tensile reading decrease and hardness reading increase at the accumulated carbide region. It is also supported by element mapping result which reveals the high intensity of manganese at the centre area of microstructure exactly same position of accumulated carbide in SEM microstructure. Microhardness finding also was in agreement with the other test and analysis. Manganese carbide can be very detrimental to the machining process and significantly reduce tool life. It is recommended from prior research that the use of manganese be reduced as much as possible. However, in this investigation, it cannot be avoided since manganese presence in high level as an austenitic promoter.
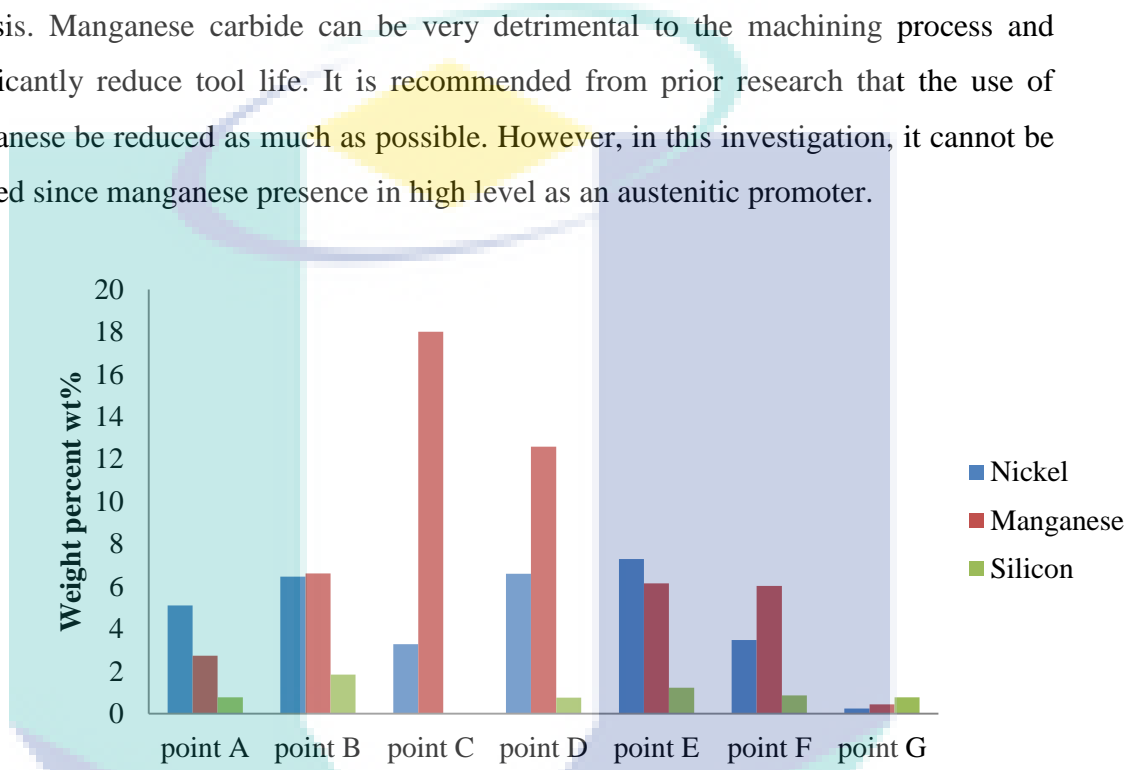

Figure 4.7   Element distribution at carbide formation

Figure 4.8 and Figure 4.9 shows microstructure of flake graphite probe location for EDX analysis. These data shows nickel reading at point D is higher than manganese because of positive segregation of nickel. This occurrence happened because manganese has been segregating at the centre area of between graphite. There are the only little amount of manganese that located at point B and Point C is where the lowest reading of manganese and nickel because this graphite area where precipitated from carbon.
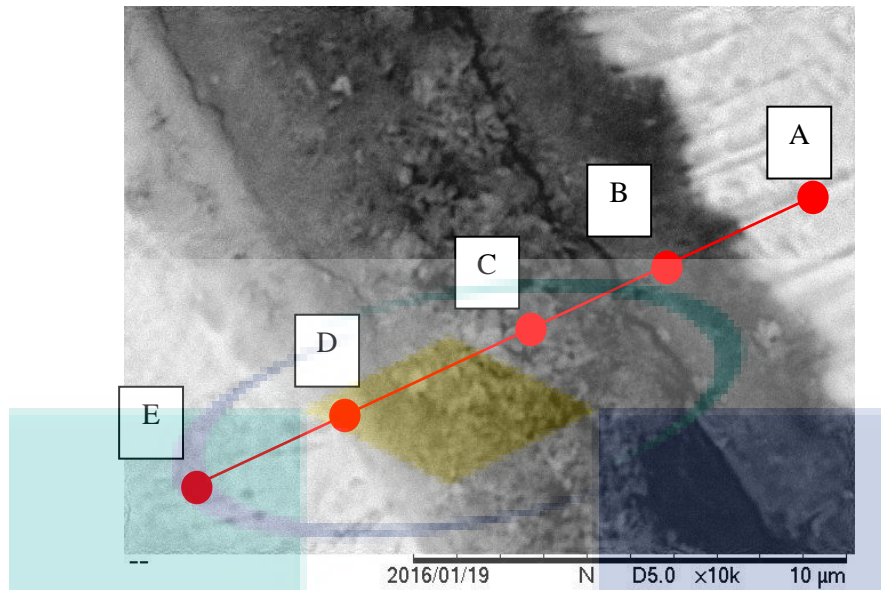
Figure 4.8   Point location to examine element distribution approximate to flake graphite structure.
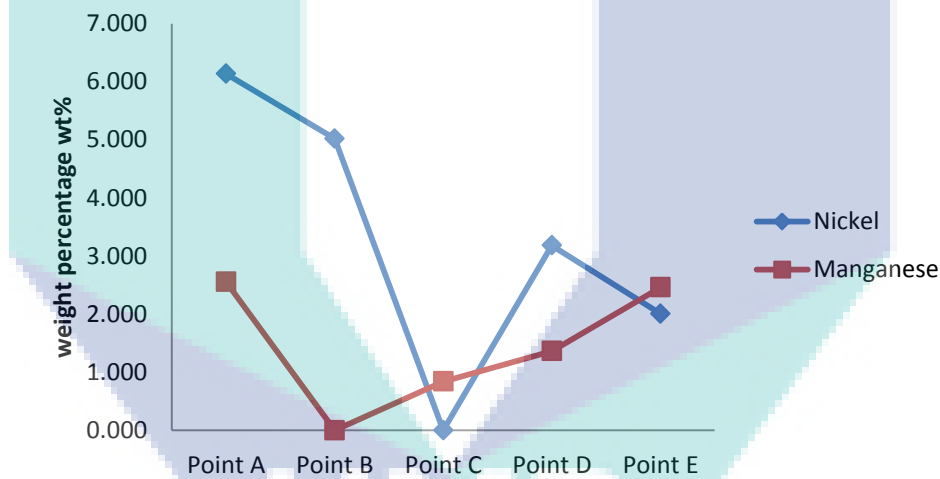

Figure 4.9   Element distribution at flake graphite

4.1.5   XRD Analysis

XRD analyses reveal the phases occurred in cast alloyed iron as shown in Figure 4.10. The analysis revealed that austenite dominates the structure of the cast sample. Beside the presence of austenitic matrix structure phase, there is also the mixed composition of carbide phase, $Mn_{23}C_6$. This reading is in line with SEM micrograph investigated which reveals the existence of carbide at LTF region alongside austenitic iron matrix. The alloyed iron solidified as austenitic structure during solidification

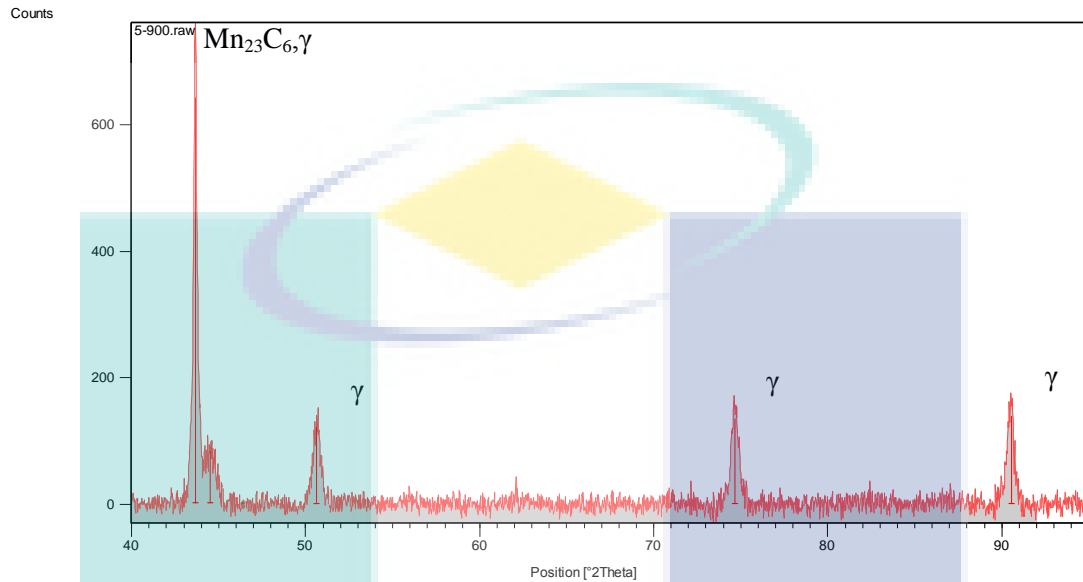together with carbide phase. There is four peaks index, as γ-Fe possessed a Face-Centered Cubic (FCC) structure.

Figure 4.10   Typical effect of manganese on AI-9 XRD phase pattern.

4.1.6   Relationship of thermal analysis, mechanical properties, and microstructure

The best way to describe solidification of cast iron is through an analysis and discussion of the thermal cooling curve (CC). It can provide a complete insight into the dynamics changes occurring during the solidification process by observing their mark on the shape of the graph. In this investigation cooling curve recorded that the eutectic temperature decreased with increasing Mn addition. This phenomenon affects the temperature range between Temperature of Eutectic Recalescence (TER) and Temperature of Eutectic Undercooling (TEU), TER–TEU, of the overall solidification. Furthermore, the changes in TER–TEU live mark on the dendrite arm spacing (DAS) and secondary dendrite arm spacing (SDAS). Once these occurrences happened then is strongly affected the mechanical properties.

The solidification cooling curves in Figure 4.11 and Figure 4.12 show that sample AI-9, AI-10, AI-11, and AI-12 have a similar curve as typical cast iron (Elliot,

1988, Sparkman, 1994 and Mampaey, 2002). Interestingly, this thermal analysis-cooling curve conducted shows that samples with high manganese content produce lower eutectic cooling curve compared to lower manganese content. This correlation is related to the effect of Mn on the eutectic temperature of the alloyed iron metastable system. Increasing Mn addition gradually lowered the solidification temperature (Jiyang, 2009a). This phenomenon may be explained by the fact that Mn expands the eutectic solidifying region away from the eutectic point of carbon equivalent (CE) 4.33. Fast cooling due to the presence of Mn potentially forces initial eutectic temperature to decrease (Henderieckx, 2008).

The implication from this occurrence increases the chances of carbide formation and prevents the existence of free graphite. Lower solidification temperature enables the formation of carbide instead of graphite as indicated in Figure 4.12 since carbide is thermodynamically stable at a lower temperature compared to graphite. Thus, the transformation of alloyed iron in cooling austenite resulted in a significant amount of carbide structure. Hence, it could affect the overall tensile strength of alloyed iron.
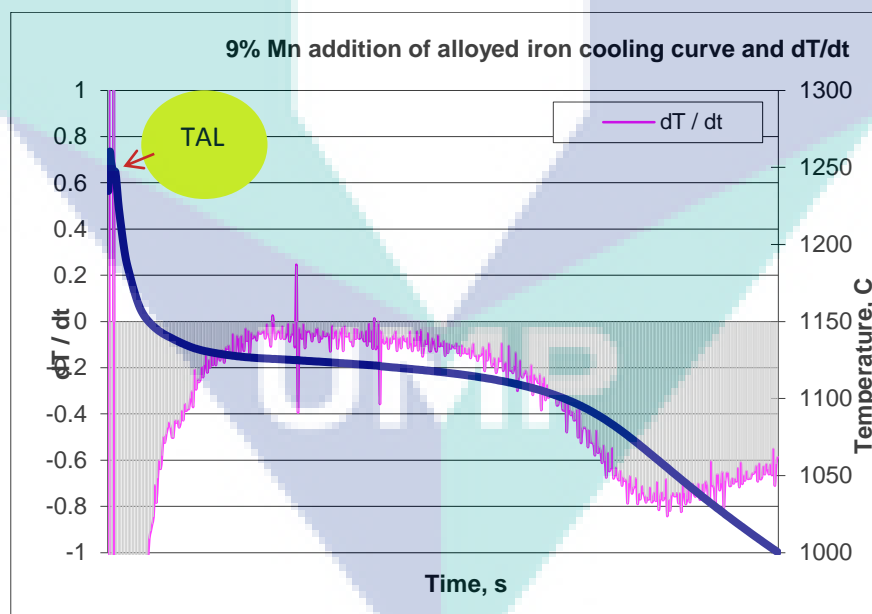

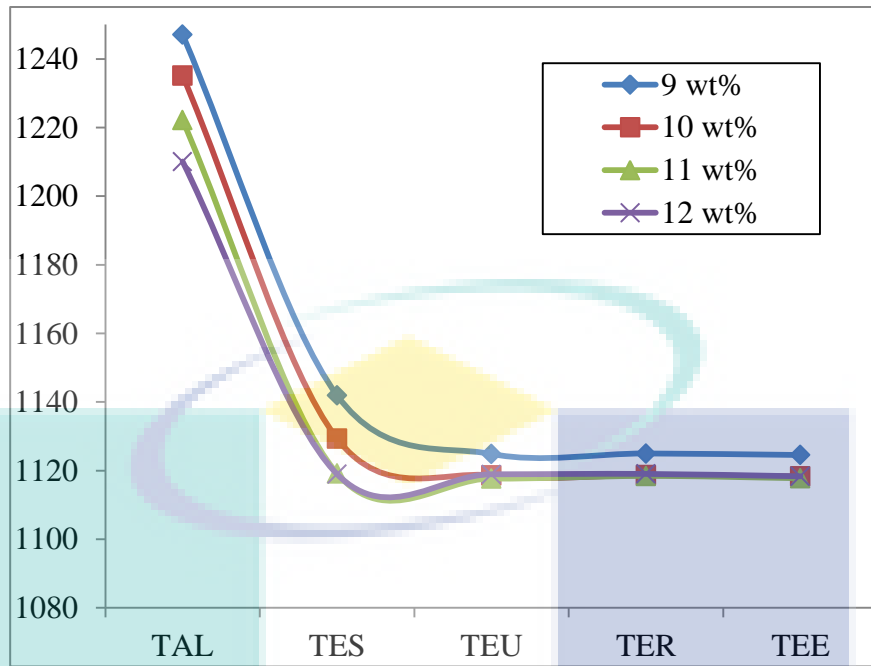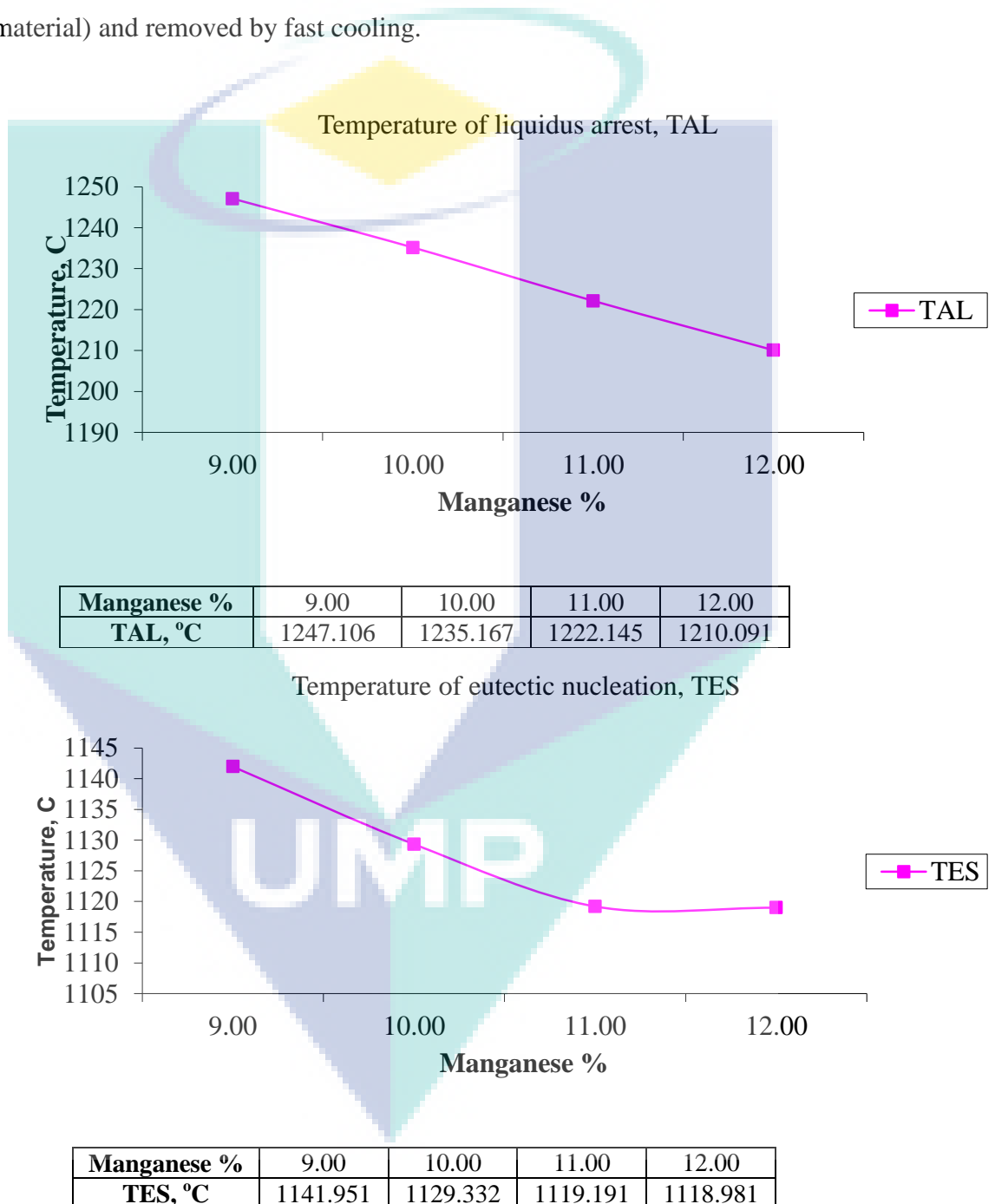Figure 4.11   Determination of thermal arrest of TAL, TES, TEU, TER, TEE

Figure 4.12   Effect of Mn wt. % on solidification cooling curves (b) comparison of temperature points for addition of Mn from 9 to 12 wt. %
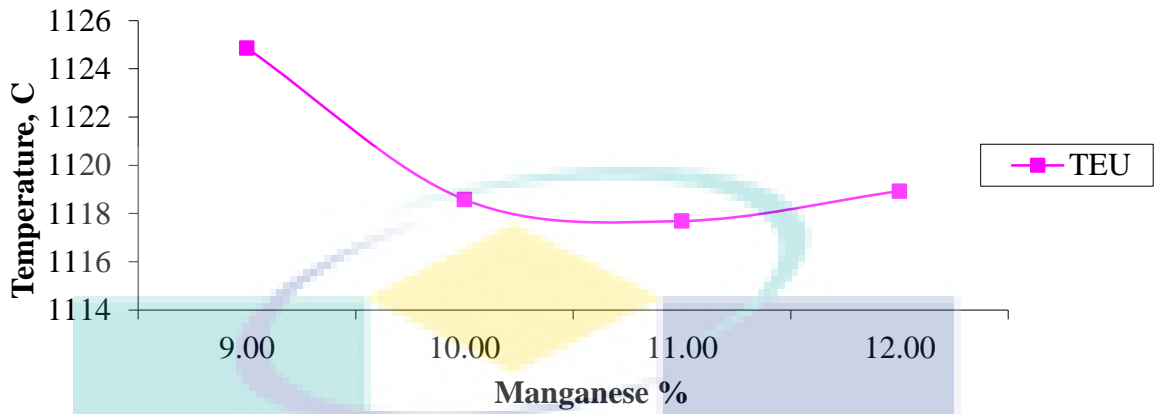
Figure 4.13 show the general solidification temperature in detail. Five thermal arrests known as TAL, TES, TEU, TER, and TEE for each alloy has been identified. From each thermal analysis conducted during solidification, phases show the solidification temperature decrement with higher Mn addition. Sample AI-9 has the highest temperature point compared to the rest of samples. TAL temperature of AI-9 is at the highest (1247°C) then drop until the lowest (1210°C) for sample AI-12. It is revealing that austenite started to nucleate and grow to the dendritic array is at a higher temperature when the Mn less compared to higher Mn addition, which indicates higher Mn utilized during alloying, solid phase will form late (Jiyang, 2009a).The similar trend applies to each of TES, TEU, TER and TEE.

TES point where the temperature for solid stage started to develop either as austenite, graphite or both also varied according to Mn addition. Simultaneously, TEU in which the temperature movement shows austenite and graphite are still growing plummet at the minimum point for higher Mn addition. Higher Mn addition produced consistent TEU at 1118° C. There is a possibility that the TEU was saturated (TEU was constant) due to no more austenite and graphite structure is growing at that temperature point. After this temperature point, the temperature of surrounding molten metal

increases up to its maximum reaching the TER temperature point.   However, for TER and TEE the thermal arrest increases as for sample AI-11 and AI-12 and overlap with AI-10 graph line (Figure 4.14). A possible explanation for this might mean that there is possibility that after 11 wt% Mn (12 wt% Mn included) the population already saturated. Mn addition balanced the heat evolved (from solidified material to liquid state material) and removed by fast cooling.

Temperature of liquidus arrest, TAL

Manganese %	9.00	10.00	11.00	12.00
TAL, ^{o}C	1247.106	1235.167	1222.145	1210.091

Temperature of eutectic nucleation, TES

Manganese %	9.00	10.00	11.00	12.00
TES, ^{o}C	1141.951	1129.332	1119.191	1118.981

Temperature of eutectic undercooling, TEU

Manganese %	9.00	10.00	11.00	12.00
TEU, °C	1124.86	1118.58	1117.688	1118.931

Temperature of eutectic recalescence, TER
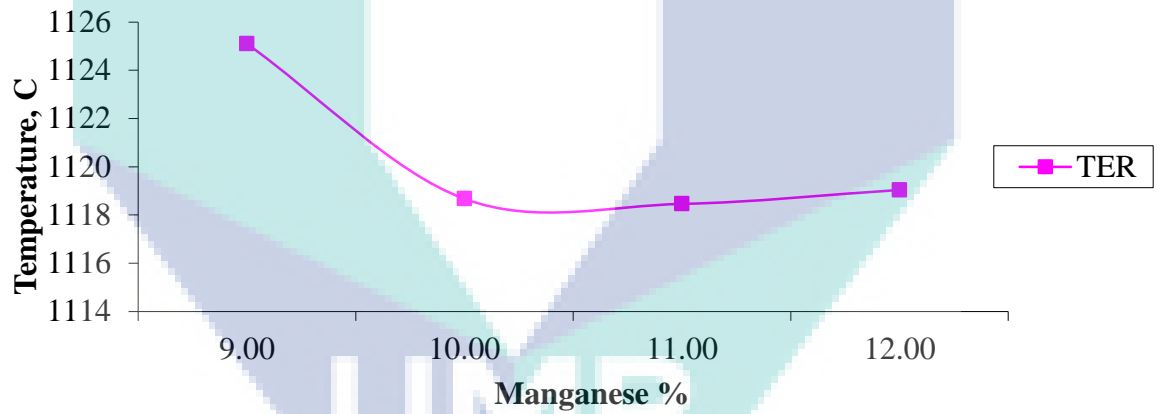
Manganese %	9.00	10.00	11.00	12.00
TER, °C	1125.1	1118.671	1118.46	1119.039

Temperature of the end of eutectic solidification, TEE

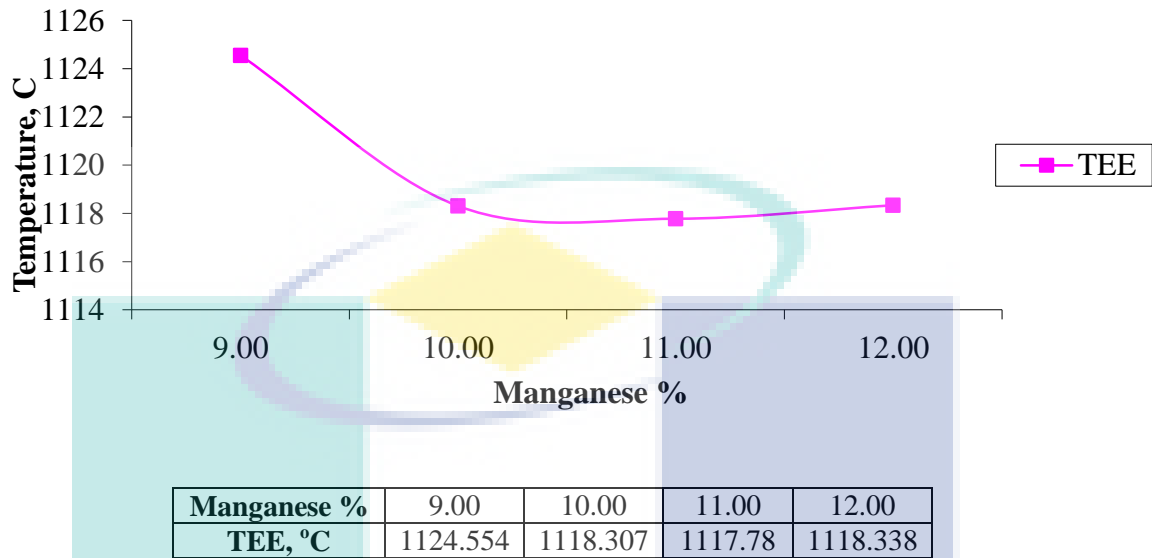| Manganese %	9.00	10.00	11.00	12.00
TEE, $^{\circ}$C	1124.554	1118.307	1117.78	1118.338

Figure 4.13   Temperature detail based on TAL, TES, TEU, TER and TEE position

The overall solidification temperature was decreased as a higher alloying element was added. It is because of the heat evolved and removed by fast cooling from nucleation site to surrounding molten metal is lesser during solidification. Taken together, alloyed iron with higher Mn addition was freeze to room temperature more quickly than less Mn alloyed iron. So less graphite and single unit grain growth are permitted for growth phase after nucleation phase finished. As a result, supposedly the size of graphite length and single unit grain or dendrite of higher Mn addition is smaller compared to lower Mn addition. The detail was discussed in Table 4.3.

4.1.7   Effect of manganese on dendrite

Figure 4.14 reveals the existence of graphite distribution, dendrite arm spacing with secondary dendrite arm spacing and carbide after solidification. The fracture surface successfully isolates the structure which overlaps by each other. The distribution is randomly organized. The dendrite is clearly seen from the edge of the specimen towards its centre. Most likely it happened due to the fact which fluid state heat transfer started from the brink of the specimen to surrounding and end at the centre of the molten metal. So the nucleation and growth of alloyed iron structure due to the heat transfer begin from specimen's edge and also last at the centre.

Higher magnification Figure 4.15, Figure 4.16 and Figure 4.17 shows a present of dendrite arm spacing structure exists among flake graphite, carbide and alloyed iron austenitic structure at the fracture surface. During fracture, there is a possibility that the crack initiated between flake graphite and austenitic structure. The force (during the tensile test) pulls each of that structure at the weakest link (flake graphite and austenitic structure). When the attraction force between flake graphite and the austenitic structure collapsed, it reveals the nature of the flake structure which is attached alongside the austenitic alloyed iron structure. The graphite flake structure is in a rosette form. However, because there is the existence of carbide phase alongside the austenitic structure, the force (during the tensile test) also pulls the bind between carbide (at the late to freeze region), austenitic structure and flake graphite. As a result, the dendrite structure which permitted the carbide to accumulate among its arms structure during solidification was exposed.
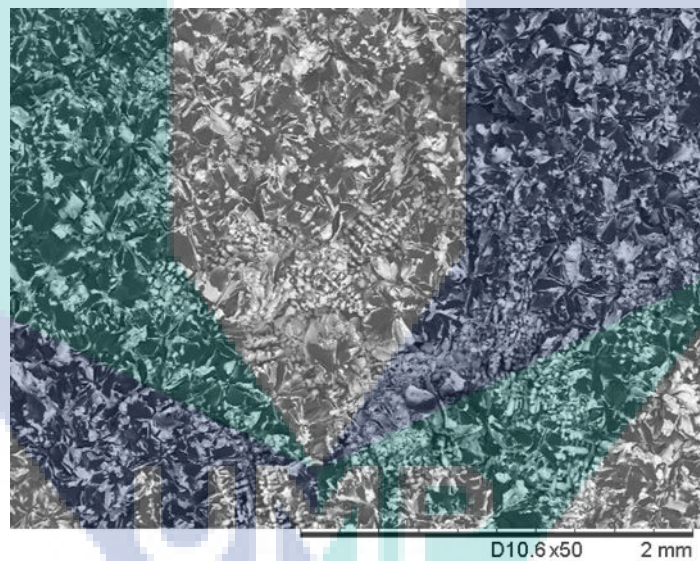

Figure 4.14   Macrograph of alloyed iron macro structure after solidification showing graphite, dendrite arm spacing, and carbide distribution
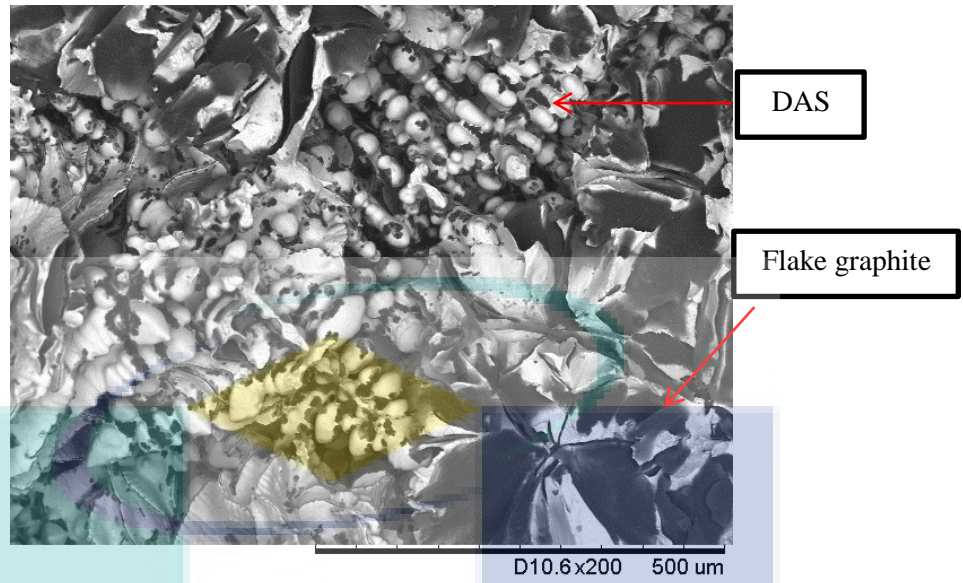
74

DAS

Flake graphite

D10.6 x200   500 um

Figure 4.15   Micrograph showing better resolution of alloyed iron structure after solidification showing graphite and dendrite arm spacing distribution

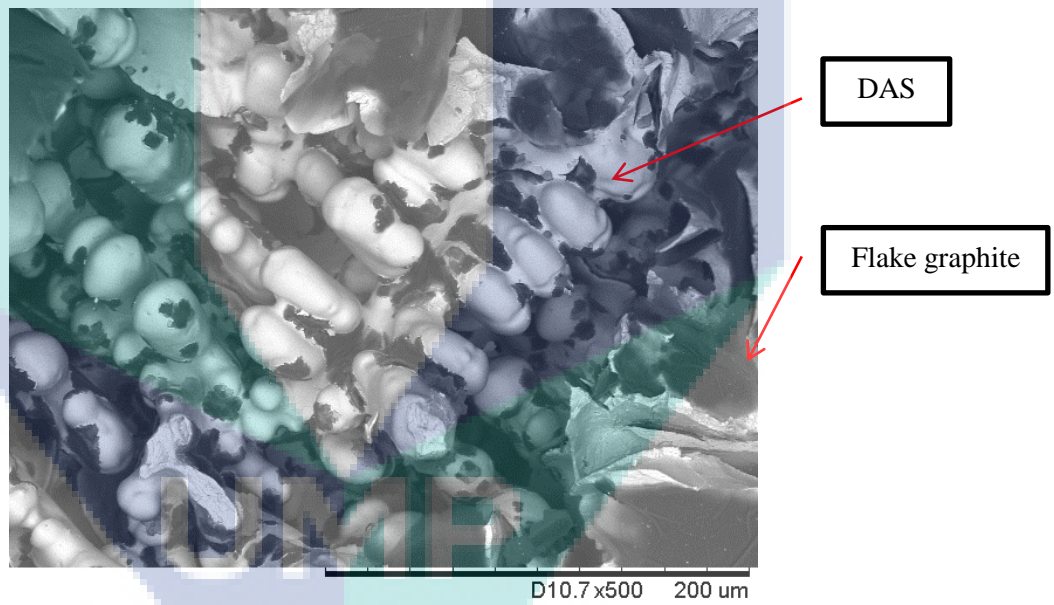DAS

Flake graphite

D10.7 x500   200 um

Figure 4.16   Micrograph showing close up of alloyed iron structure after solidification showing graphite and dendrite arm spacing distribution
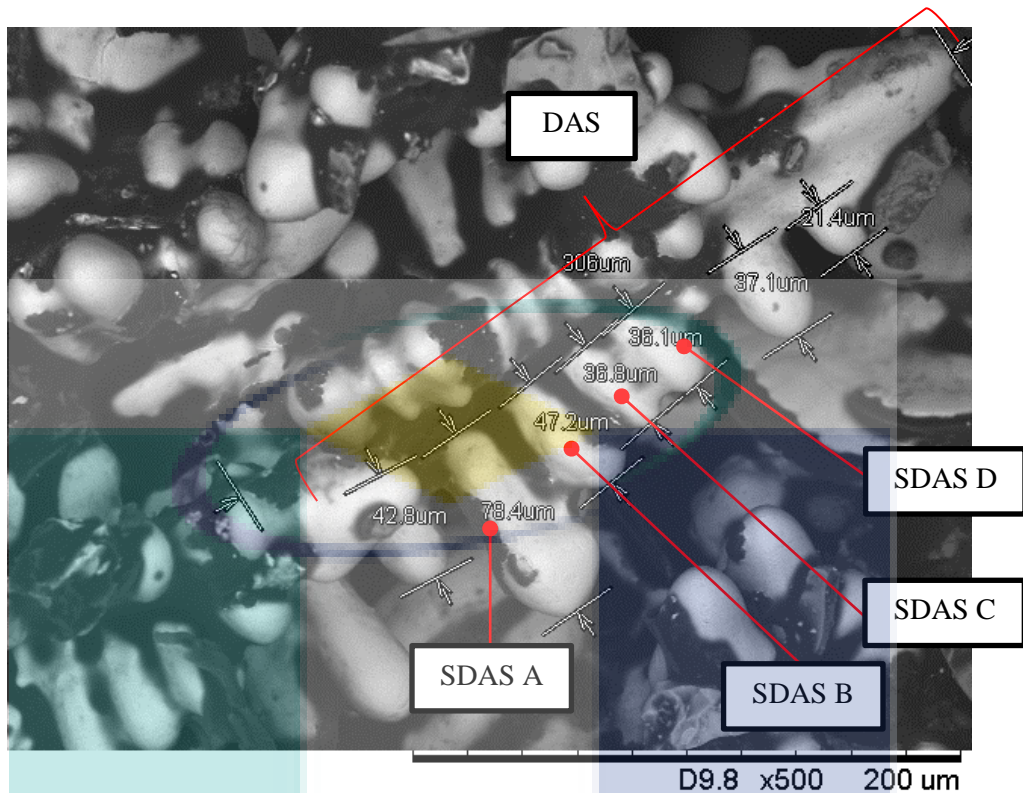
Figure 4.17   Measurement of alloyed iron dendritic structure

A higher percentage of manganese is evidently decreasing overall solidification temperature. The decrease in solidification temperature then avoids further growth of dendrite size during solidification growth phase. So the dendrite size of higher Mn is relatively smaller compare to the minimum addition of alloying element. The edge of grain which is surrounding the dendrite structure becomes more relatively bigger in size. The bigger the edge of the grain region is the less material strength (Rashidi et al., 2013). So the material strength is attached directly by bigger region of the edge of the grain consequently the material is prone to failure compare to the minimum addition of alloying element. The crack occurrence at the edge of the grain due to force applied is relatively is easier transferred from each other when the age of the grain become bigger.

Table 4.3   Comparison of dendrite structure parameter based on Mn wt. % addition of alloyed iron

% Mn	Length, µm				
	DAS	SDAS A	SDAS B	SDAS C	SDAS D
9	390.0	128.0	98.4	176.0	89.0
10	352.0	139.0	132.0	136.0	103.0
11	306.0	42.8	78.4	47.2	36.8
12	238.0	59.3	71.4	52.8	39.6

It can be summarized that after iron was alloyed, the strength decreased compared to the conventional cast iron. The phenomenon is due to several factors.

Firstly, the graphite embedded in alloyed iron structure is a flake shape. This look similar to needle flake shape does not act as crack arrester once a force was applied. So the crack propagated along the flake graphite and continuously transfers between another flake graphite. As a result, any force deploy towards this alloyed iron was distributed along its flake graphite distribution. After the force was fully distributed, the alloyed iron structure will collapse.

Secondly, there is a presence of dendritic structure after the austenitic alloyed iron solidified towards room temperature. Most of the alloyed iron solidified as dendritic structure (D. M. Stefanescu, 2005). Dendritic structure trapped and encouraged microsegregation of elements during solidification. As a result, the uneven element segregation enhances uneven cooling for solidification purpose. Then the uneven cooling was promoted a micro shrinkage phenomenon alongside dendrite arm spacing. Thus there is a void occurred alongside dendrite arm spacing which will weaken the overall structure of the alloyed iron once a force was applied.

Thirdly, the carbide was also detected in alloyed iron structure at the 'late to freeze' region. Carbide existed mostly at the last region which solidified during solidification of molten metal. These areas trapped and also encourage microsegregation of elements and intermetallic phase during solidification. As a result, the uneven element segregation was enhancing uneven cooling which promoted a micro shrinkage phenomenon at the outer space of dendritic structure during solidification. This situation created an ideal condition for avoiding occurrence which minimizing alloyed iron strength once a force was applied.
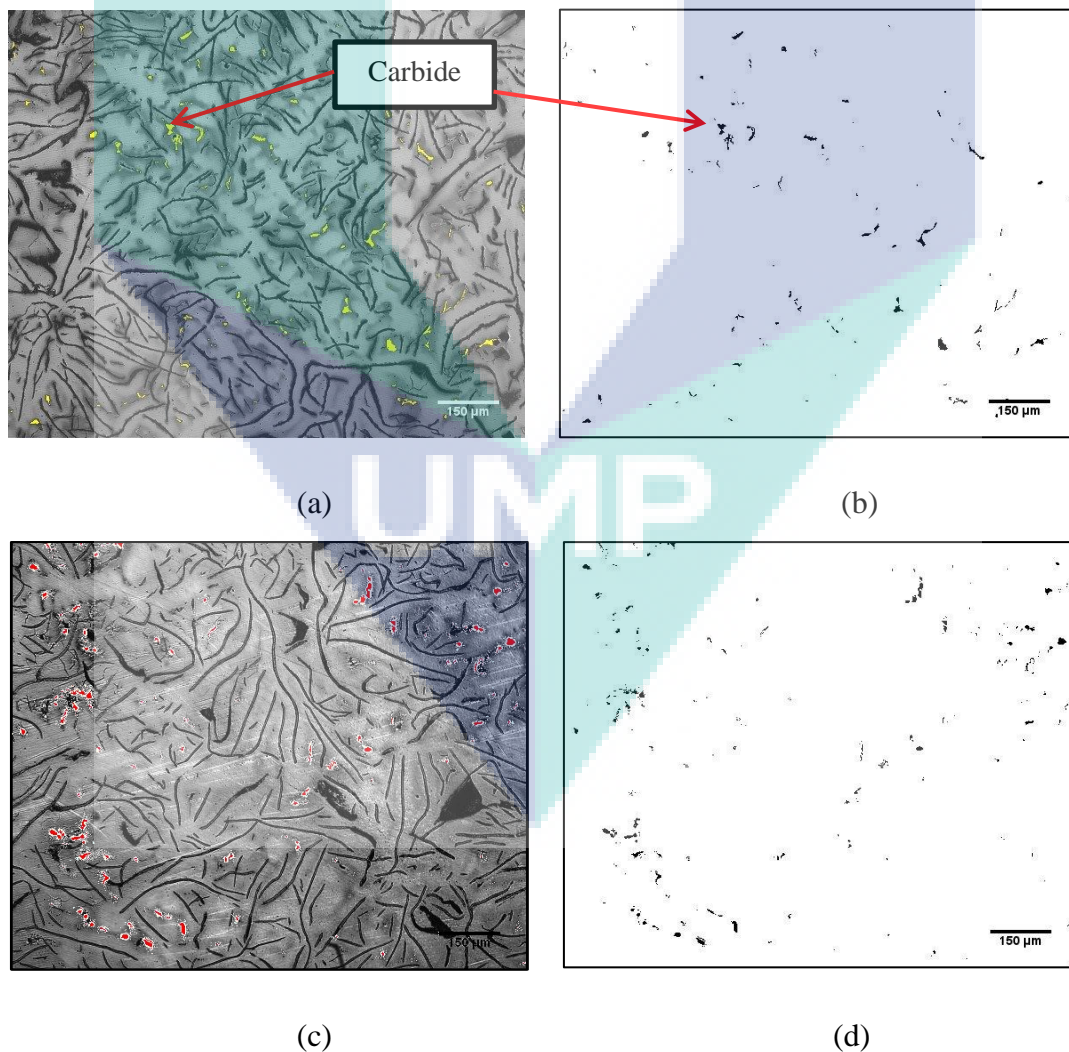
4.2   Annealing

4.2.1   The effect of annealing on microstructure

One criticism of how much manganese affect during solidification on Ni-resist. The occurrence of elements segregation mechanism during solidification encourages carbide formation as revealed in section 4.1. However, heat treatment already well known used in heat treated Ni-resist. Influence of annealing parameter on the carbide

77

formation varies with each of heat treatment temperature parameter. It should then be possible to find indications of carbide growth in the microstructure and to reduce its formation since it is undesirable.

Sample AI-9 was chosen for further study due to its high mechanical properties compared to another sample parameter. It was investigated by tracing the micro-segregation inside each microstructure by using image analyser colour intensity/contrast technique, SEM, and mechanical properties. The result from this investigation illustrates the presence of carbide segregation shape for all parameter heat treatment. As an example in

Figure 4.18 shows the heat treated microstructure of the Mn-Ni-resist alloy with carbide mapping picture.

(a)

(b)

(c)

(d)

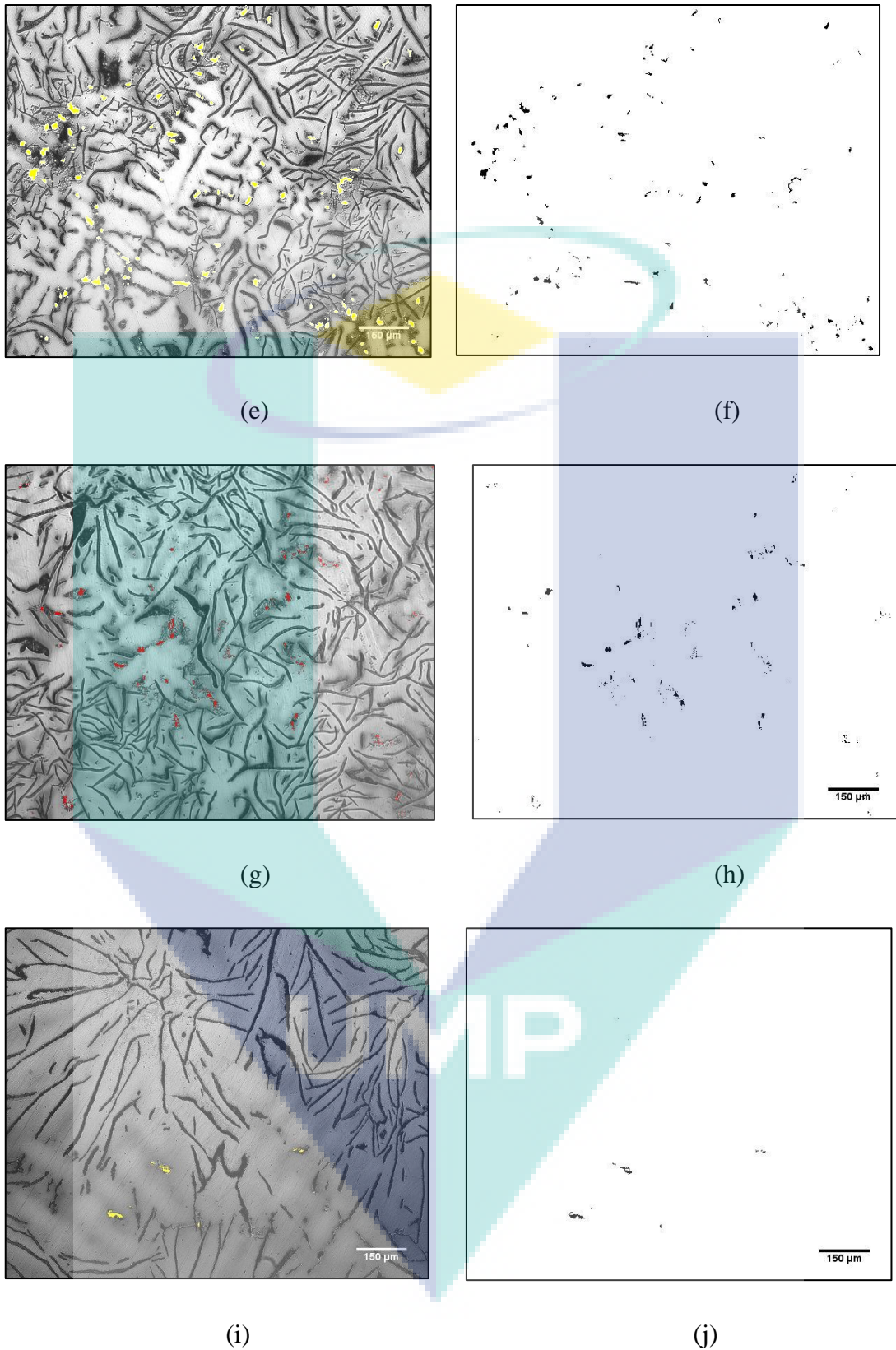(e)

(f)

(g)

(h)

(i)

(j)

Figure 4.18   Microstructure of the modified M-N-resist under 10X magnification: (a) As-cast condition, (c) Annealing 700°C, (e) Annealing 800°C (g) Annealing 900°C (i) Annealing 1000°C. With image analysis on carbide (b)(d)(f)(h)(j)

Before anneal	After anneal

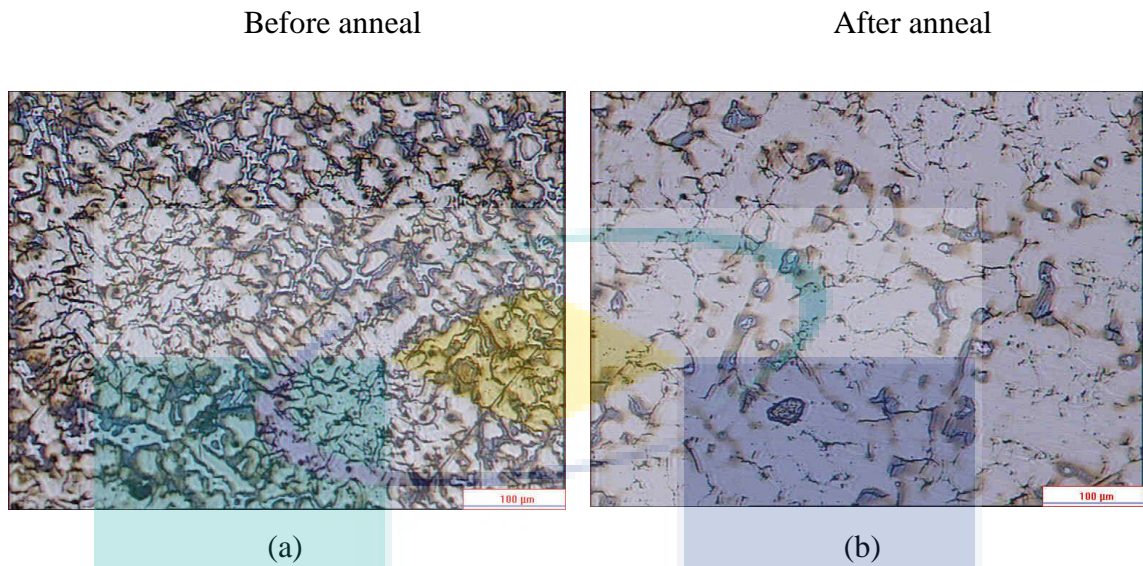|	
(a)	(b)

Figure 4.19   Comparison of alloyed iron (a) before annealing process and (b) after annealing process using picral etchant. The flake graphite and carbide distribution were dispersed and dissolved whenever annealing process takes effect

Figure 4.18 (a) to (j) was exemplified the sequence of carbide formation throughout the microstructure. The samples was divided into five group of the sample based on temperature parameter. The sample was namely according to its annealing temperature and condition. Carbide was observed dissolves progressively from sample without heat treatment (as-cast) to the 1000°C. Based on the carbide distribution, the rate of carbide dissolution was slow at low temperature (700°C – 900°C) but very fast when at high temperature (1000°C). It is remarkable that the carbide formation observed in

Figure 4.18(g) and Figure 4.20(i) is dissolved aggressively as stated. This finding corroborates the ideas of A. N. Volkov (1974) and Lyadskii et al. (1967), who suggested that annealing above 600°C leads to a reduction of the carbide inclusion. Appendix C has more figures for more references on the distribution of carbide.

The carbide formation was decreased considerably at 900°C to 1000°C. This parameter can be considered as spheroid annealing since it has same temperature parameter (Walton, 1993). However, the finding is contradicted because it is supposedly not adversely affect the strength. As overall, the dissolution was successfully decreased carbide formation depending on the holding temperature

compare to the as-cast condition. Increasing annealing temperature shows decreasing pattern of the carbide appearance in the microstructure as clearly also shown in Figure 4.19. This result may be explained by the fact that the diffusion of manganese from carbide to the austenite matrix as stated by Lev (1962).

4.2.2   The effect of annealing on dendrite shape

Annealing temperature restructured the alloyed iron austenitic and carbide structure as shown in Figure 4.20. Better resolution of dendrite structure based on macro structure micrograph was observed in Figure 4.21 which shows a composite of DAS and SDAS attached by each of them. The dendritic structure was clearly heading its way toward inner circle of casting cavity (which was not seen clearly in the as-cast sample). This observation occurred because most of the graphite and carbide which covered the entire layer of the dendritic structure was transform to a finer mesh after annealed. This observation is right up until $900^{o}C$ annealing temperature. Exceeding $1000^{o}C$ the austenitic formation which acts as the binding structure was also affected. Its structure reshuffles to the unsymmetrical shape of dendritic trees shown in Figure 4.22.
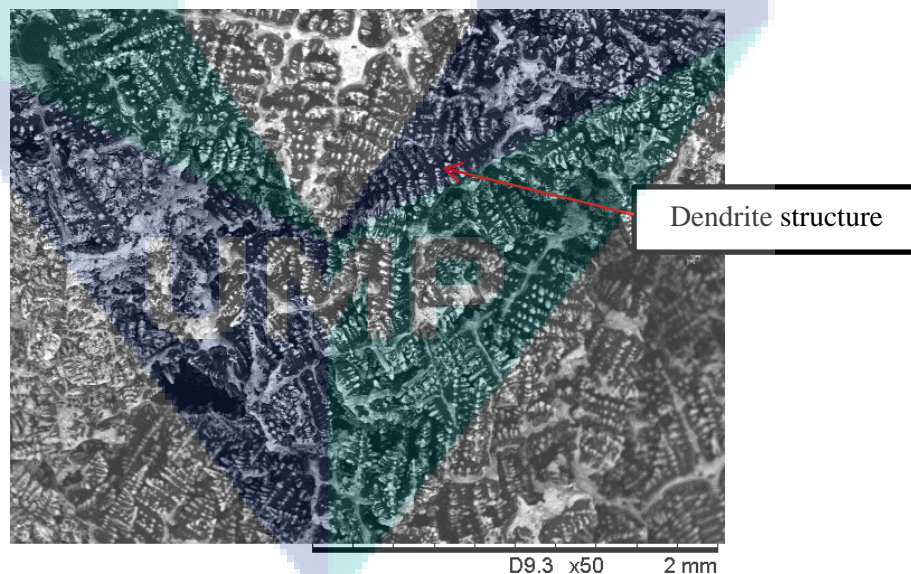

Figure 4.20   Macrograph of alloyed iron macro structure after annealing below $1000^{o}C$
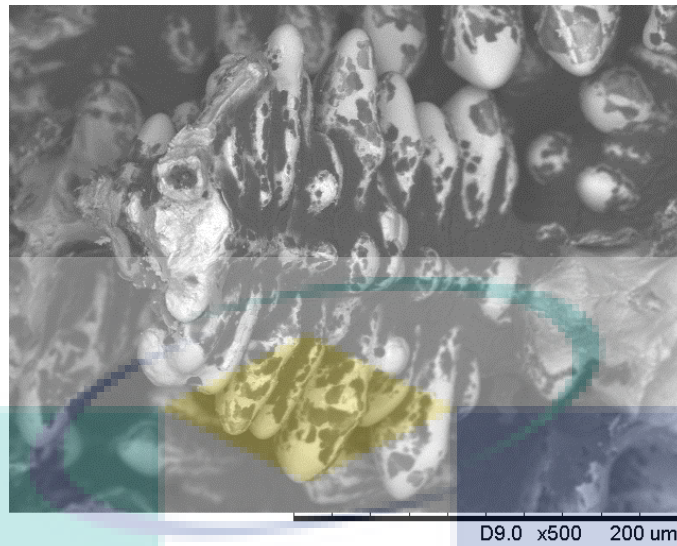
Figure 4.21   Micrograph of alloyed iron microstructure showing transformation of graphite structure from flake to a finer mesh (without any recognized structure) after annealing 900°C
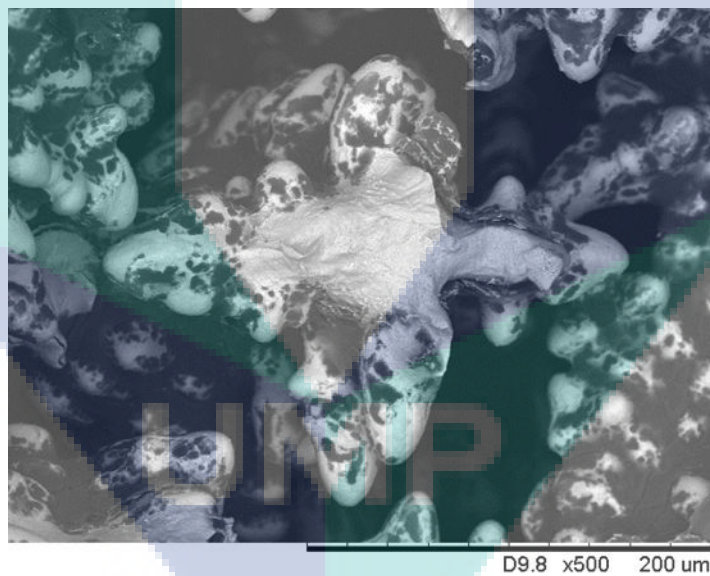

Figure 4.22   Higher magnification micrograph of alloyed iron microstructure showing the transformation of graphite structure from flake to a finer mesh at 1000°C. The austenitic structure was also reshuffled from common dendrite form to an unsymmetrical shape

4.2.3   The effect of annealing on carbide size/area

Quantitative analysis of

Figure 4.18 was recorded in Table 4.4, and this data are illustrated in Figure 4.23. Result for average area of a single unit of carbide graph shows that there has been a slight increase of reading from 55.34 µm2 to 24.56 µm2. This chart pattern also happened to be same with the total carbide area which indicated the sample with low-temperature parameter and as-cast produce high carbide reading with 6918.38 µm2 (as-cast) and slowly decreases to 4155.21µm2 (900°C). While high-temperature parameter is (1000°C) produces low reading as 835.13 µm2. This trend can be seen in percentage mode as in Figure 4.23(a) which shows a decreasing trend of carbide area fraction As-cast iron with 0.54% carbide decreased to 0.51% for sample 700°C, 0.49% for sample 800°C and 0.32% for sample 900°C. Surprisingly, higher dissolution of carbides was observed in the sample 1000°C as compared to the carbide dissolution of sample 900°C.

Table 4.4   Quantitative microstructure analysis

Condition / Sample name	carbide			
	Area average (μm^2) (single unit of carbide)	Percentage (%)	Total carbide area (μm^2)	Number of carbides
As-Cast	55.34	0.54	6918.38	125
700°C	45.40	0.51	6583.50	145
800°C	38.73	0.49	6312.24	163
900°C	34.92	0.32	4155.21	119
1000°C	24.56	0.06	835.13	34

The number of carbides is reading shows increasing reading up to 800°C which is from 125 units to 163 units and decreasing to 34 units at 1000°C. It is due to the irregular size of carbide. Some of them are big, and some are small. So the final area can be seen in the percentage of average carbide area as Figure 4.23(b)

A sharp decline of carbide dissolution in the 1000°C sample possibly resulted from the contribution of approximate temperature to the transition region line A$_1$ which is in the partial melting region. Figure 4.23 clearly shows dendritic structure was affected by the higher degree of annealing temperature. The dendritic structure was transformed from dendritic tree identical structure to become unsymmetrical shape structure.

Furthermore, an analysis of thermal analysis reveals the decreased of overall solidification temperature point with the higher addition of Mn percentage. Whole TAL, TES, TEU, TER, and TEE temperature point decreased whenever Mn % addition increased. This lower A_1 effect by the presences of manganese as austenite stabilizer also lowered the temperatures A_1 (Dasgupta et al., 2012) and believed to drop near to 1000°C. So there are higher chances of the austenitic dendritic structure was affected during 1000°C as well. This discovery supported the previous investigation by Nili-Ahmadabadi and Feghahati (2013) which reported that a heat treatment involving an austenitizing at partial melting temperature was sufficient and a higher rate of dissolution to reduce free carbides present in samples.

As shown in Figure 4.18 the shape and distribution of the carbide particles are irregular. The carbide disperses and dissolves through the matrix as the annealing temperature increased. Increasing the holding temperature of the annealing decreases the carbide size before solidification approximation, and as a sequence, there is the tendency of the carbide dispersed together as well. Carbide spread but still grouping at the LTF region as shown in Figure 4.19. Either it is believed to dissolve slowly into austenite as the annealing temperature increased required a further examination. It is evidently shown in Table 4.4, a result of the number and small size carbide grouping in inter graphite region. The growth of small dispersed carbide becomes the dominant pattern for entire matrix. The trend of carbide dispersion can be seen clearly in the graph in Figure 4.23.
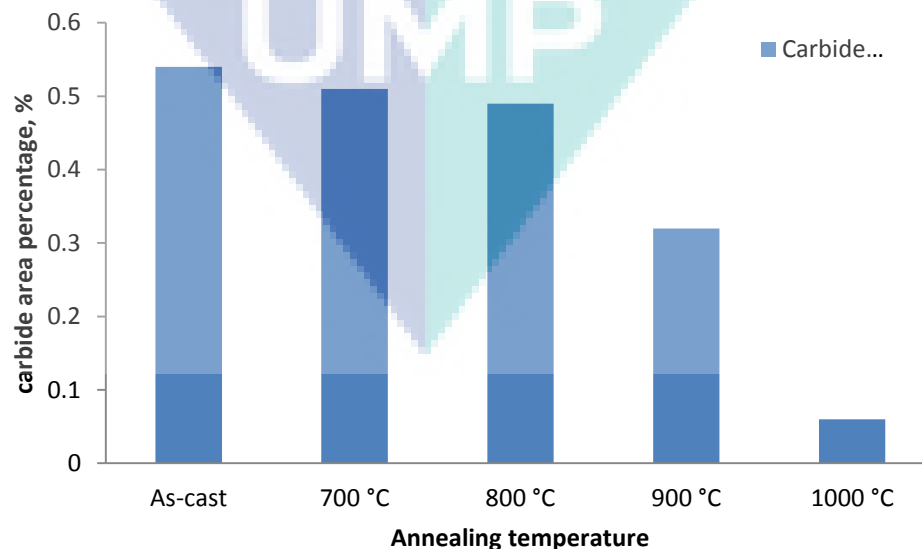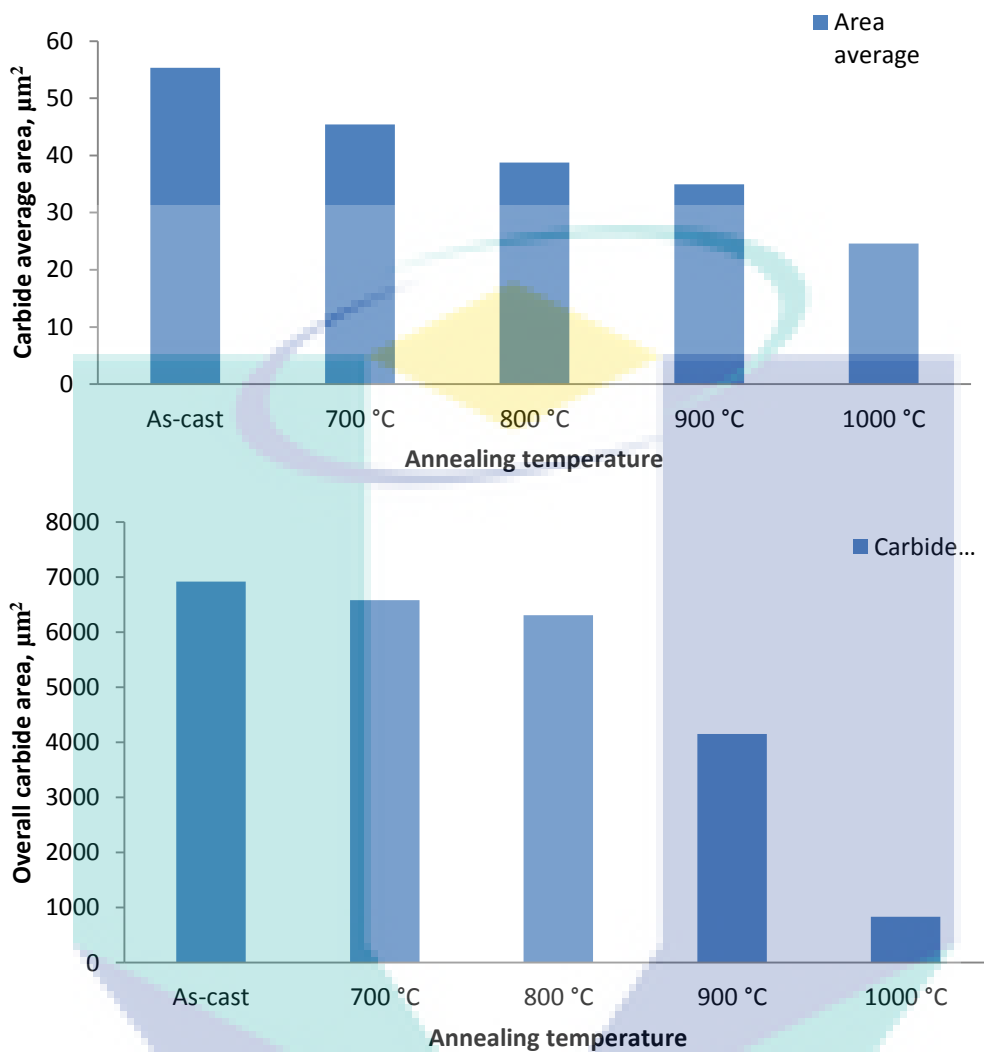
Figure 4.23   Graph for carbide distribution according to a percentage, average single carbide form and overall carbide area in the microstructure

4.2.4   The effect of annealing on strength

Table 4.5 shows the influence of annealing parameter to the mechanical properties of AI-9 sample. It is apparent from this Table 4.5 that the heat treatment had a strong effect on the structure and mechanical properties. When the alloyed iron was annealed, ultimate tensile strength gradually increased until the annealing temperature increases reach 1000°C but the proportion of macro hardness slowly decreased. This shows a positive correlation between the annealing parameter, mechanical strength, and macro hardness reading. As the annealing temperature increase, the mechanical properties are refurbished.

Table 4.5   Mechanical properties of high manganese austenitic cast iron

Materials	Room temperature test		
	Ultimate Tensile Strength (MPa)	Elongation (%)	Macro hardness (HRB)
As-cast	60.10	1.04	102.53
Annealing 700°C	66.67	1.14	100.93
Annealing 800°C	68.89	1.34	93.63
Annealing 900°C	71.76	1.74	90.48
Annealing 1000°C	75.01	1.92	80.55

From the readings shown in Table 4.5 and Figure 4.24, it is a very promising result that reveals heat treated alloyed iron was relatively strong with the highest tensile strength is achieving 75.01 MPa compare to as-cast condition only 60.10 MPa. It cannot be argued that this situation occurs due to the annealing temperature in dissolving carbide, graphite, and dendritic structure formation as discussed before. The high-value tensile strength of Mn-Ni-resist related to its annealing temperature in controlling carbide formation. This outcome is aligned with the previous microstructure analysis which indicated less carbide discovered whenever annealing temperature increased (up until 1000°C) (Cox, 1988; A. N. Volkov, 1974).

Figure 4.24   Comparison of tensile properties : (a) ultimate tensile strength, (b) elongation

Higher annealing temperature increased the tendency of carbide to disperse and scatter around the wide last to freeze (LTF) region. Most probably this is the cause of a number of carbides recorded in Table 4.4 increase from as-cast to 800°C (125 to 163).

Though, the trend is only rising until 800°C then the trend of carbide number sharply drop from 119 to 34 at a higher temperature (reaching 1000°C). This condition influence alloyed iron solidification structure which effects solid phase transformation and reshuffle back including austenitic dendritic, graphite and carbide. It also possibly exerts important effects on the mechanical properties.

4.2.5 The effect of annealing on properties (Hardness)

Figure 4.25 illustrates the influence of varying annealing temperature on hardness values in all of the samples. This curve reveals that hardness is slightly decreased with increasing annealing temperature. The highest value of hardness for the sample 700°C corresponding to the plentiful fraction of carbide in its structure compared with the other samples.
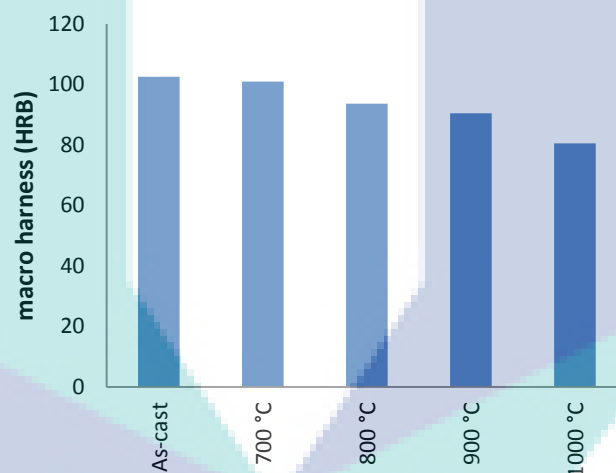

Figure 4.25   Macro-hardness of the alloyed iron

While lowest hardness is reading sample 1000°C, the carbide content is much lower in the matrix, resulting in lower macro-hardness. It can be suggested that the macro-hardness of the alloyed iron is primarily affected upon addition of the heating temperature and phase constituent in the microstructure. According to the ASTM-A436 standard, the hardness values for Ni-resist (Type 1) have been reported in the range of 131 up to 149 Brinell. In this study, the hardness values were in the range of 80 up to 101 Brinell for annealed samples. It seems the relationship between the tensile properties and macro-hardness of alloyed iron is shown that proper annealing heat treatment practice evidently results in decreasing hardness values and increase tensile

properties. It is suggested that an annealing process minimized the formation of carbide due to element segregation governs.

4.2.6 Relationship of properties and macro hardness

The result obtained from tensile strength and hardness are presented and compared in Figure 4.26. It is apparent from this figure that when the hardness increased the tensile strength gradually decreased. These two records also supported by elongation reading Figure 4.26(b) which shows increment when tensile increased and hardness decreased. This result is going as expected. The finding of these properties is which corroborate the results of a large amount of the previous work in this method (Lyadskii et al., 1967; Stanchev et al., 1976; A. N. Volkov et al., 1968).
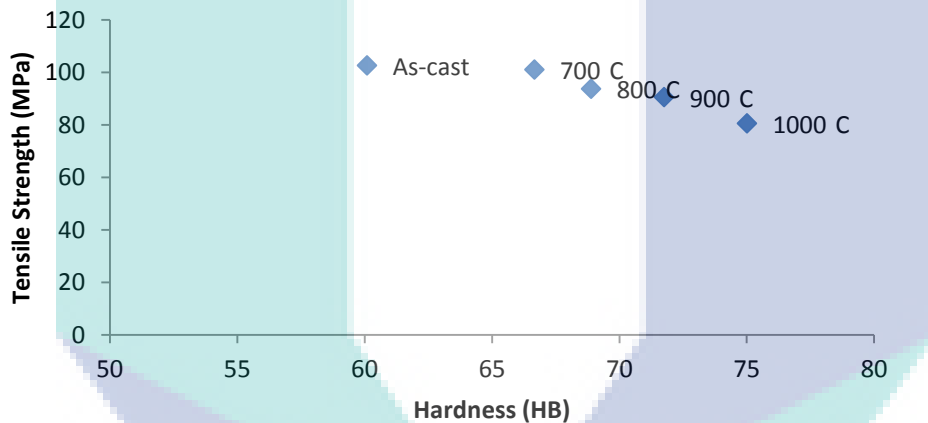

Figure 4.26   Relationship between the tensile strength and macro hardness

It can be summarized that after alloyed iron was heat treated, the strength was slightly increased, and better compare to the as cast alloyed iron. The phenomenon is due to several factors.

Firstly, there is no more important flake graphite shape after the annealing process. Flake shape was transformed to a finer mesh. So the crack propagation (with flake graphite) after the load was applied is lesser (with finer mesh graphite shape). So the crack transferred between flake graphite to another does almost not exist. As a result, any force deployed towards annealed alloyed iron is no longer distributed along graphite distribution. Instead, all forces applied had to spread between austenitic dendritic structure and LTF region. Consequently, less crack site is available, and a

higher load is required to break the entire structure. Thus the tensile strength is improved as well.

Secondly, the carbide located around LTF region was dispersed to a smaller area as shown in Figure 4.19. So that, the void left between LTF regions fulfil by carbide, and other positive segregation elements were lesser. The same phenomenon as previously discusses in the first factor is happening again. The force deployed towards annealed iron distributed probably evenly between austenitic dendritic structure and smaller form of carbide. With a minor crack site due to a lower form of carbide, a higher load is required to break the overall alloyed iron structure. This implication improves tensile strength exceeding 10% compare to as cast alloyed iron.
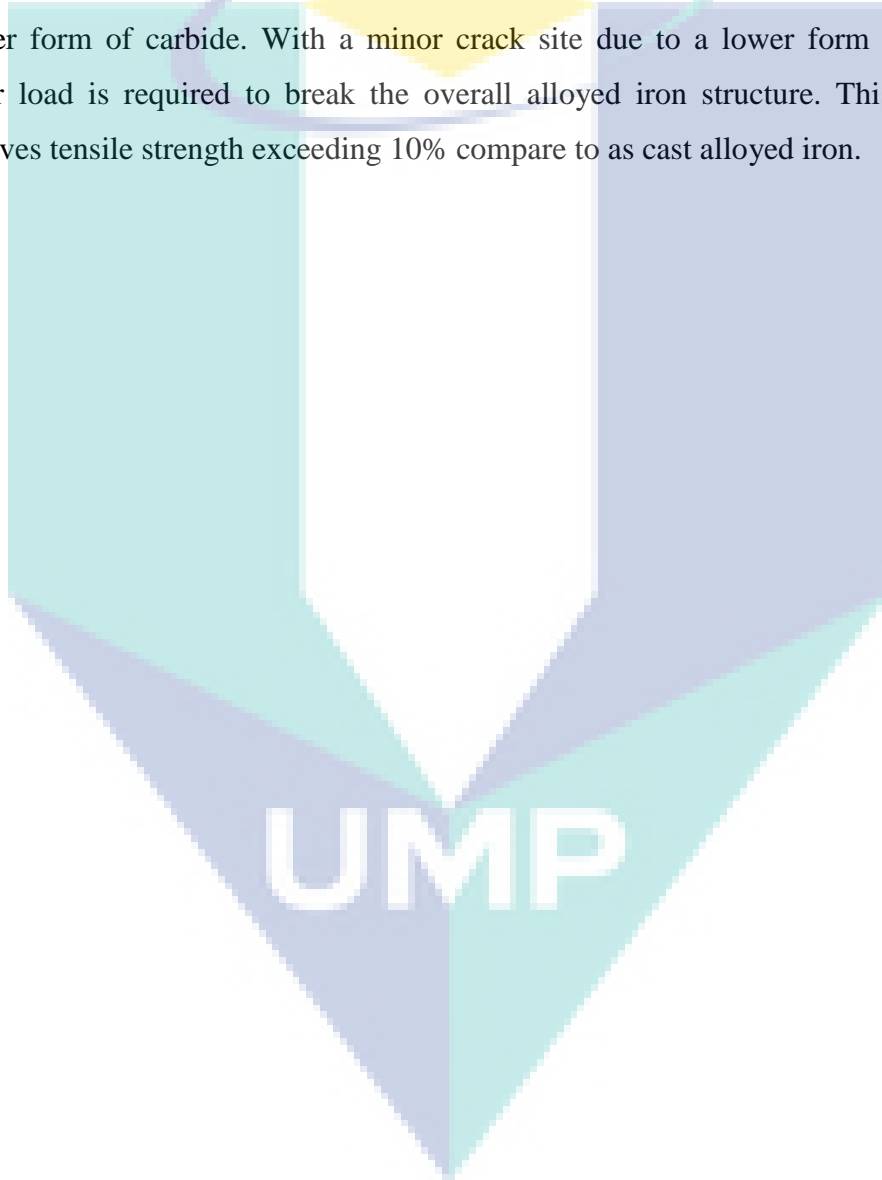
CHAPTER 5

CONCLUSION

5.1   Conclusion

Based on the above results and discussion and research finding, the research objectives have been achieved, and the following conclusions can be drawn from the present study:

1. To introduce the novel usage of manganese as one of alloying element in Ni-resist, a clear understanding of effect of manganese on the solidification, mechanical properties and microstructure are required. Macrostructure micrograph reveals the existence of flake graphite distribution, dendrite arm spacing with secondary dendrite arm spacing and carbide after solidification. It is concluded that the addition of 9 wt %Mn to 12 wt %Mn to the Ni-resist increased the amount of carbide found on the outer frame of flake graphite. The formation of carbide is due to element segregation of manganese in inter graphite region. These findings suggest a role for manganese in promoting carbide and its effect on mechanical properties.

2. Thermal analysis conducted during solidification phases shows the decreasing of solidification temperature with higher Mn addition. 9 wt. % has the highest temperature point compared to the more Mn addition alloyed iron. TEU and TER temperature point for higher Mn addition shows are a lesser value compared to a lower Mn addition alloyed iron. Consequently, the size of graphite length and single unit grain or dendrite of higher Mn addition is smaller compared to lower Mn addition. DAS of 9 wt. % with 390µm compared to 12 wt. % with 238.0µm. Moreover, SDAS have the same pattern of reading.

3. Increasing the annealing temperature reduces more segregated carbide in the LTF region in microstructure resulting in an improvement in tensile strength and lowering hardness reading. As-cast sample has the lowest tensile strength of 60.10 MPa but produces with highest macro hardness 102.53 HB. While 1000°C evidently has the highest tensile strength with 75.01Mpa recorded and lowest macro hardness with 80.55 HB recorded. Less precipitation of carbide, $Mn_{23}C_6$ phase observed at grain boundaries of Mn-Ni-resist by increasing annealing temperature. There is a possibility that annealing temperature minimizes the segregation existence in alloyed iron.

The outcome of this research can be seen in Appendix D where the list of publication and conferences involved during this research.

5.2 Further Improvement

Further research is needed in the determination of the relationship between the heat treatment method and alloying element to the mechanical properties, cooling curve, and microstructure obtained by more standard means. Given the successful of a recent investigation on understanding the effect of alloying element and heat treatment of austenitic iron, there is promising evident that current approach to reducing the dependence of nickel in Ni-resist and increase the ability to produce the Ni-resist model. It could be achieved by modified and adapted to predict optimum austenite promoter/stabilizer, given the appropriate resources of time and financial support.

Another promising and yet hardly explored the field in austenitic cast iron is inoculation control of solidification also its understanding implement together with other heat treatment method.

REFERENCES

436, A. A. (2001). Standard Specification for Austenitic Gray Iron Castings. *ASTM International: Annual Book of ASTM Standards, iron and steel products*.

A128, A. (2001). Standard Specification for Steel Castings, Austenitic Manganese. *ASTM International: Annual Book of ASTM Standards, 1*.

A247, A. (2001). Standard Test Method for Evaluating the Microstructure of Graphite in Iron Castings. *ASTM International: Annual Book of ASTM Standards*.

A439, A. (2001). Standard Specification for Austenitic Ductile Cast Iron Casting. *ASTM International: Annual Book of ASTM Standards, iron and steel products*.

A644, A. (2003). Standard Terminology Relating to Iron Castings. *Annual Book of ASTM Standard, 1*(Reapproved), 70. doi:10.1016/S0016-0032(35)90652-4

A. Janus, & K. Granat. (2014). Heat treatment of Ni–Mn–Cu cast iron. *Archives of Civil and Mechanical Engineering, 14*(4), 602-607. doi:10.1016/j.acme.2014.02.006

A. Janus, & M. Stachowicz. (2014). Thermodynamic Stability of Austenite NI-Mn-Cu Iron. *Metalurgija*(53), 353 - 356.

Ahmadabadi, M. N., Niyama, E., Tanino, M., Abe, T., & Ohide, T. (1994). Chemical composition and structural identification of eutectic carbide in 1 pct Mn ductile iron. *Metallurgical and Materials Transactions A, 25*(5), 911-918. doi:10.1007/bf02652266

Alabbasian, F., Boutorabi, S. M. A., & Kheirandish, S. (2016). Effect of inoculation and casting modulus on the microstructure and mechanical properties of ductile Ni-resist cast iron. *Materials Science and Engineering: A, 651*, 467-473. doi:10.1016/j.msea.2015.09.024

Alzafin, Y. A., Mourad, A. H. I., Zour, M. A., & Abuzeid, O. A. (2009). Stress corrosion cracking of Ni-resist ductile iron used in manufacturing brine circulating pumps of desalination plants. *Engineering Failure Analysis, 16*(3), 733-739. doi:http://dx.doi.org/10.1016/j.engfailanal.2008.06.013

Aptekar', L. I., & Abramenko, Y. E. (1977). Structure and properties of austenitic nickel cast irons. *Metal Science and Heat Treatment, 19*(4), 280-292. doi:10.1007/bf00700810

Asenjo, I., Larranaga, P., Sertucha, J., Suárez, R., Gómez, J. M., Ferrer, I., & Lacaze, J. (2007). Effect of mould inoculation on formation of chunky graphite in heavy section spheroidal graphite cast iron parts. *International Journal of Cast Metals Research, 20*(6), 319-324. doi:10.1179/136404608x286138

Barton, R. (1958). Constitution, production and mechanical properties of Ni-Resist. *B.C.I.R.A. Journal of Research and Developmenmt, 7*, 299-308.

Bhadeshia, H. K. D. H. (2002). Thermal analyses techniques. Differential thermal analysis. *University of Cambridge, Material Science and Metallurgy*.

Boudot, A., Gerval, V., Oquab, D., Lacaze, J., & Santos, H. (1997). The role of manganese and copper in the eutectoid transformation of spheroidal graphite cast iron. *Metallurgical and Materials Transactions A, 28*(10), 2015-2025. doi:10.1007/s11661-997-0158-7

Cabanne, P.-M. (2006). Thermal analysis: A useful technique for the foundryman. *Sorelmetal Technical Services*(103), 1-4.

Calister, W. D., & Rethwisch, D. G. (2010). *Materials Science And Engineering - An Introduction* (8TH EDITION ed.): John Wiley & Sons, Inc.

Chisamera, M., Riposan, I., & Liliac, M. (1995). High Active Inoculant Ferroalloy To Control Graphite Morphology And Nucleation Ability In Cast Iron. *INFACON7, Publishers: FFF, Trondheim, Norway*, 743 - 749.

Chisamera, M., Riposan, I., Stan, S., Stefan, E., & Costache, G. (2009). Thermal analysis control of in-mould and ladle inoculated grey cast irons. *China Foundry, 6*(2), 145-151.

Chisamera, M., Stan, S., Riposan, I., Costache, G., & Barstow, M. (2008). Solidification Pattern of In-Mold and Ladle Inoculated Low Sulfur Hypoeutectic Gray Cast Irons. *Buletinul Institutului Politehnic Din Iasi, 4*(8), 41 - 56.

Covert, R. (1998). Properties and Applications of Ni Resist and Ductile Ni Resist Alloys. *https://nickelinstitute.org*(11018).

Cox, G. J. (1988). Properties of alloy austenitic iron. *The Foundryman, 81*(Part 9), 453 - 443.

Dasgupta, R. K., Mondal, D. K., Chakrabarti, A. K., & Ganguli, A. C. (2012). Kinetics of austenitisation of ductile irons containing two different contents of manganese and copper. *International Journal of Cast Metals Research, 25*(4), 239-245. doi:10.1179/1743133611Y.0000000022

Davis, J. R. (1996). *Cast Irons* (J. R. Davis Ed.): ASM International.

Dorazil, E. (1991). *High strength austempered ductile cast iron*: Ellis Horwood.

E8/E8M, A. (2001). Standard Test Methods for Tension Testing for Metallic Metarials. *ASTM International: Annual Book of ASTM Standards, 03.01 : Mechanical Testing, Elevated and Low-Temperature Tests, Metallography*. doi:10.1520/e0008_e0008m-09

ELKEM. (2004). Technical Information 2 - Inoculation of Cast Iron. from Elkem ASA, Foundry Products

ELKEM. (2012). Cast Iron - Inoculation.

Elliott, R. (1988). Solidification Of Cast Iron *Cast Iron Technology*. London: Butterworth-Heinemann.

Emadi, D., Whiting, V. L., Nafisi, S., & Ghomashchi, R. (2005). Applications of thermal analysis in quality control of solidification processes. *Journal of Thermal Analysis and Calorimetry, 81*(1), 235-242. doi:10.1007/s10973-005-0772-9

Fallon, M. (1993). Heat and corrosion resistant of austenitic ductile iron. *BCIRA Technology*(9315), 8–14.

Farahany, S., Ourdjini, A., & Idris, M. H. (2012). The usage of computer-aided cooling curve thermal analysis to optimise eutectic refiner and modifier in Al–Si alloys. *Journal of Thermal Analysis and Calorimetry, 109*(1), 105-111. doi:10.1007/s10973-011-1708-1

Fatahalla, N., AbuElEzz, A., & Semeida, M. (2009). C, Si and Ni as alloying elements to vary carbon equivalent of austenitic ductile cast iron: Microstructure and mechanical properties. *Materials Science and Engineering: A, 504*(1-2), 81-89. doi:10.1016/j.msea.2008.10.019

Forrest, R. D. (1983). Austenitic ductile iron. *foundry trade journal international, 5*(18), 138 - 142.

Gagne, M., & Labreque, C. (2007). Effect of Wall Thickness on Graphite Morphology and Properties of D5-S Austenitic Ductile Iron. *AFS Transactions, 115*(Paper 07-004(05)).

95

Geoffrey, S. (2014). Understanding Segregation to Predict Solidification *Modern Casting, 104,* 35 - 38.

Giacopini, A., Boeri, R. E., & Sikora, J. A. (2013). Carbide dissolution in thin wall ductile iron. *Materials Science and Technology, 19*(12), 1755-1760. doi:10.1179/026708303225009445

Glicksman, M. E. (2011). Microsegregation *Principles of Solidification: An Introduction to Modern Casting and Crystal Growth Concepts* (pp. 345-368). New York, NY: Springer New York.

Gundlach, R., Meyer, M., & Winardi, L. (2015). Influence of Mn and S on the Properties of Cast Iron Part III—Testing and Analysis. *International Journal of Metalcasting, 9*(2), 69-82. doi:10.1007/bf03355617

Harding, R. (1986). *Prospects for the Exploitation of ADI.* Paper presented at the 2nd International Conference on Austempered Ductile Iron, Ann Arbor, Michigan.

Hasse Fredriksson, & Ulla A ̊ kerlind. (2006). Materials Processing during Casting *Microsegregation in Alloy– Peritectic Reactions and Transformations*. England: John Wiley & Sons.

Hayrynen, K. L. (2002). The Production of Austempered Ductile Iron (ADI). *2002 World Conference on ADI.*

Henderieckx, I. G. (2008). Ductile Iron - solidification mechanism. *Gietech BV Technical Information*.

Hoskin, M. A. (1962). Critical Problems in the History of Science: Proceedings of the Institute for the History of Science at the University of Wisconsin, September 1-11, 1957. Marshall Clagett. *Isis, 53*(2), 230-231. doi:doi:10.1086/349553

I. Riposan, M. Chisamera, S. Stan, & D. White. (2009). Complex (Mn, X)S compounds - major sites for graphite nucleation in grey cast iron. *China Foundry, 6*(4), 352 - 357.

Jagmohan Datt, U. B. (2013). Influence of Composition and Austempering Temperature on Machinability of Austempered Ductile Iron. *International Scholarly and Scientific Research & Innovation, 7*(2), 116-121.

Janus, A., & Kurzawa, A. (2013). Effect of Nickel Equivalent on Austenite Transition Ratio in Ni-Mn-Cu Cast Iron. *Archives of foundry engineering, Volume 13*(Issue 2/2013), 53–58.

Jenkins, L. R., & Forrest, R. D. (1993). Ductile Iron (10th editi ed., pp. 64).

Jiyang, Z. (2009a). Colour Metallography of Cast Iron - Grey Iron (III). *China Foundry, 6*(4), 366-374.

Jiyang, Z. (2009b). Colour Metallurgraphy of Cast Iron - Introduction *China Foundry*. China: China Foundry.

Johansson, M. (1977). Austenitic-Bainitic Ductile Iron. *Trans. AFS, Vol 85*, 117-122.

Jolley, G., & Gilbert, G. N. J. (1967). Segregation in Nodular Iron and its Influence on Mechanical Properties. *The British Foundryman*(3), 72–92.

Kalinina, L. T., Mayurnikov, A. V., Porublev, N. I., & Mayurnikov, V. V. (1975). Effect of copper on isothermal decomposition of austenite in silicon-manganese cast iron. *Metal Science and Heat Treatment, 17*(1), 87-88. doi:10.1007/bf00663102

Lyadskii, V. B. (1963). Wear resistance of austenitic manganese cast iron in the case of friction between unlubricated cast irons. *Metal Science and Heat Treatment, 5*(11), 656-658. doi:10.1007/bf00660559

Lyadskii, V. B., Mairansaev, M. U., & Teshaev, S. T. (1967). Effect of Annealing On the Hardness and Resistance to Abrasive Wear of Austenitic Manganese Cast Iron. *Tadzhik Agricultural Institute. Translated from Metallovedenie Termicheskaya Obrabotka Metallov*(8), 57 - 58.

Mampaey, F. (2002). Solidification Mode and Feeding Behavior of Austenitic Cast Iron. *AFS Transactions, 2*(24), 1 - 20

McKay, & Robert, J. (1936). Nickel and corrosion-resisting nickel alloys. *Industrial and Engineering Chemistry, 28*(12), 1391-1397. doi:10.1021/ie50324a012

Morrison, J. C. (1998). Practical production of Ni-resist castings. *Foundry Manage Technology, 126*, 54–64.

Murthy, K. N., Sampathkumaran, P., & Seetharamu, S. (2009). Abrasion and erosion behaviour of manganese alloyed permanent moulded austempered ductile iron. *Wear, 267*(9-10), 1393-1398. doi:10.1016/j.wear.2008.12.033

Nili-Ahmadabadi, M., & Feghahati, S. (2013). Use of modelling to optimise homogenisation of high Mn heavy section ductile iron castings using partial melting. *International Journal of Cast Metals Research, 20*(2), 53-57. doi:10.1179/136404607x239708

Olsen, S. O., Skaland, T., & Hartung, C. (2005). *Inoculation of Grey and Ductile Iron - A Comparison Of Nucleation Sites and Some Practical Advises*. Paper presented at the 14th International Baltic Conference Materials Engineering.

Oshima, T. (2007). Efforts to Save Nickel in Austenitic Stainless Steels. *ISIJ International, 47*(3), 359–364.

Owhadi, A., Hedjazi, J., Davami, P., Fazli, M., & Shabestari, J. M. (1997). Microsegregation of manganese and silicon in high manganese ductile iron. *Materials Science and Technology, 13*(10), 813-817. doi:10.1179/mst.1997.13.10.813

Ozaki, R., Okada, A., & Miyake, H. (1968). Influences of Carbon, Silicon, Manganese and Sulfur on the Eutectic Cell Number in Gray Cast Iron. *THE JOURNAL OF THE JAPAN FOUNDRYMEN'S SOCIETY, 40*(1), 26-36. doi:10.11279/imono.40.1_26

Park, G.-D., Heo, H.-J., Na, H.-S., & Kang, C.-Y. (2012). Effect of the Cu Composition Ratio on the Phase Transformation in Low Ni Austenite Cast Iron, Fe-3%C-16%(Ni+Mn+Cu). *Journal of Korean Institute of Metals and Materials, 50* (6), 419-425. doi:10.3365/KJMM.2012.50.6.419

Paulik, F., Paulik, J., & Erdey, L. (1966). Derivatography. *Talanta, 13*(10), 1405-1430. doi:http://dx.doi.org/10.1016/0039-9140(66)80083-8

Pearce, J. (2008). Inoculation of cast irons practice and developments. *foundry trade journal international*, 28 - 32.

Popovski, V. (2004). Determining the Optimum Level of Inoculant Addition by Thermal Analysis – A Case Study. *ELKEM ASA Research*, 1 - 8.

Popovski, V., Misterek, C., & Kaiser, L. (2005). *Metallurgical Comparisons Operating Conditions,Inoculant Types and Fade Effects In Gray Iron.* Paper presented at the AFS Cast Iron Inoculation Conference, Schaumburg, Illinois.

Poyet, P., Couchinave, P., & Dancoisne, P. I. (1984). Effects of Nickel substitution by Manganese in Austenitic S.G. Cast Iron for Low-Temperature Uses. *MRS Online Proceedings Library Archive, 34*, 345 (349 pages). doi:doi:10.1557/PROC-34-345

Putatunda, S. K. (2003). Influence of austempering temperature on microstructure and fracture toughness of a high-carbon, high-silicon and high-manganese cast steel. *Materials & Design, 24*(6), 435-443. doi:http://dx.doi.org/10.1016/S0261-3069(03)00090-6

Rashidi, M. M. (2014). *Manganese As Austenitic Matrix Stabilizer For Ductile Ni-resist Alloy Using In-mould Magnesium Treatment Method.* (philosopy Degree), University Technology Malaysia.

Rashidi, M. M., & Hasbullah, I. M. (2013). Effect of inoculation on microstructure, mechanical and corrosion properties of high manganese ductile Ni-resist alloy. *Materials & Design, 51*, 861-869. doi:10.1016/j.matdes.2013.04.064

Rashidi, M. M., & Hasbullah, I. M. (2014). The effects of solidification on the microstructure and mechanical properties of modified ductile Ni-resist iron with a high manganese content. *Materials Science and Engineering: A, 597*, 395-407. doi:10.1016/j.msea.2013.12.070

Rashidi, M. M., Hasbullah, I. M., & Shayfull, Z. (2013). The Effect of Inoculation on Properties of Modified Ductile Ni-Resist Alloy. *Key Engineering Materials, 594-595*, 98-112. doi:10.4028/www.scientific.net/KEM.594-595.98

Rashidi, M. M., & M. Hasbullah, I. (2013). Microstructure and mechanical properties of modified ductile Ni-resist with higher manganese content. *Materials Science and Engineering: A, 574*, 226-234. doi:10.1016/j.msea.2013.02.038

Roula, A., & Kosnikov, G. A. (2008). Manganese distribution and effect on graphite shape in advanced cast irons. *Materials Letters, 62*(23), 3796-3799. doi:10.1016/j.matlet.2008.04.056

S.C.Borse, Y. E. M. (2014). Review on Grey Cast Iron Inoculation. *International Journal of Innovative Research in Science, Engineering and Technology, 3*(4), 30 - 36.

Seidu, S. O., Owoeye, S. S., & Owoyemi, H. T. (2015). Assessing the effect of copper additions on the corrosion behaviour of grey cast iron. *Leonardo Electronic Journal of Practices and Technologies*(26), 49-58.

Sertucha, J., Larrañaga, P., Lacaze, J., & Insausti, M. (2010). Experimental Investigation on the Effect of Copper Upon Eutectoid Transformation of As-Cast and Austenitized Spheroidal Graphite Cast Iron. *International Journal of Metalcasting, 4*(1), 51-58. doi:10.1007/bf03355486

Shebatinov, M. P., & Abramenko, Y. E. (1986). Properties and wear resistance of austenitic cast iron. *Metal Science and Heat Treatment, 28*(6), 425 - 431. doi:10.1007/BF00836891

Skaland, T. (1999). Ductile Iron Production - A Comparison of Alternative Treatment Methods. *ELKEM ASA Research*, 1 - 19.

Sparkman, D. A. (2010). Thermal Analysis Metrics by Derivatives.

Stanchev, D. I., Rublev, V. I., Sednev, Y. G., & Filatov, A. M. (1976). Effect of heat treatment on structure and properties of manganese cast iron. *Metal Science and Heat Treatment, 18*(6), 514-516. doi:10.1007/bf00774934

Stefanescu, D. M. (1993). Ferrous Casting Alloy *ASM handbook, Vol. 15 - Casting* (Vol. Vol. 15, pp. 1362 - 1615): ASM International.

Stefanescu, D. M. (2005). Solidification and modeling of cast iron—A short history of the defining moments. *Materials Science and Engineering: A, 413-414*, 322-333. doi:10.1016/j.msea.2005.08.180

Stefanescu, D. M. (2015). Thermal Analysis—Theory and Applications in Metalcasting. *International Journal of Metalcasting, 9*(1), 7-22. doi:10.1007/bf03355598

Verhoeven, J. D. (2007). Solidification *Steel Metallurgy for the Non-Metallurgist* (pp. 165-174): ASM International.

Volkov, A. N. (1974). Stability of austenite in steel G13L and cast irons with manganese. *Metal Science and Heat Treatment, 16*(2), 173-175. doi:10.1007/bf00649803

Volkov, A. N., Lyadskii, V. B., & Stanehev, D. I. (1968). *Effect of Heat Treatment on the Wear Resistance of Manganese Cast Irons*. Metallovedenie i Termicheskaya Obrabotka 1Ketallov, (5).

Walton, C. F. (1993). ASM Handbook-Vol 4 - Heat treating *Heat treating* (10th Editi ed., Vol. 4, pp. 1451 - 1516): ASM International.

Warda, R. (1998). Ductile Iron Data For Engineers. *http://www.ductile.org/*.

Yaer, X., Shimizu, K., Matsumoto, H., Kitsudo, T., & Momono, T. (2008). Erosive wear characteristics of spheroidal carbides cast iron. *Wear, 264*(11-12), 947-957. doi:10.1016/j.wear.2007.07.002

Yang, Y. L., Cao, Z. Y., Lian, Z. S., & Yu, H. X. (2011). A Study on Microstructure of Ductile Ni-Resist Cast Iron for Exhaust Manifolds and Mechanical Property at the Condition of Alternative Thermal Cycles. *Advanced Materials Research, 194-196*, 95-99. doi:10.4028/www.scientific.net/AMR.194-196.95

Yatsenko, A. I., & Martsiniv, B. F. (1968). Effect of nickel on the transformation of austenite in gray cast iron. *Metal Science and Heat Treatment, 10*(11), 890-894. doi:10.1007/bf00649218

Zeng, D., Xie, C., Hu, Q., & Yung, K. C. (2001). Corrosion resistance enhancement of Ni-resist ductile iron by laser surface alloying. *Scripta Materialia, 44*(4), 651-657. doi:http://dx.doi.org/10.1016/S1359-6462(00)00620-5

Zhang, L., Du, Y., Xu, H., Liu, S., Liu, Y., Zheng, F., . . . Tang, C. (2009). Phase equilibria and thermal analysis in the Fe–Mn–Ni system. *International Journal of Materials Research, 100*(2), 160-175. doi:10.3139/146.110002
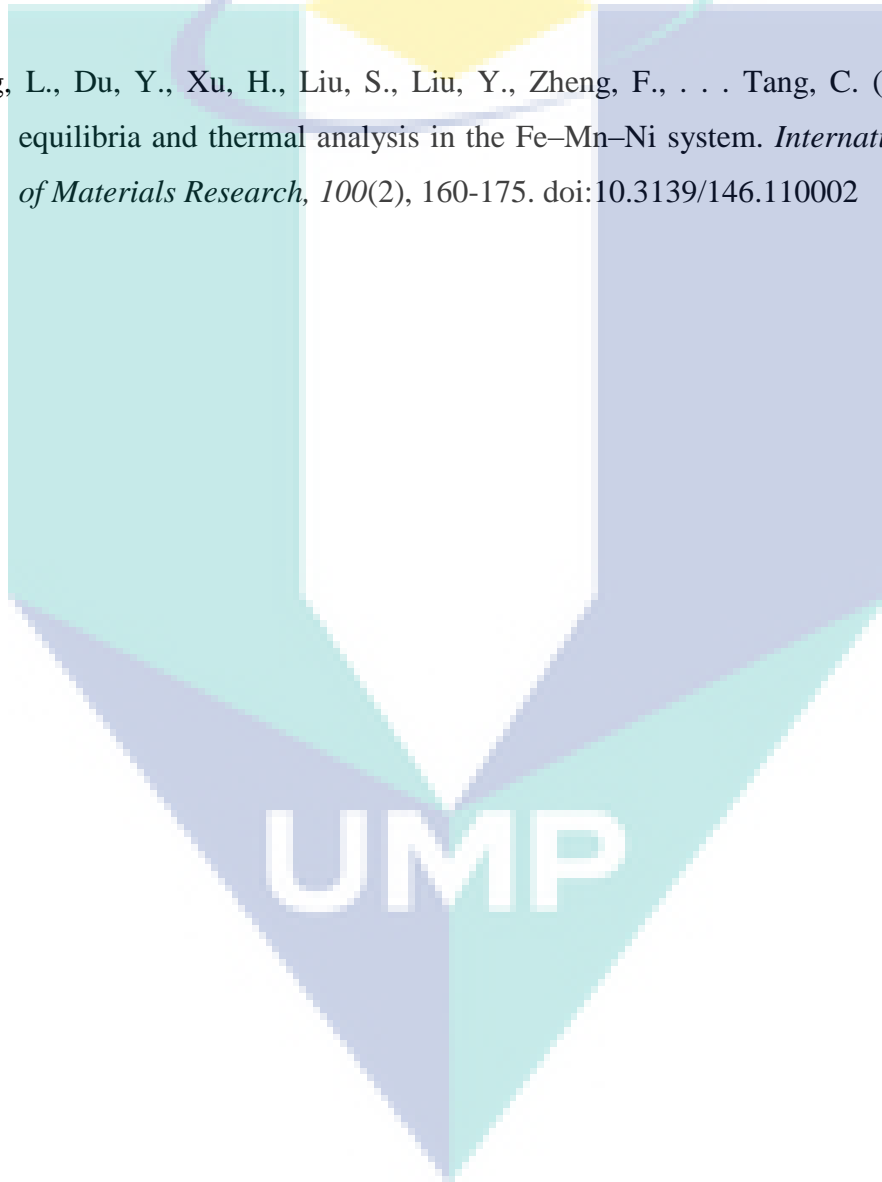
APPENDIX A
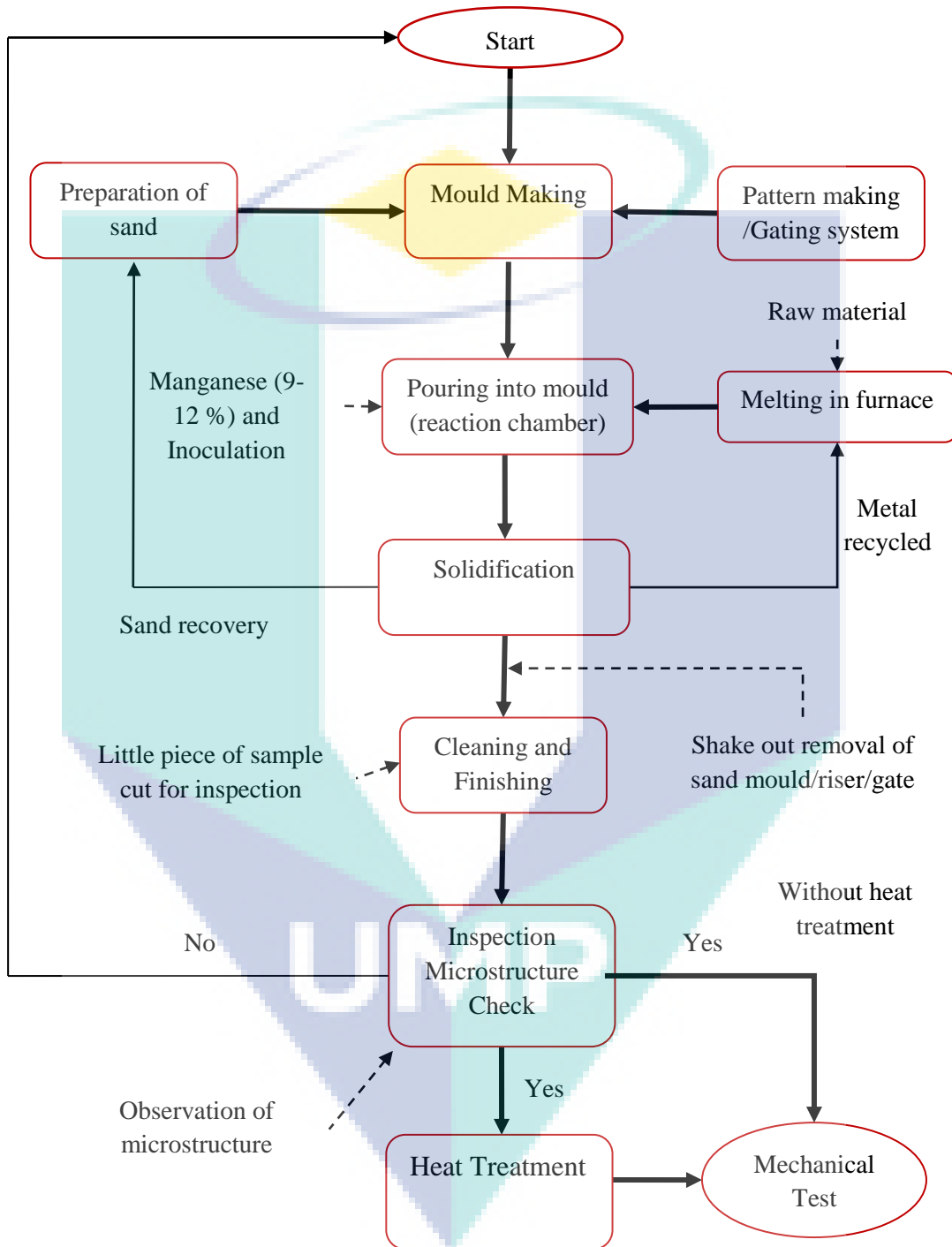
Casting General Flow Chart

APPENDIX B

Calculation to determining alloying composition;

To decrease carbon content in base iron (equation 3.1)

$$a \text{ wt\%} = \frac{\frac{b}{100} \times m + \frac{c}{100} \times n}{m+n} \times 100 \qquad \qquad \textbf{(3.1)}$$

Where,

a = preferred carbon content in melt product.

b = carbon content in pig iron.

c = carbon content in steel.

m = mass of pig iron in kg.

n = mass of steel in kg.

With 26.4 kg pig iron and 3.8 kg steel,

$$a \text{ wt\%} = \frac{\frac{4.5}{100} \times 26.4 + \frac{0.19}{100} \times 3.8}{26.4+3.8} \times 100$$

Base iron mix carbon = 3.96% after adjustment during alloying

To increase Ni content in base iron (equation 3.2)

$$T \text{ wt\%Ni} = \frac{t}{100} \ m + n \qquad \qquad \textbf{(3.2)}$$

Where T is targeted mass of Nickel and t percentage of nickel in the melt.

Percentage of Ni (t) required is as minimum 10%, and m+n is 30.2 kg

$$T \text{ wt\%Ni} = \frac{10}{100} \ 30.2 \ kg$$

X Wt % Ni = 3.02 kg Ni required for adjustment during alloying

To increase Mn content in base iron (equation 3.3)

$$X \text{ wt\% Mn} = \frac{\frac{x}{100} \times (m+n)}{\frac{86}{100} Mn \text{ in } FeMn} \tag{3.3}$$

Where,

X   =   mass of Ferro-Manganese required.

x   =   percentage of manganese in the melt.

With 30.2 kg base iron

$$X \text{ wt\% Mn} = \frac{\frac{9}{100} \times (30.2 \text{ kg})}{\frac{86}{100}} \qquad \textit{(This example for 9\% of manganese)}$$

X wt. % Mn = 3.16 kg Mn required for adjustment during alloying
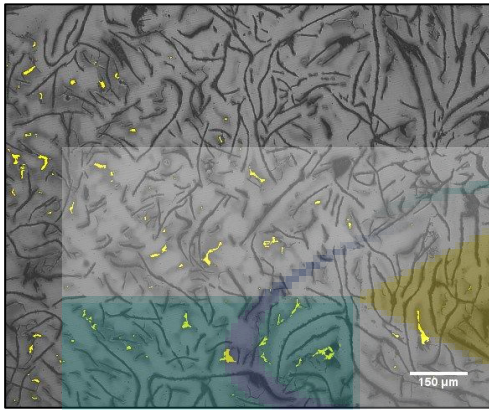
APPENDIX C

(a)
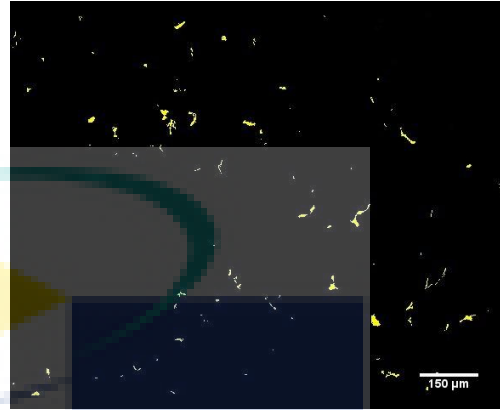
(b)
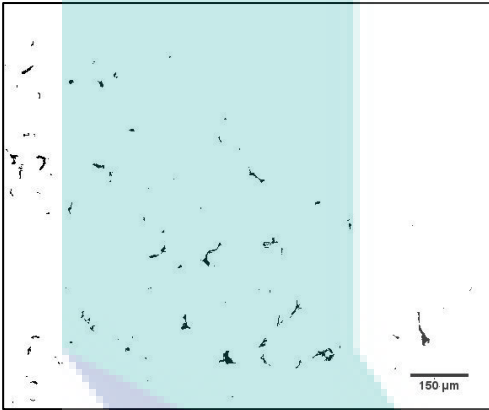
(c)
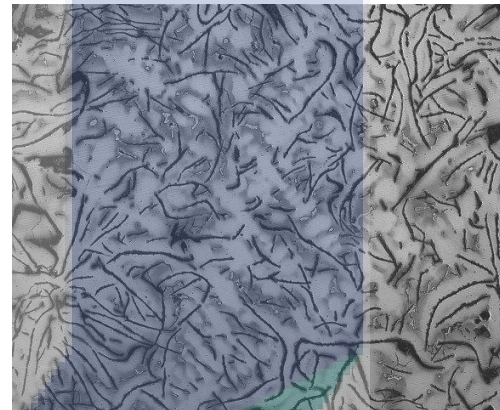
(d)
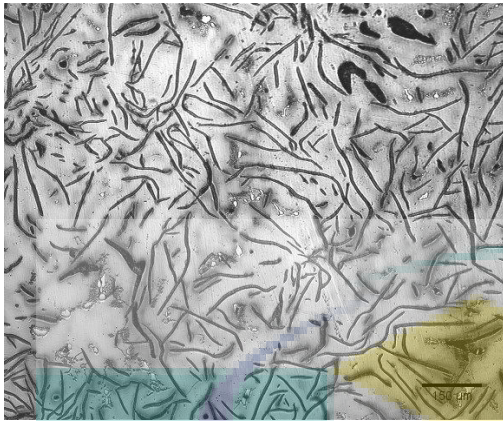
As cast condition
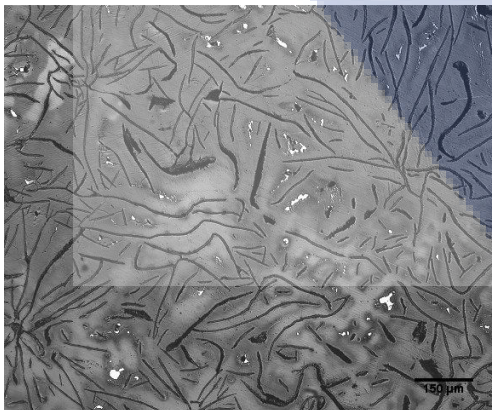
(a)
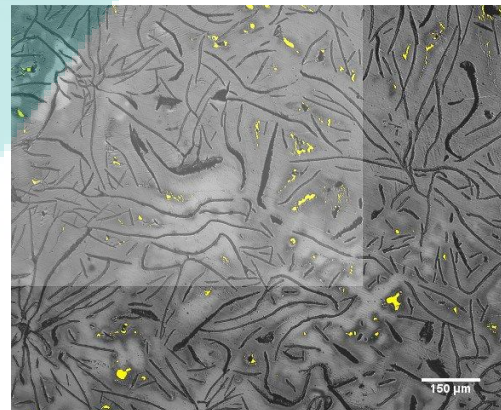
(b)
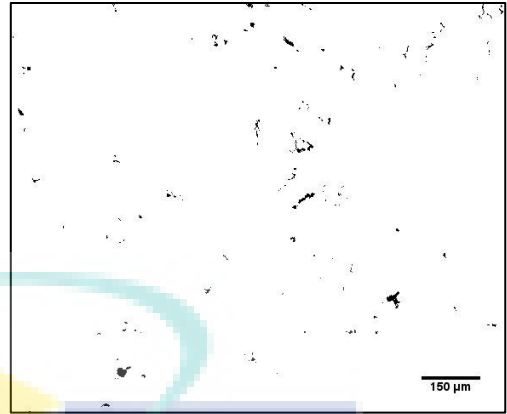
(c)   (d)

Annealing 700°C
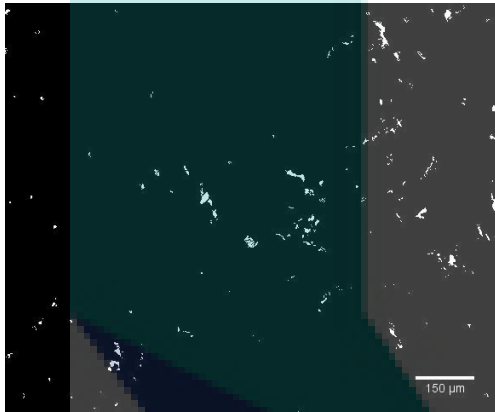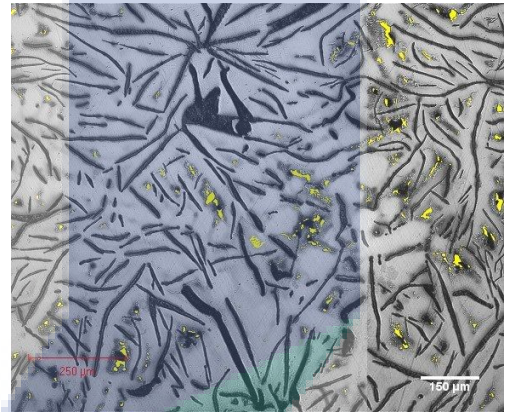
(a)   **(b)**

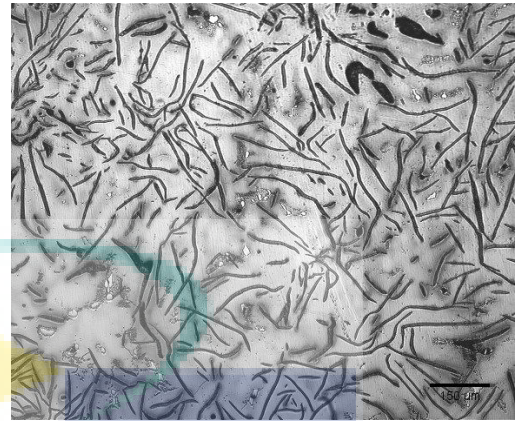**(c)**   **(d)**
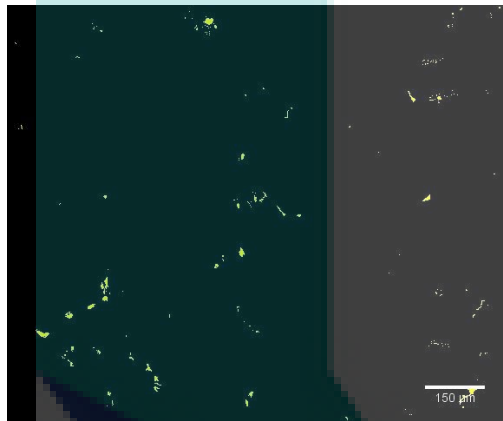
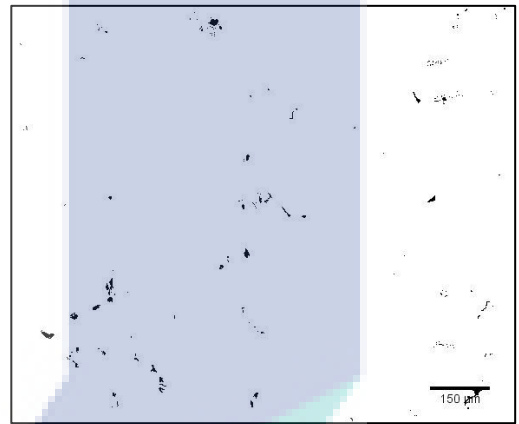**Annealing 800 °C**

108

(a)

(b)

(c)

(d)
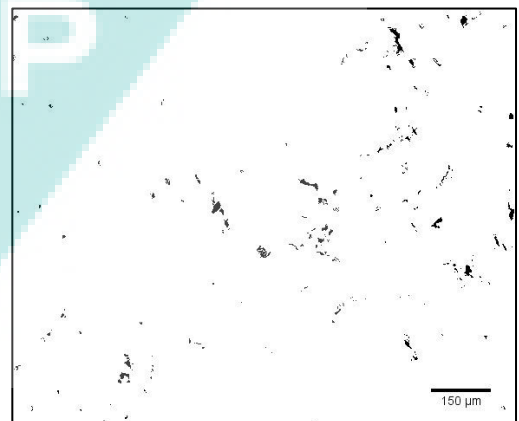
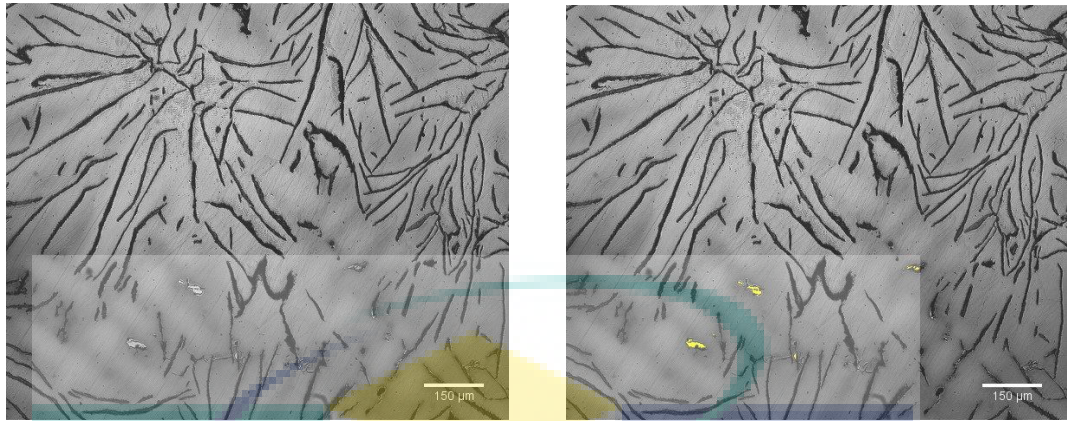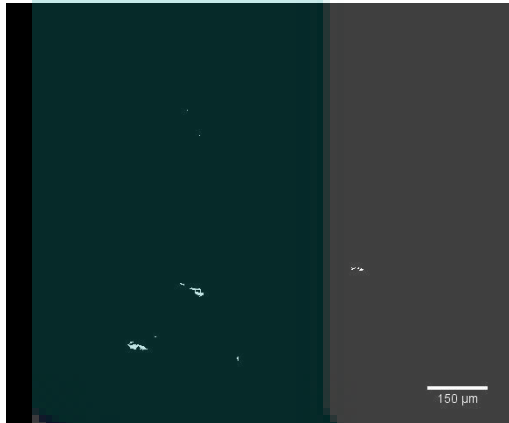**Annealing 900 °C**

(a)

(b)

(c)

(d)

Annealing 1000 °C

APPENDIX D

List of Publications and Conferences

Presented Paper in National and International Conferences

1. **K. M. Ahmad**, M. M. Rashidi, M. Ishak (2016), Microstructure and Mechanical Properties of Austenitic Compacted Cast Iron with Additive Manganese, MATEC Web Conf. Volume 78, 00009 (2016), 3rd International Conference on Mechanical Engineering Research 2015 (3rd ICMER2015), 19 August 2015, Kuantan, Pahang Malaysia. DOI: 10.1051/matecconf/20167400009

2. **K. Muzafar**, M. M. Rashidi, I. Mahadzir, Z. Shayfull (2016), Investigation on Microstructure Of Heat Treated High Manganese Austenitic Cast Iron, MATEC Web Conf. Volume 78, 01079 (2016), 2nd International Conference on Green Design and Manufacture 2016 (ICONGDM 2016), 1st - 2nd May 2016, Phuket, Thailand. DOI: 10.1051/matecconf/20167801079

3. **K. Muzafar**, M. M. Rashidi, I. Mahadzir, Z. Shayfull (2016), Effect on Mechanical Properties of Heat-Treated High Manganese Austenitic Cast Iron, MATEC Web Conf. Volume 78, 01081 (2016), 2nd International Conference on Green Design and Manufacture 2016 (IConGDM 2016), 1st - 2nd May 2016, Phuket, Thailand. DOI: 10.1051/matecconf/20167801081

Conferences attended

1. **Presenter**, 3rd International Conference on Mechanical Engineering Research 2015 (3rd ICMER2015), Zenith Hotel, 19 August 2015, Kuantan, Pahang Malaysia.